ABSTRACT

Title of Document: STRUCTURAL DETERMINANTS FOR ALLOSTERY AND FUNCTIONAL SWITCHING IN THE *E. COLI* BIOTIN REGULATORY SYSTEM.

Saranga Naganathan, Ph.D., 2008

Directed By: Professor Dorothy Beckett,
Department of Chemistry and Biochemistry

The *Escherichia coli* protein, BirA, functions as an allosteric transcriptional repressor and a metabolic enzyme. BirA catalyzes synthesis of its intermediate, bio-5'-AMP, from biotin and ATP. In its repressor function, binding of bio-5'-AMP promotes homodimerization that is a prerequisite to DNA binding at the biotin biosynthetic operon. As an enzyme, BirA forms a heterodimer with the biotin carboxyl carrier protein and transfers biotin to activate the first committed step of fatty acid synthesis. Based on structural data the unliganded repressor is characterized by four flexible loops that are ordered in the ligand-bound homodimers. Two of these loops participate in intermediate binding. The biotin binding loop (BBL) orders over biotin and participates directly at the dimer interface. The adenylate binding loop (ABL), located distal to the interface orders over the adenine ring. Single site mutations in a hydrophobic cluster of the ABL are investigated for small ligand binding and dimerization employing isothermal titration calorimetry and sedimentation equilibrium techniques. Results indicate that coupling between adenylate binding and dimerization is compromised in each mutant. Further, the

ligand-induced disorder-to-order transition in the ABL is shown to be integral to the allosteric response. The ABL and BBL are also examined for their role in the structural mechanism of intermediate-induced protein:DNA interaction. Based on a structural model of the repressor:DNA complex, electrostatic interactions are predicted between the flexible loops and the DNA backbone. The DNA binding properties of mutants in the loops are assessed by the DNase I footprinting technique. Contrary to predictions, results indicate no direct participatation of the loops in the protein:DNA interaction. Finally, the same loops are inspected for their role in mutually exclusive, isoenergetic protein:protein interactions. Combined with mutant proteins previously examined in homodimerization, additional mutants in the flexible loops are investigated in alternate protein:protein interactions. The hetero- and homo-dimerization processes are monitored by inhibition DNase I footprinting titrations, a kinetic assay, and sedimentation equilibrium measurements. Results indicate an overlap in structural determinants important for both interactions. Further, “hotspots” have evolved that are exclusive to one but not the other protein:protein interaction that is associated with each function of BirA.

STRUCTURAL DETERMINANTS FOR ALLOSTERY AND FUNCTIONAL SWITCHING IN THE *E. COLI* BIOTIN REGULATORY SYSTEM.

By

Saranga Naganathan

Dissertation submitted to the Faculty of the Graduate School of the
University of Maryland, College Park, in partial fulfillment
of the requirements for the degree of
Doctor of Philosophy
2008

Advisory Committee:
Professor Dorothy Beckett, Chair
Professor David Fushman
Assistant Professor Barbara Gerratana
Professor George Lorimer
Associate Professor Richard Stewart

Acknowledgements

I am inexpressibly grateful to my parents and my sister, Sahana, for their constant love, support and confidence in me. I am extremely indebted to my husband, who has over these years been patient and stood by me even through long distances. Thank you Kaushik, for your consistent encouragement, love and providing me with strength at every step. Here is to our future..…

I would like to thank Dr. Beckett for her guidance and confidence in me. Thank you for all the opportunities, facilities and resources to learn and develop my scientific skills. You have worked very hard with me on my speaking and writing skills with patience and perseverance. I thank you for providing the opportunity to present posters and attend conferences. I especially thank you for your support and consideration in the final stages on my degree.

I thank Dr. Herman Kraybill for the fellowship. I was so inspired by him on our first meeting and have immense admiration and respect for him.

I am extremely grateful to the members of my committee, Dr. David Fushman, Dr. George Lorimer, Dr. Victor Munoz, Dr. Barbara Gerratana and Dr. Richard Stewart. Thank you for your encouragement and advice through the years.

Emily, thank you for everything! I joined the lab not knowing how to pipette, or even make buffers. You guided me and helped me through every step, teaching me so many skills and techniques with patience. Thank you for making me laugh and telling the best stories I have heard. It was an absolute pleasure working with you.

I would like to thank current and previous lab members for creating a conducive, healthy and fun work environment. I especially thank the undergraduates who kept the spirit going everyday! It has been a wonderful experience meeting people with so many different backgrounds, goals, ideas and personalities. I have learned so much from every one of you. I especially thank Dr. Patrick Brown, who in the final stages of writing his dissertation taught me how to perform ITC experiments just as I had joined the lab. I thank Maria and Joy for valuable discussions and times of laughter. I also thank Dr. Keehwan Kwon and Jennifer Grason for the preparation of some mutant proteins I utilized in my research.

I thank Dr. Zachary Wood for providing an exciting project. Although it proved somewhat challenging, it was a great learning experience.

Graduate school was a wonderful experience. It would have been impossible to make it through without my closest friends. I have met some wonderful people and made great friends over the years and I thank them all for making these years valuable.

Table of Contents

List of Tables

List of Figures

I. General Introduction

Decades ago François Jacob wrote, "…*evolution does not produce innovations from scratch. It works with what already exists, either transforming a system to give it a new function, or combining several systems to produce a more complex one (1).*" The remarkable ability of proteins to develop multifunctional properties and to integrate them through the conservation of sequence and/or structure is of considerable evolutionary significance. The *E. coli* Biotin Regulatory System is an excellent model to investigate this phenomenon. The work presented in this thesis is focused on elucidating the structural basis of multi-functionality in this system.

The central component of the *E. coli* Biotin Regulatory System, BirA, is a bifunctional protein. It funnels biotin into metabolism or regulates biotin biosynthesis by switching between two alternate interactions *(2, 3).* BirA binds substrates biotin and ATP to catalyze synthesis of its intermediate, bio-5'-AMP*(4)*. Binding of this small molecule allosterically activates the transcription repression function of BirA through driving formation of a homodimer that binds the biotin operon *(5-7)*. BirA also forms a heterodimer with a biotin acceptor protein, apoBCCP, a subunit of the acetyl-CoA carboxylase enzyme (ACC). This results in biotin transfer to ACC, thereby activating the enzyme that catalyzes the first committed step of fatty acid synthesis. Alternative protein:protein interactions regulate the functional switch in BirA.

The BirA system serves as a model for investigating structural features important to protein:ligand, protein:protein and protein:DNA interactions in the context of its multi-functionality. The focus of this thesis is three-fold: (1) to elucidate the role of a flexible loop important in intermediate binding to the allosteric response in BirA, (2) to investigate the role of flexible loops involved in intermediate binding and homodimerization in the structural mechanism of effector-induced protein:DNA interaction, and (3) to investigate the role of the same flexible loops to the functional switch between transcriptional regulation and metabolism. The topics covered in this general introduction are intended to provide the reader with background on the *E. coli* Biotin Regulatory System and to place this work in a broader context.

A. Allosteric Regulation

Regulation of protein function through allostery is a concept that emerged from early research on feedback inhibition of enzymes*(8, 9).* In the original allosteric model a protein contains a regulatory site distinct from the catalytic site that is responsible for regulating protein function. The catalytic activity of a protein can be activated or attenuated by binding of an activator or inhibitor at the distant regulatory site. The mechanism of regulation can be explained by a conformational change in the protein that accompanies binding thereby altering the catalytic activity of the protein *(10, 11).* Monod called this regulatory site an "allosteric" binding site *(12, 13).* Many allosteric systems can be explained by two models: the concerted MWC model by Monod, Wyman and Changeux, and the sequential model by Koshland, Nemethy and Filmer. These models provide mechanical views of allostery. In general they

postulate two conformations of an enzyme, the tense (T) and relaxed (R) states, that exhibit differential affinities for a substrate. Binding of a small molecule to the allosteric site shifts the equilibrium between the two states. In a broader and more current view of allostery, macromolecules exist as ensembles that are shifted in response to small ligand binding or post-translational modification, thereby affecting functional properties. The resulting allosteric response is in essence a change in the thermodynamic properties of the system and is realized through a conformational and/or dynamic change in the macromolecule.

Understanding allosteric regulation requires elucidation of the mechanisms by which a signal associated with effector binding is propagated through the macromolecule to affect its functional features. In some systems the allosteric signal is transmitted *via* a conserved network of interactions from the ligand binding site to a distant regulatory site. In others, the signal is transmitted over large distances to effect global conformational and/or dynamic changes. One approach to understanding allostery is through experimental determination of the significance of structural and dynamic changes in a macromolecule for the functional response.

Allostery operates in many cellular processes including metabolism, signal transduction, and transcription regulation *(14, 15)*. The *E. coli* protein, BirA, serves as an excellent model for studying allostery. Extensive thermodynamic and structural studies have enabled an understanding of the mechanism of allosteric activation in BirA. Additionally, data have also provided clues to structural features important to

allosteric signal transmission. The following brief introduction to the *E. coli* Biotin Regulatory System provides the necessary background that has lead to the research presented in the second chapter of the thesis.

The central component of the *E. coli* Biotin Regulatory System, BirA, is a bifunctional protein that functions as a metabolic enzyme and a repressor of transcription initiation *(2, 3)* (Figure 1). As an enzyme BirA catalyzes the two-step biotinylation of the biotin carboxyl carrier protein (apoBCCP), a subunit of the acetyl-CoA carboxylase enzyme (ACC). In the first step, apoBirA monomer binds the substrates biotin and ATP to catalyze synthesis of the intermediate, bio-5'-AMP. The bio-5'-AMP bound form, holoBirA, covalently links the biotin moiety to the ε-amino group of a specific lysine residue of BCCP*(4).* Biotin, when linked to BCCP, is the transient carrier of a carboxylate group in its transfer from the donor, bicarbonate, to the acceptor, acetyl-CoA, and thus plays the role of an essential cofactor in the first committed step of fatty acid biosynthesis. As a transcriptional repressor two BirA monomers bind specifically to the 40-base pair biotin operator sequence (bioO) blocking access of the RNA polymerase to the two divergent overlapping promoters, P_a and $P_{b,}$ and repressing transcription of the biotin biosynthetic operon *(5, 6).* Formation of the repression complex occurs *via* two coupled reactions in which dimerization is followed by DNA binding *(16).* ApoBirA is not the active species in bioO binding. Rather the bio-5'-AMP-bound repressor binds bioO with high affinity. Hence, bio-5'-AMP, serves as an intermediate in biotin transfer to BCCP and as a corepressor of BirA in its transcription repression function.

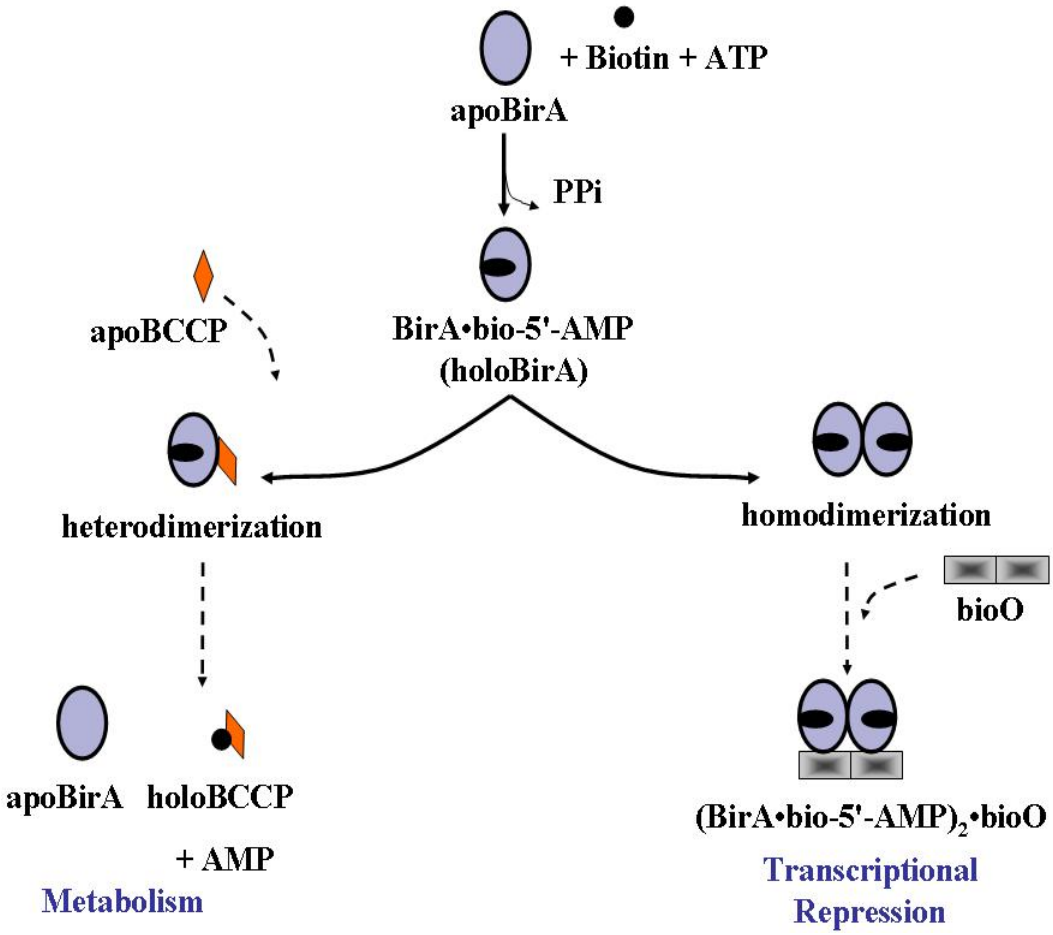

Figure 1. A schematic of the *E. coli* Biotin Regulatory System

The activated enzyme, BirA-bio-5'-AMP, switches between functioning as a biotin holoenzyme ligase and a transcriptional repressor.

As evidenced by the x-ray crystallographic structure, gel filtration, and sedimentation equilibrium studies apoBirA, the unliganded form of BirA is monomeric *(17, 18).* It is a 35.3 kDa protein of 321 amino acids comprising three domains (Figure 2). The N-terminal DNA binding domain contains a winged-helix-turn-helix motif, characteristic of many DNA binding proteins. The central domain contains a 7-stranded mixed beta-sheet packed against 5 alpha helices, and five loops of which four loops are partially disordered in the crystal structure and are indicated in the figure. The central domain contains the ligand binding site and biochemical data also indicate its direct role in dimerization and indirect role in DNA binding. The C-terminal domain contains a β-sandwich motif and structural data indicate its involvement in dimerization.

The mechanism of allosteric activation of BirA has been studied extensively using equilibrium thermodynamic and kinetic techniques *(19-26).* Binding of the allosteric activator, bio-5'-AMP, to two apoBirA monomers drives dimerization. Results of time-resolved DNase I footprinting and equilibrium thermodynamic measurements of repression complex assembly reveal a two-step process of dimerization followed by DNA binding *(16).* Sedimentation equilibrium measurements indicate that binding of bio-5'-AMP enhances BirA dimerization by -4.4 kcal/mol *(17, 27).* This difference in the dimerization energetics for apoBirA and BirA bound to bio-5'-AMP, is equal to the difference in total assembly energetics of the repression complex for the two species. Thus allosteric activation is thermodynamically centered in the dimerization step *(27).* Therefore, elucidation of

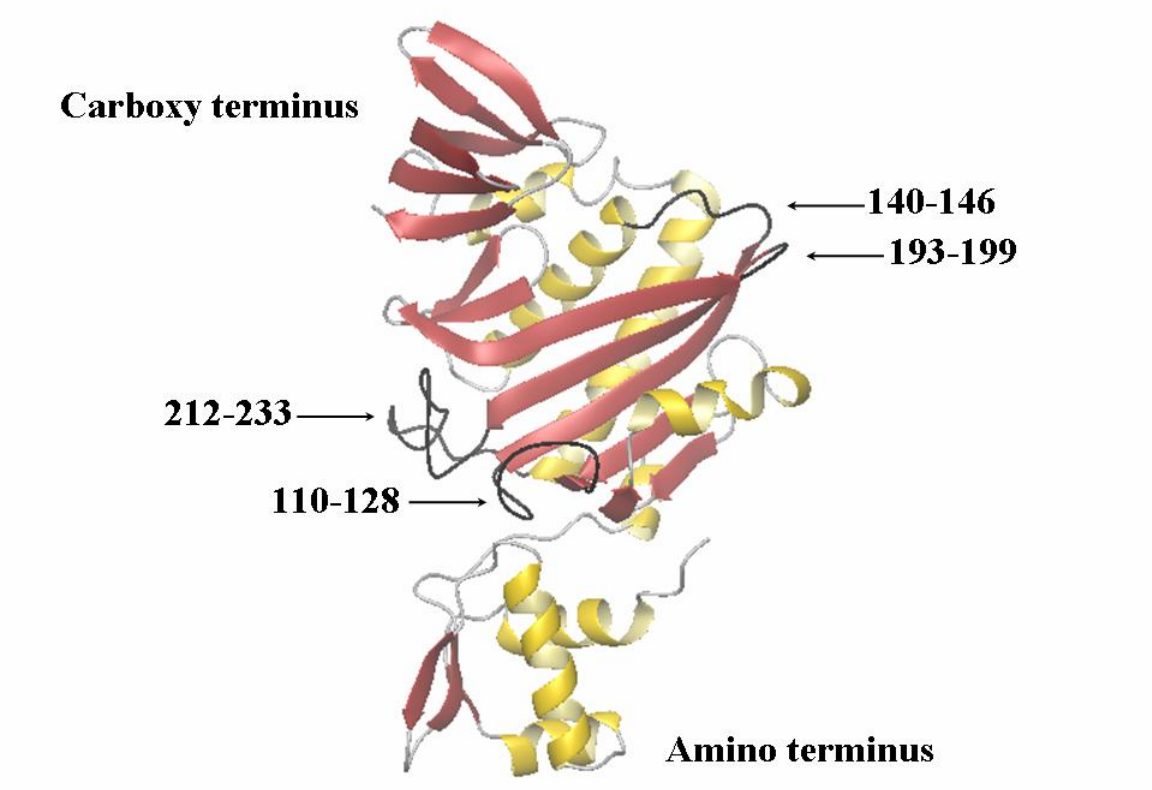

Figure 2. A model of the three-dimensional structure of apoBirA obtained from X-ray crystallography *(18)*. The four partially disordered loops are indicated in black. The model was generated using the program MolMol *(28)* with the Protein Data Bank file 1BIA as input.

the allosteric mechanism in BirA requires determination of the structural and dynamic changes in the BirA monomer that accompany activation of dimerization by bio-5'-AMP.

The magnitude of the allosteric response in BirA can be modulated using analogues of the corepressor, bio-5'-AMP (Figure 3). Based on their ligand binding properties and abilities to promote repressor dimerization and bioO binding, these small ligands are characterized as weak and strong activators *(29).* Bio-5'-AMP and its analog biotinol-AMP (btnOH-AMP) are strong allosteric activators while *d*-biotin, a substrate in bio-5'-AMP synthesis, and the sulfamoyl analog of bio-5'-AMP (btn-SA) are weak activators of BirA dimerization. While biotin binding results in no enhancement of dimerization, btn-SA binding results in a modest enhancement of -1 kcal/mol. By contrast, btnOH-AMP binding which affords an enhancement of -3.4 kcal/mol, a value comparable with that for bio-5'-AMP of -4.4 kcal/mol, serves as a good mimic of the intermediate. High resolution structures of the repressor bound to the weak activator, biotin, and strong activator, btnOH-AMP, have been determined by x-ray crystallography and are discussed below *(30, 31).* Comparison of structures and thermodynamic data on apoBirA, and the ligand-bound dimers has provided a better understanding of the mechanism of allosteric activation in BirA. Moreover, the structural data have offered valuable information on the structural and dynamic changes in the BirA monomer concomitant with ligand binding.

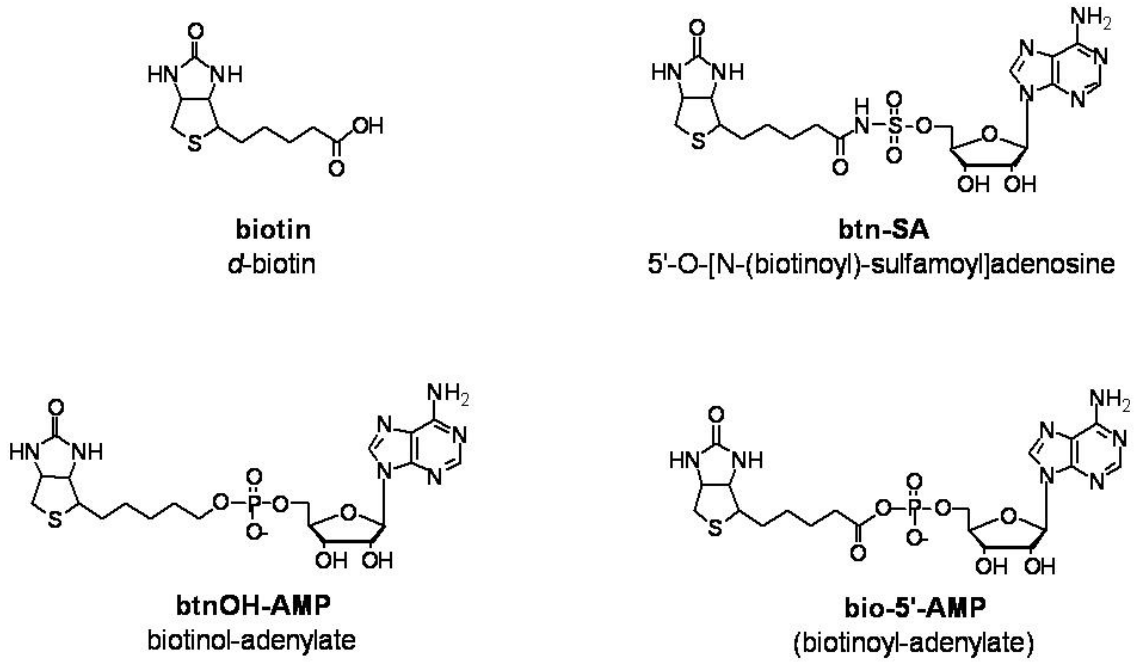

Figure 3. Chemical structures of the corepressor, bio-5'-AMP, and its analogs. Small ligands are categorized as weak (top) and strong (bottom) allosteric activators of BirA.

The x-ray crystallographic structure of biotin-bound BirA has been determined to 2.4 Å resolution. The structure reveals that the repressor is dimeric *(30)* (Figure 4A). The dimerization interface is located at the central domain of each monomer and is formed by side by side β-strands to form an extended β sheet. In forming the dimer each monomer buries 920 $Å^2$ of solvent accessible surface area. A striking feature of this structure is that 3 of the 4 partially disordered loops in apoBirA structure appear ordered in the biotin-bound dimer. These loops are composed of residues 110-128, 140-146 and 193-199 and participate at the dimer interface. Loop 110-128 is referred to as the biotin binding loop as it is ordered over the biotin moiety in the crystal structure. Mutations of residues in these loops exhibit defective dimerization and DNA binding properties *(32, 33).* The fourth loop comprising residues 212-234, remains disordered in this dimer structure.

The biotin binding loop contains the glycine rich sequence $_{115}$GRGRRG$_{120}$ which is conserved in all biotin ligases *(33).* Kinetic and thermodynamic analyses of mutants G115S, R118G and R119W of this sequence demonstrated that they are involved in biotin and bio-5'-AMP binding, dimerization, and bioO binding *(32).* Based on the biotin-bound dimer structure, these three residues do not interact with the biotin moiety. However, other residues within the sequence directly contact the ligand. R116 contributes two main-chain hydrogen bonds to biotin and G117 packs against the alkyl tail of biotin. While these studies clearly demonstrated the structural determinants important for biotin binding, those required for ATP binding remained unknown.

Biochemical studies have demonstrated a role for the fourth disordered loop 212-234 in corepressor binding. Early evidence was obtained from proteolytic digestion experiments performed with the protease subtilisin that cleaves the BirA backbone between residues 217-218 located in the loop *(34)*. The time course of subtilisin-catalyzed proteolysis of apoBirA and BirA bound to bio-5'-AMP were determined. Binding of the corepressor resulted in a decreased proteolysis rate, indicating protection of the fourth loop upon binding bio-5'-AMP. Further, the hydroxyl radical footprinting technique was utilized to probe structural and conformational changes that take place in the BirA monomer upon ligand binding *(35)*. Results indicated a decreased reactivity of the BirA backbone to hydroxyl radical agents as a consequence of ligand binding. Bio-5'-AMP binding resulted in 90-100% protection of segment 215-220 of the fourth loop. Based on these combined biochemical results, it was surmised that the fourth loop becomes ordered upon binding the corepressor and that its ordering may result in enhanced dimerization.

The ordering of the fourth loop concomitant with corepressor binding was confirmed by structural data. Bio-5'-AMP contains a reactive mixed anhydride bond and is inherently unstable, which precluded its use in determining the corepressor-bound structure of BirA. However, the corepressor analog, btnOH-AMP, is a strong allosteric activator that mimics bio-5'-AMP in its ability to enhance dimerization of BirA and DNA binding. The x-ray crystallographic structure of btnOH-AMP-bound BirA has been determined to 2.8 Å resolution and reveals the repressor as a dimer *(31).* As in the biotin-bound dimer structure, the dimer interface is formed *via* a β-

strand of the central domain. While the dimer interface of the BirA-biotin and the BirA-btnOH-AMP complexes are similar, the energetic difference between the weak and strong activator-induced dimerization is -3 kcal/mol. A comparison of the two dimer structures reveals some differences. Consistent with greater thermodynamic stability, the dimer interface in the btnOH-AMP-bound dimer is larger and extends to the C-terminal domain. However, the most significant structural difference is the ordering of the fourth flexible loop in the btnOH-AMP-bound dimer. This loop, comprising residues 212-234 is located distal to the dimer interface. It is folded over the purine ring of the adenylate moiety and is therefore called the adenylate binding loop (Figure 4B).

A common approach to understanding allosteric control in macromolecular systems involves determination of how conformational and/or dynamic changes that occur at the allosteric ligand binding site are transmitted to a distinct site to affect function. A brief review of two systems is provided in this section. In the first, small ligand binding to an allosteric site alters its local conformation. The allosteric signal associated with binding is transmitted through a conserved network of residues to affect a distant site. In the second system, small ligand binding similarly alters local structural features at the allosteric site. By contrast, in this system the allosteric signal is realized *via* a global conformational change. However, in both examples local changes at the effector binding site affect the functional response at a distance.

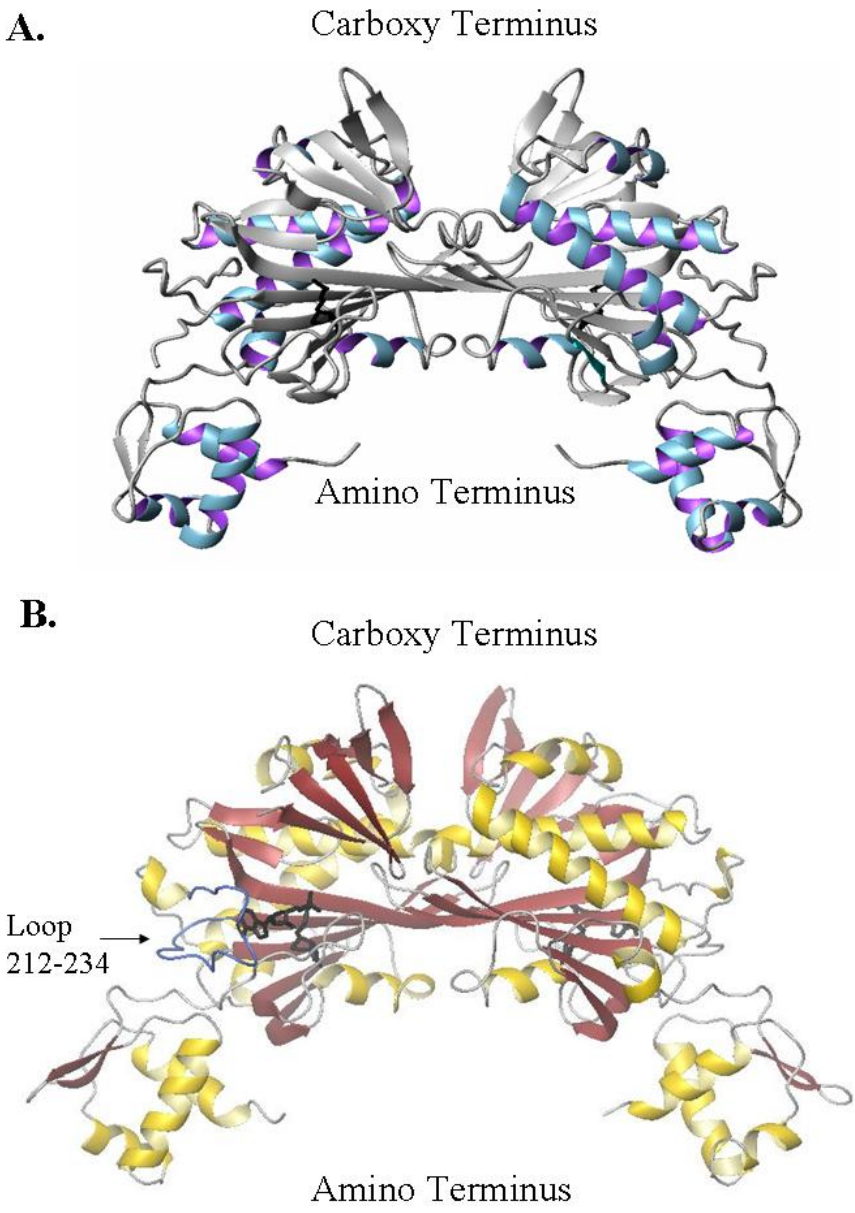

Figure 4. Models of the three dimensional structures of Ligand-bound BirA dimers determined by X-ray crystallography *(30, 31)*. (A) BirA bound by *d*-biotin. *d*-biotin is shown in black. (B) BirA bound by biotinol-adenylate. Biotinol-adenylate is shown in black. The fourth loop is shown in blue. The models were generated using the program MolMol *(28)* with the Protein Data Bank files 1HDX (A) and 2EWN (B) as inputs.

1. Hsp70

Hsp70s are the 70-kDa heat shock proteins that are essential members of the cellular chaperone machinery. These chaperones function in *de novo* folding of newly synthesized polypeptides and the disaggregation and refolding of stress-denatured proteins *(36, 37).* Hsp70 is composed of two binding domains including the C-terminal substrate-binding domain (SBD) and the N-terminal ATPase domain. Short hydrophobic peptide stretches within polypeptide substrates interact transiently with the substrate binding domain of Hsp70. The functionality of the SBD is regulated by the nucleotide status of the ATPase domain through control of the conformational state of the substrate-binding domain. While ATP binding to the ATPase domain results in low affinity of Hsp70 proteins for their substrates, the affinity is high when ADP or no nucleotide is bound. Additionally, the interdomain allostery in this system is bidirectional. That is, substrate binding to the SBD induces a conformational change in the ATPase domain to stimulate ATP hydrolysis, thereby resulting in a high substrate affinity state.

Several approaches have been taken to understand the allosteric mechanism of regulation in Hsp70. Structural data have provided some information on the active sites of each domain and interdomain communication. The x-ray crystallographic structure of a two-domain construct of the bovine Hsc70 in its nucleotide free-state has been determined *(38).* The structure shows the contact sites between the substrate-binding and ATPase domains. The interdomain contacts are formed by one side of a helix A of the substrate binding domain which rests in a groove of the

ATPase domain with two domains are connected by a linker (Figure 5). Combined structural, biochemical and amide hydrogen-deuterium exchange studies have helped elucidate the mechanism of allosteric regulation in Hsp70 *(39, 40).* Biochemical data indicate that a conserved proline located in the ATPase domain and an arginine located at the surface of the domain are important to the allosteric mechanism *(41).* A signal transduction pathway has been identified that starts with the conserved proline and arginine residues of the ATPase domain surface *(42).* Mutant proteins assessed for ATPase activity and effects on interdomain communication by fluorescence techniques enabled identification of key residues that constitute the signaling network. These include two positively charged surface exposed residues in the ATPase domain and an aspartate residue in the linker connecting the two domains (shown in Figure 5). The aspartate is essential for stimulating ATPase activity. ATP binding to the ATPase domain causes local changes within the domain that are relayed to the SBD. The transmission of the response upon ligand binding occurs *via* this signaling network of residues resulting in a bend in the linker between the domains, thereby triggering a low affinity state of the SBD. Local changes in the ATPase domain upon ligand binding affect the functional activity of the distant substrate binding domain.

2. Thrombin

Thrombin is an allosteric serine protease that belongs to the chymotrypsin family *(43).* It is generated in the blood form its precursor prothrombin and plays two opposing roles in blood coagulation *(44).* It acts as a procoagulant in converting

substrate, fibrinogen, into an insoluble fibrin clot that anchors platelets to the site of lesion to initiate wound repair *(45, 46).* By contrast, thrombin also acts as an anticoagulant by activating protein C *(47).* Na^{2+} binding allosterically controls the procoagulant function of thrombin, and the anticoagulant function is driven by the cofactor thrombomodulin. The review here focuses on the former function of thrombin.

Structural, mutagenesis and kinetic investigation allowed identification of three forms of the enzyme, E (*), E, and E:Na(+), that interconvert under the influence of ligand binding to distinct domains. The transition between the Na(+)-free, E, and the Na(+)-bound, E:Na(+), is accompanied by conformational changes in the enzyme *(48).* E (*) is most likely an inactive form of thrombin, unable to interact with Na(+)and substrate *(49).* Extensive structural and biochemical investigations on these forms have provided an understanding of the mechanism of allosteric regulation in thrombin.

There are currently over 50 structures of thrombin bound by Na+ *(50).* Combined with the structural data, alanine scanning mutagenesis of thrombin has revealed an allosteric core of residues that cluster around the Na+ site. Mutations in this cluster result in energetic defects in Na+ binding *(51).* Structures of the Na+ free and Na+ bound forms have been determined. While they bear many similarities, distinct differences have been identified at the allosteric core *(52).* Several of these

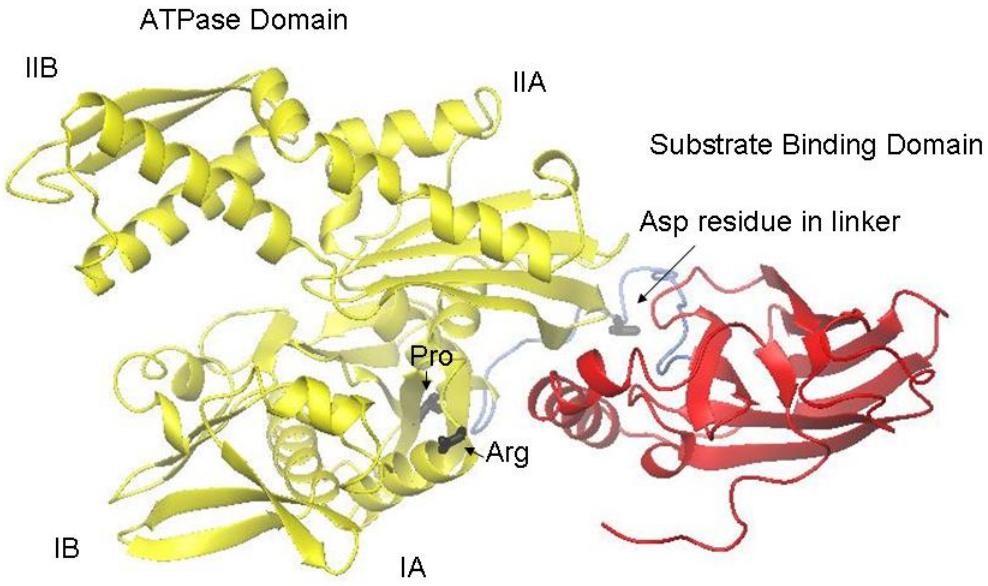

Figure 5.The structure of the Bovine Hsc70 protein *(38)*.

The ATPase domain (yellow) and substrate binding domains (red) of the two-domain construct of the bovine heat shock protein 70. The linker is shown in blue and key residues are indicated in black. The model was generated using the program MolMol *(28)* with Protein Data Bank file 1YUW as input.

structural determinants within the core are involved in the transition between the Na+ free and Na+ bound forms as evidenced from kinetic analyses *(53).* While Na+ binding directly alters the conformation of the core, the resulting allosteric signal is propagated through the entire protein to globally alter conformation, thereby affecting function.

Several approaches have been employed to probe the overall conformational state of thrombin in response to Na+ binding. Ligands that bind to specific domains of thrombin have been utilized to probe more local changes within domains. The use of chromogenic substrates has provided valuable information on how the active site participates in the allosteric transition *(51).* Another approach has been to analyze the interaction between thrombin and macromolecular ligands that probe a larger surface of the enzyme. For example, the potent natural inhibitor, hirudin *(54)*, mimics the binding strategy of fibrinogen *(55, 56)* and serves as an excellent probe of the conformational state of the enzyme. These methods have identified structural determinants critical to transition of thrombin from one form to the other and have offered some idea of the molecular basis of allostery in thrombin. Overall, the allosteric response associated with Na+ binding to thrombin is realized through global conformational transitions that promote its response to injury.

The second chapter of this thesis is focused on understanding allostery in the biotin repressor protein by determining the significance of the structural/dynamic changes associated with intermediate binding. The response is realized through

ligand-induced dimerization of the protein. In this study, corepressor-induced folding of the adenylate binding loop, which is located distal to the dimerization interface, is investigated for its role in the allosteric response.

B. Allosteric Regulation of Transcription Factors

The biotin repressor, BirA, belongs to a large family of allosteric transcription factors. The allosteric mechanisms associated with small ligand binding to regulate transcription have been extensively studied in many systems. The third chapter of the thesis focuses specifically on elucidating the structural mechanism by which small ligand binding alters the affinity of the protein:DNA interaction in the *E. coli* Biotin Regulatory System.

In order to maintain the normal cell viability in response to changes in nutrient levels the expression of many genes must be modulated. This regulation is often carried out at the level of transcription initiation. A good example to illustrate the importance of regulating gene expression is in *C. diphtheriae*. This organism expresses iron binding proteins which sequester iron for biological activities. Increased levels of iron uptake can result in formation of reactive hydroxyl radical species that can damage biological molecules *(57).* Alternatively, low levels of iron uptake may result in expression of virulence factors. Hence in response to iron levels in the cell expression of genes that encode iron binding proteins are regulated at the transcriptional level.

Many transcriptional regulators are allosteric DNA binding proteins. Structurally, they typically have an effector binding domain and a DNA binding domain. The DNA binding domain of the transcription factor contains the DNA-recognition elements required for a specific protein:DNA interaction. Allosteric regulation of transcription factors involves binding of a small ligand to a regulatory site/effector binding domain, distal from the DNA binding site. Small ligand binding is accompanied by a conformational change in the protein that alters the protein's affinity in site specific DNA binding. The resulting protein:DNA interaction is critical for regulating transcription initiation. Transcription initiation is regulated by the action of two classes of transcription factors including activators and repressors. While activators enhance transcription initiation, repressors inhibit this process. The discussion below on the mechanism of allosteric control of transcription factors is focused on repressors.

The mechanisms of allosteric regulation of many transcriptional repressors have been determined. In the classical mechanism, repressors exist as preformed oligomers, and effector binding affects the affinity for DNA by altering the conformation of the DNA recognition elements in the repressor. Among the repressors that exhibit this mechanism are the lactose repressor (LacR), tryptophan repressor (TrpR), purine repressor (PurR) and nickel repressor (NikR). In the non-classical mechanism, binding of the effector alters the self-assembly properties of the repressor. The resulting change in oligomeric state affects the binding affinity for

DNA. The diphtheria toxin repressor (DtxR), luecine responsive element (LrpA) and the biotin repressor (BirA) belong to this class of repressors.

Allosteric regulation of the biotin repressor, BirA, follows the non-classical mechanism. As described in the section on Allosteric Regulation, the mechanism involves two coupled processes. Binding of the allosteric activator, bio-5'-AMP, to apoBirA drives dimerization that is followed by DNA binding. The ligand-bound BirA homodimer binds to a 40 base-pair, inverted palindromic sequence of the biotin operator (bioO) to repress transcription initiation at the two divergent overlapping promoters, P_a and P_b of the biotin operon *(5, 6).* The N-terminal DNA binding domain comprises a winged-helix-turn-helix (wHTH) motif that forms site-specific contacts with the DNA. While the recognition helix of the motif contacts the major groove of DNA, the wing extends into the minor groove. Alteration in the amino acid sequence of the recognition helix of the wHTH results in loss of repression at the biotin control region. A combination of solution techniques, including DNase I footprinting, methylation protection and hydroxyl radical footprinting, have revealed the contact regions between the BirA dimer and the biotin operator *(35).* Two of the regions include the N-terminal DNA binding domain of each monomer that interacts with the two 12 base-pair termini of the 40 base-pair biotin operator sequence.

The structural mechanisms by which effector binding alters the protein:DNA interaction has been studied in various systems. In some transcriptional repressors the ligand binding site is located at the interface. Binding of the ligand alters the

structural features of the protein:DNA interface, thereby affecting transcriptional regulation. In others, the ligand binding site is located distal to the protein:DNA interface. Here, ligand binding creates a new structural module in the repressor for interaction with DNA. A brief review of two examples is presented to illustrate these distinct structural mechanisms and to provide a context for the research performed in chapter three.

1. Tryptophan Repressor

The Trp repressor, TrpR, regulates transcription of the *trp*ABCDE operon, which encodes the enzymes utilized in the biosynthesis of L-tryptophan from chorismate, in response to L-tryptophan *(58).* Each monomer consists of a N-terminal helix-turn-helix DNA binding domain and a C-terminal domain. Three α-helices of the C-terminal domain of each monomer pack against each other to form the dimer interface that is stabilized by a hydrophobic core. TrpR functions as a homodimer in binding to its operator sequence and is allosterically activated by tryptophan binding.

Comparison of the structures of apoTrpR and holoTrpR determined by x-ray crystallography and NMR *(59-62)* have enabled some understanding of the allosteric activation mechanism of the tryptophan repressor by L-trp. Based on structural and biochemical analyses, different mechanistic models have been proposed. In one, binding of L-trp to the protein dimer acts like a wedge between the core domain and the DNA binding domain, thereby positioning the recognition helix of each monomer in the proper geometry for tight, complimentary alignment with the two operator half-

sites *(63).* In another, L-trp binding induces complete folding of portions of the helix-turn-helix domain of TrpR which increases the affinity for DNA.

While the mechanistic models previously proposed were based on comparison of structures of apo- and holo-repressors, structural data on the repressor:DNA complex has provided a more complete understanding of the mechanism. TrpR was the first transcription factor for which a crystal structure was obtained for the repressor:operator complex *(64).* The tryptophan repressor interacts with DNA in the absence/presence of L-trp and the L-trp binding site is located at the protein:DNA interface. In the absence of tryptophan, the protein:DNA interaction is non-specific. ApoTrpR binds two L-tryptophan molecules prior to site-specific binding to the operator. Sequence-specific holorepressor binding is distinguished from the non-specific aporepressor binding by a 6500 fold difference in dissociation constants *(65).* The structural mechanism of effector-induced changes in the protein:DNA interaction has been determined by structural and biochemical methods. Structural determinants important to the repressor:operator interaction have been identified *(59).* The protein:DNA interaction between the tryptophan repressor dimer and DNA is governed largely by electrostatics. TrpR carries a relatively large net negative charge which results in repulsive interactions with the DNA. Structurally, the tryptophan binding pocket located at the repressor:operator interface undergoes an enhancement in positive potential upon effector binding, as compared to the aporepressor. This is supported by biochemical studies with tryptophan and its analogs that indicate an overall change in electrostatics upon effector binding. Direct contacts between the

effector and the DNA play an essential role in altering the electrostatic details of the interaction *(66).* In this system the allosteric ligand participates in the binding mechanism through direct alterations in the structural features of the interface.

2. Nickel Repressor

In the presence of nickel, the nickel repressor, NikR, represses transcription of the operon *nikABCDE* that encodes the nickel importer/permease *(67, 68).* Biochemical studies have shown that one nickel (II) ion binds each subunit of the homotetramer with high affinity in the picomolar concentration regime *(69, 70).* Nickel binding enhances the NikR affinity for its 28-base pair palindromic operator sequence by 250 fold. High resolution structures of apoNikR and metal bound NikR have been determined by x-ray crystallography *(71, 72).* The structure of apoNikR from *E. coli* reveals a modular domain architecture, with two dimer ribbon-helix-helix (RHH) DNA binding domains flanking a tetrameric metal-binding domain (MBD). Comparison of the apo- and metal-bound repressor structures reveals a disorder-to-order transition of a flexible loop in the nickel binding site upon binding metal. Preliminary structural and biochemical results provide insight into the mechanism of activation of NikR by metal ions.

Recent structural approaches undertaken to elucidate the structural mechanism of nickel-induced DNA binding of NikR reveal formation of a new structural module upon metal binding that directly interacts with DNA. Formation of the NikR-operator complex results in extensive polar interaction between the repressor and DNA. These

include specific and non-specific interaction from the RHH domain and non-specific interaction from the MBD *(72)* (Figure 6). The structure of the NikR repressor:operator complex indicates that the RHH DNA binding domains interact in the standard mode with the DNA backbone. They form specific contacts *via* hydrogen bonds between the side chain of two residues of a β-sheet and the nucleotide bases in the major groove of DNA. Mutation of these residues results in defective NikR binding to the operator, thus supporting the observation *(68).* The non-specific interactions contributed by the RHH domain include about 14 nonspecific interactions with the DNA backbone. Although biochemical measurements have not been performed to test these non-specific interactions, they have previously been observed in other members of the RHH family *(73, 74).* These non-specific interactions serve to anchor the domain to the DNA by properly orienting the specificity-determinants of the β-sheet of the RHH in the major groove of the DNA. Additionally, nickel binding induces a disorder-to-order transition of two loops in the metal binding domains. This change in conformation results in non-specific interactions between the side chains of two positively charged residues within the loops and the DNA backbone. Although these structural observations have not yet been assessed by biochemical methods, these data suggest formation of a new structural module upon metal binding in NikR that contributes to the structural mechanism of the protein:DNA interaction.

The third chapter of the thesis is focused at elucidating the structural mechanism of allosteric activator induced interaction of the biotin repressor and its

site-specific DNA sequence. In particular, the role of flexible loops involved in ligand binding and dimerization are examined for their role in direct interaction with DNA.

C. Regulating protein function *via* protein:protein interaction

The functional properties of many proteins are regulated in response to cellular requirements. Regulation of protein function can occur through interaction with another protein partner. For example, the *E. coli* global transcription regulator MIc, modulates production of glucose-specific PTS (phosphotransferase system) components *(75).* Glucose-bound MIc activates transcription of the *ptsG* gene that encodes glucose permease. In turn, at high glucose concentration, an increased production of glucose permease controls MIc-dependent gene expression. The glucose-bound enzyme, in its non-phosphorylated state, sequesters MIc in a protein:protein interaction, rendering it unavailable for transcription activation *(76).* Many enzymes like glucose permease can control gene expression in response to the availability of their substrates/effector through interaction with transcription factors. Table 1. includes some examples from *E. coli*.

In many biological regulatory processes protein function is modulated *via* exchange of one protein partner for another. For example, the transcription factor CHOP can associate with itself or other members of the C/EBP family. The choice of protein partner dictates transcriptional regulation at different target genes *(77, 78).* Similarly, the choice of a dimerization partner of proteins that belong to the mammalian basic helix- loop-helix/PAS family is critical to regulating transcription at

Table 1. Control of Gene Expression by Enzyme-Transcription Factor Interaction

Enzyme/ catalyzed reaction	Substrate/Effector	Target Protein
PtsG, Glucose permease	Glucose	MIc *(76)*
MalK, ATP binding subunit of the maltose transporter	Maltodextrins, Maltotriose	MalT *(80)*
PyrH, UMP kinase	Pyrimidines	PepA *(81)*
DhaL, DhaK, dihydroxyacetone kinase	Dihydroxyacetone	DhaR *(82)*

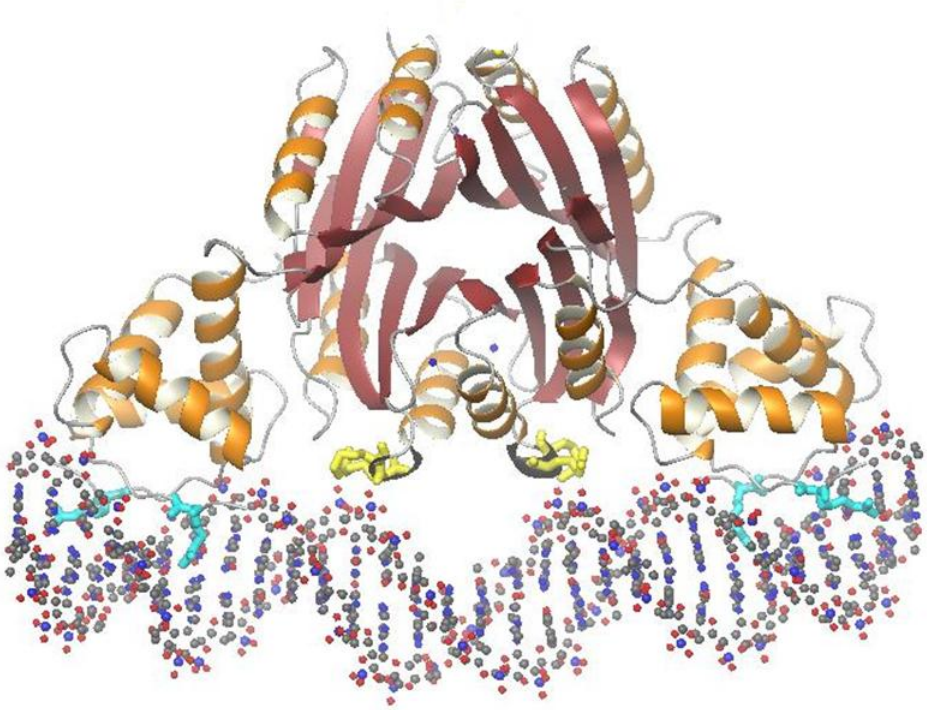

Figure 6. Structural Determinants of the NikR-Operator DNA Interaction *(72)*. Displayed are the specific contacts of the RHH domain (cyan) and the non-specific contacts of the MBD loops (yellow) with the operator in the NikR:operator complex. Model was generated using the program MolMol *(28)* with Protein Data Bank file 2HZV as input.

different genes *(79)*. Several analogous systems in which a single protein switches between alternative interactions to regulate function have been identified.

Control of a portein's biological function can occur through the use of the same surface of one protein in alternative protein:protein interactions. For instance, HAUSP (Herpesvirus-associated ubiquitin-specific protease) interacts with p53 tumor-suppressor and with MDM2 to regulate the p53-MDM2 pathway. MDM2 is an E3 ubiquitin ligase that ubiquitylates itself and p53, thereby serving in a complex auto-regulatory feedback loop *(83, 84)*. HAUSP serves in deubiquitylation in its interaction with both proteins *(85, 86)*. The HAUSP-p53 interaction stabilizes p53 resulting in p53-dependent apoptosis. By contrast, the HAUSP-MDM2 complex leads to suppression of MDM2 activity, in turn, stabilizing p53. Although the regulation of this pathway *via* two distinct protein:protein interactions is complex, an examination of the structures indicates that both interactions utilize the same surface groove in the N-terminus of HAUSP *(87)*. Another example is plakoglobin (γ- catenin), which interacts with desmosome proteins (Dsg and Dsc) belonging to the cadherin superfamily, to enable desmosome (intracellular junction) assembly. Alternatively, plakoglobin can interact with α-catenin to from adherens junctions. The regulation of distinct junction assemblies by plakoglobin occurs v*ia* protein:protein interactions that use the same surface in the C-terminal domain of plakoglobin *(88)*. A common theme in such systems is utilization of a single protein surface in alternative protein:protein interactions, thereby making the functions mutually exclusive.

In some systems, alternative protein:protein interactions regulate distinct functional features of a protein. The same surface of one protein is utilized in specific interaction with different protein partners, thereby rendering them mutually exclusive. One of the best studied systems is β-catenin. β-catenin functions as a transcriptional coactivator and in cell-cell adhesion *(89).* As a coactivator of transcription initiation β-catenin interacts with members of the T-cell factor (Tcf)/lymphoid enhancer factor (LEF) family of transcription factors *(90).* Alternatively, β-catenin interacts with cadherins in its cell adhesion function. The functional switch in β-catenin is controlled by the availability of the protein. Structural data indicate that the same surface of β-catenin is used to form complexes with E-cadherin and the transcription factor, Tcf-3 (Figure 7). In the former interaction the armadillo repeat sequence of β-catenin, interacts with the cytoplasmic catenin binding domain of E-cadherin. The same surface of the armadillo repeat sequence interacts with the amino terminal segment of the Tcf-3. Close inspection of the structures reveal similar chemistries at the two interfaces *(91, 92).* The ability of a single protein to form interactions with two different protein partners with promiscuity and specificity is remarkable. Although there is evidence in many systems that such alternate functions are mutually exclusive, an understanding of their mechanisms of regulation requires elucidation of the structural, thermodynamic and kinetic features of formation of alternative protein:protein interactions.

The biotin repressor/ biotin holoenzyme ligase, BirA, which is a bifunctional protein provides another example in which the same surface of one protein is used for

alternative protein:protein interactions. Extensive structural, thermodynamic and kinetic studies have been performed to investigate the functional switch in BirA. The fourth chapter of the thesis focuses on investigating the structural features of two mutually exclusive interactions that dictate the functional switch.

The mechanism of control of the functional switch of holoBirA from transcription repressor to biotin ligase has been extensively studied. As described earlier, binding of the intermediate, bio5'-AMP to BirA populates the activated monomer, holoBirA. HoloBirA participates in homodimerization or heterodimerization with the acceptor protein, apoBCCP, a subunit of the acetyl-CoA carboxylase enzyme. *In vivo* and *in vitro* data indicate that the concentration of the acceptor protein plays an important role in control of the functional switch *(93, 94).* *In vitro* studies show that apoBCCP engages holoBirA for biotin transfer, thereby depleting the holoBirA pool available for homodimerization. Thermodynamic measurements for formation of the homodimer and heterodimer reveal that they are isoenergetic, indicating a kinetically controlled switch *(95, 96).*

Structurally, the functional switch reflects formation of two mutually exclusive processes. A structural model of holoBirA-apoBCCP has been formulated and is supported by results of biophysical and biochemical studies of BirA and BCCP mutants *(93, 97, 98).* Comparison of the experimentally determined structure of the

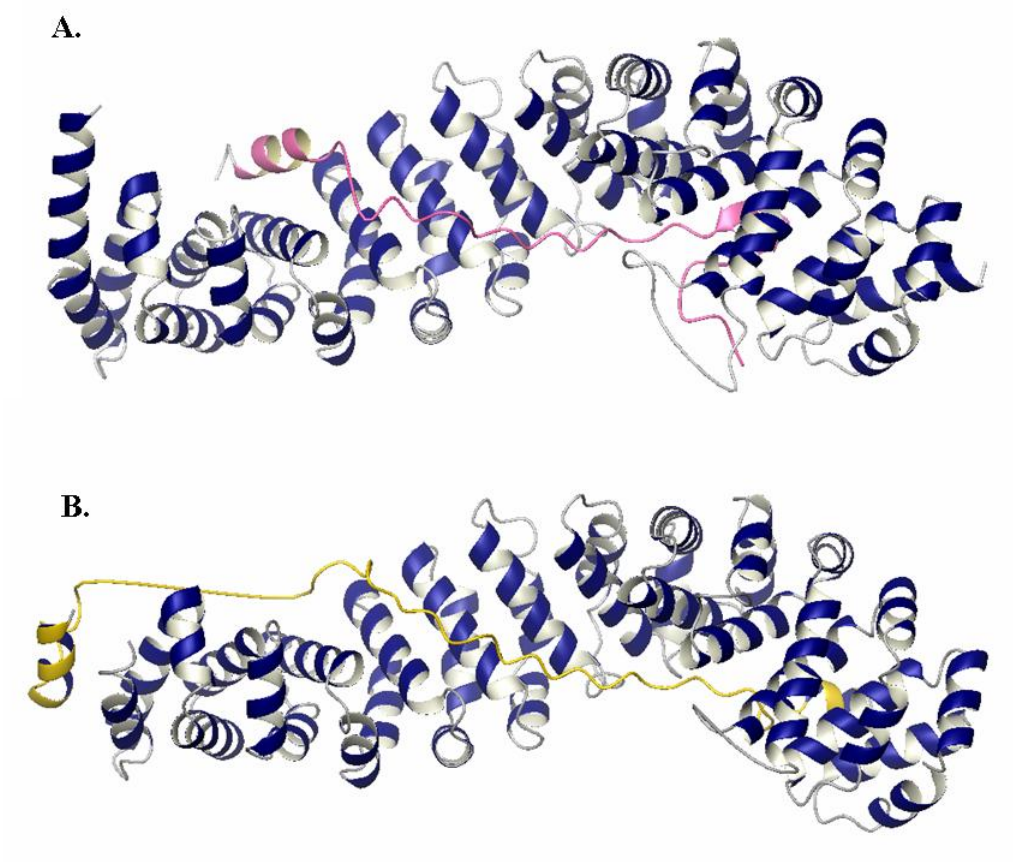

Figure 7.Structural Models of β-Catenin in alternative protein:protein interactions. (A) Complex of β-catenin and N-terminal segment of the transcription factor, Tcf-3. (B) Complex of β-catenin and the cytoplasmic domain of E-cadherin. Models were generated using the program MolMol *(28)* with Protein Data Bank files 1G3J for (A) and 1I7W for (B) as inputs.

holoBirA homodimer and the hypothetical structural model of the holoBirA-apoBCCP complex reveals that the same surface of BirA is utilized in both protein:protein interactions. The homodimer is formed *via* an antiparallel interaction between the same β-strand of the central domain of each holoBirA. By contrast the heterodimer interaction uses the same β-strand of holoBirA in a parallel interaction with a β-strand of apoBCCP to form an extended β-sheet. Although the same surface of BirA is utilized for homodimerization and heterodimerization, there is evidence that the chemistries of the two interfaces are distinct. In order to examine the structural features of alternative protein:protein interactions of BirA, in the fourth chapter of the thesis, the flexible loops involved in intermediate binding and homodimerization are investigated for their roles in heterodimerization.

D. Organization of the Dissertation

The first chapter of this dissertation is an Introduction that provides concepts and a literature review of specific systems with respect to allostery, allosteric regulation of transcription factors and regulation of protein function *via* protein:protein interactions.

The second chapter presents work that was published in the Journal of Molecular Biology. The work focuses on investigating the role of a hydrophobic cluster in a flexible loop of the biotin repressor that orders over the adenine ring in the ligand-induced allosteric response in the protein. The approach involved site-directed mutagenesis of residues in the hydrophobic cluster. The mutant proteins were

subjected to detailed thermodynamic analysis of small ligand binding and dimerization properties by isothermal titration calorimetry and sedimentation equilibrium techniques. Further, structural probing by partial proteolysis and heat capacity measurements by isothermal titration calorimetry were performed to assess the affect of mutations in the cluster on ligand-linked folding of the flexible loop. Overall, the results indicate that formation of the hydrophobic cluster is critical to a disorder-to-order transition of the loop and that this transition is integral to the allosteric response in BirA

The third chapter describes and tests predictions of a model for the repressor dimer:biotin operator complex. The model was entirely constructed and proposed by Dr. Zachary A. Wood, who is presently at the University of Georgia. It was generated based on combined structural and biochemical data. The aim of this work is to investigate the role of the effector in influencing the structural features of the protein:DNA interface of the *E. coli* biotin repressor dimer and its specific DNA sequence, bioO. The model predicts electrostatic interactions between positively charged residues of the effector binding loops of BirA and the backbone of the biotin operator backbone. Proteins in which these positively charged residues were changed to alanine were subjected to the DNase I footprinting titrations to asses their bioO binding properties. These results revealed that the energetics of dimer:DNA complex assembly were unaffected upon abolition of all putative electrostatic contacts. Overall, contrary to predictions based on the structural model, the effector binding loops do not directly interact with the DNA.

The fourth chapter describes work that focused on the alternative protein:protein interactions that control the functional switch in BirA. The structural determinants important to BirA homodimerization and heterodimerization with acceptor protein, apoBCCP, were investigated using a combination of mutagenesis and biochemical methods. Single site mutation of residues that directly disrupt the protein:protein interface and those that perturb the thermodynamic coupling between intermediate binding and homodimerization were investigated for defects in heterodimerization. The ligand binding and homodimerization properties of select mutant proteins were previously characterized by another graduate student in this laboratory, Dr. Keehwan Kwon. Results indicated an overlap in structural features important to both protein:protein interactions.

The fifth chapter summarizes how the results obtained in this research have provided an understanding of the structural basis for multi-functionality in the *E. coli* biotin repressor/biotin ligase. A discussion of future prospects for research is also included in this section. The final chapter provides details on the Materials and Methods employed for all research presented in this dissertation.

II. Nucleation of an Allosteric Response *via* Ligand-induced Loop Folding

A. Introduction

Allostery is ubiquitous in cellular processes including metabolism, signal transduction, and transcription regulation *(14, 15).* Consequently, allosteric control operates in a broad range of macromolecules including oligomeric metabolic enzymes (aspartate transcarbamylase) *(99)* chaperonin machines (GroEL) *(100)*, transcription regulatory proteins (lactose repressor) *(101)*, multi-domain signal transduction proteins (N-WASP) *(102)*, and small molecule-activated riboswitches (Adenine riboswitch) *(103).* Understanding allostery requires elucidation of the mechanism(s) by which a signal associated with small ligand binding or post-translational modification is relayed through the macromolecule to effect functional changes. In many cases this signal is transmitted over a large distance. One route to understanding allostery in biological macromolecules is experimental determination of the significance of structural and dynamic changes in the macromolecule for the functional response.

The *Escherichia coli* repressor protein, BirA, is the central component of the biotin regulatory system and serves as an excellent model for the study of allostery. BirA is a bifunctional protein that is both a key metabolic enzyme and a repressor of transcription initiation *(2, 3).* As an enzyme, BirA, or biotin holoenzyme ligase, catalyzes the two-step biotinylation of the Biotin Carboxylase Carrier Protein (BCCP), a subunit of the acetyl-CoA carboxylase, which catalyzes the first

committed step of fatty acid biosynthesis. BirA first catalyzes synthesis of biotinyl-5'-AMP (bio-5'-AMP) from its substrates biotin and ATP and then transfers the biotin moiety of the intermediate to the ε-amino group of a specific lysine residue on BCCP *(4).* Biotin, when linked to BCCP, is the transient carrier of a carboxylate group in its transfer from the donor, bicarbonate, to the acceptor, acetyl-CoA, and thus plays the role of an essential cofactor in the first committed step of fatty acid biosynthesis. As a transcription repressor, the BirA homodimer binds the biotin operator, bioO, thereby preventing transcription initiation at the biotin biosynthetic operon *(5-7).* It is not the apoBirA monomer, but rather the holo- or adenylate-bound dimer that is the active species in biotin operator binding. Hence, bio-5'-AMP is both the corepressor of BirA in its transcription repression function and the intermediate in its catalysis of biotin transfer to the BCCP subunit of acetyl-CoA carboxylase.

ApoBirA, the unliganded form of BirA, is monomeric, as evidenced by its crystal structure and gel filtration and sedimentation equilibrium studies *(18).* The protein is composed of three domains. The N-terminal DNA binding domain adopts a winged-helix-turn-helix motif that directly contacts the DNA in the repression complex. The central domain is organized into a 7-stranded mixed β-sheet packed against 5 α-helices, and five surface loops of which four are partially disordered. This domain contains the catalytic site and biochemical data indicate its direct role in dimerization and indirect role in DNA binding. The C-terminal domain contains a β-sandwich motif and structural studies indicate its involvement in repressor dimerization *(30).*

The mechanism of allosteric activation of BirA involves corepressor-linked repressor dimerization. Binding of the bio-5'-AMP to apoBirA is positively coupled to repressor dimerization (Figure 8). This mechanism of allosteric activation of BirA has been studied extensively using equilibrium thermodynamic and kinetic techniques *(5, 16-18, 32, 35).* Sedimentation equilibrium measurements indicate that adenylate binding enhances BirA dimerization energetics by -4 to -5 kcal/mol *(17, 27).* Kinetic and equilibrium thermodynamic measurements of repression complex assembly reveal a two-step process of dimerization followed by DNA binding *(16).* Finally, comparison of apoBirA and holoBirA in dimerization and the two-step assembly of the repression complex indicates that allosteric activation is thermodynamically centered in the dimerization step *(27).* Therefore, elucidation of the allosteric mechanism in BirA requires determination of the structural and dynamic changes in the BirA monomer that accompany activation of dimerization by bio-5'-AMP.

The magnitude of the allosteric response in BirA can be modulated using analogues of the physiological effector, bio-5'-AMP. Based on their ligand binding properties and abilities to promote repressor dimerization and bioO binding, these small ligands are categorized as weak and strong allosteric activators. Bio-5'-AMP and its analog biotinol-AMP (btnOH-AMP) are strong allosteric activators while *d*-biotin, a substrate in bio-5'-AMP synthesis, and the sulfamoyl analog of bio-5'-AMP (btn-SA) are weak activators of BirA dimerization. While biotin binding results in no

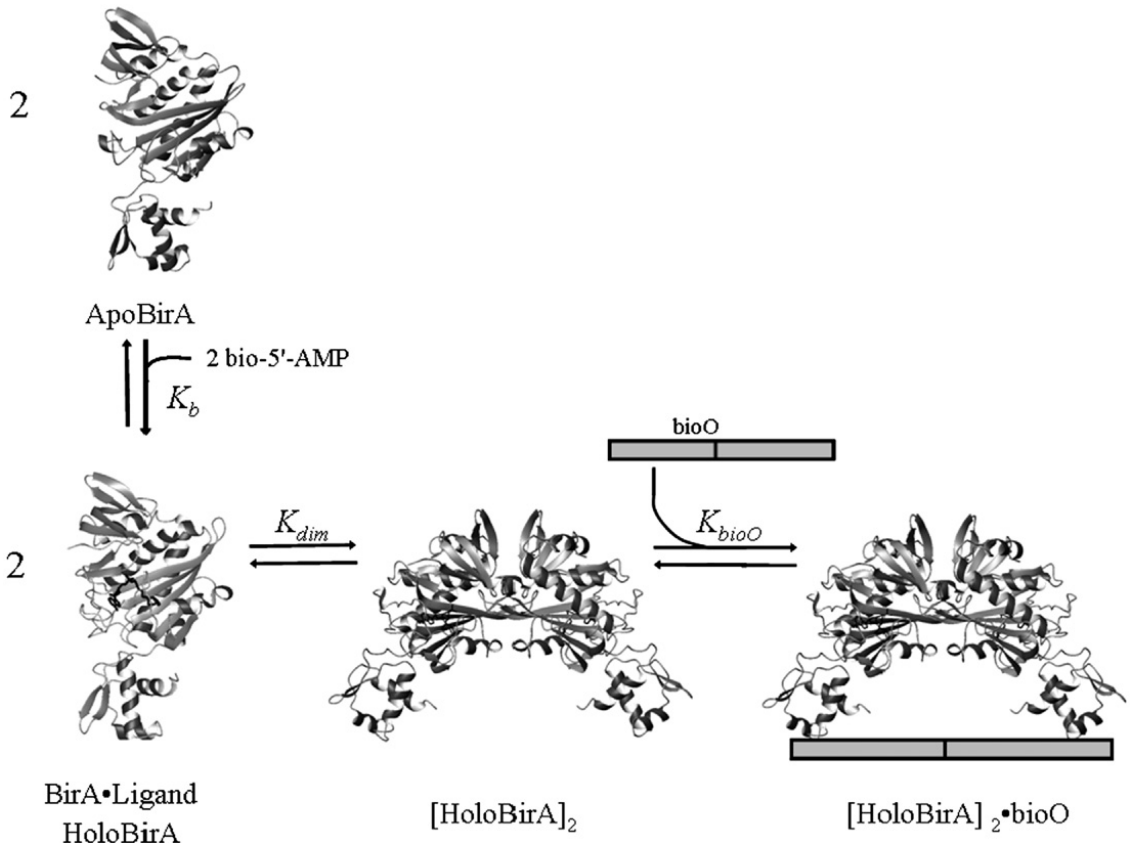

Figure 8: Allosteric activation of the biotin repressor by its physiological corepressor, bio-5'-AMP. Binding of the ligand is positively coupled to repressor dimerization. The resulting dimer subsequently binds site-specifically to the biotin operator sequence, bioO. ApoBirA refers to the unliganded protein and holoBirA is the bio-5'-AMP-bound species. K_b, K_{dim}, and K_{bioO} refer to the equilibrium constants governing bio-5'-AMP binding, holoBirA dimerization, and holoBirA dimer binding to bioO, respectively.

enhancement of dimerization, btnSA binding affords an enhancement of -1 kcal/mol *(104).* The designation of weak effector for biotin is based on its modest (-1 kcal/mole) enhancement of bioO binding. High resolution structures of the repressor bound to the weak activator, biotin, and strong activator, btnOH-AMP, have been determined by x-ray crystallography *(30, 31).* In both structures the repressor is dimeric, with the dimerization interface located at the central domain of each monomer and formed by side-by-side alignment of β-sheets to form an extended β sheet.

Comparison of the structures of apoBirA, and the BirA-biotin and BirA-btnOH-AMP complexes provides clues about conformational changes that may be important for allosteric activation of the BirA monomer. In both dimer structures, 3 of the 4 partially disordered loops in apoBirA are ordered and form part of the dimer interface. One of these three interface loops, referred to as the biotin-binding loop or BBL, is folded over the biotin moiety in both structures. While the dimer interface of the BirA-biotin and the BirA-btnOH-AMP complexes bear these similarities, the energetic difference between a weak and strong activator-induced dimerization, is large (-3 kcal/mol). Further comparison of the two dimers reveals some differences. For example, consistent with its greater stability, the dimer interface in the adenylate-bound species is larger and extends to the C-terminal domain. However, the greatest structural difference is not found at the dimer interface. Rather, it is the ordering of a fourth flexible loop in the adenylate-bound dimer, which remains disordered in the BirA-biotin dimer structure. This loop, consisting of residues 212-234, is distal to the

dimer interface and is folded over the purine ring of the adenylate moiety *(31).* It is therefore referred to as the adenylate binding loop or ABL (Figure 9A).

Details of the ABL structure in the adenylate-bound dimer provide insight into one structural feature that may be pivotal to the allosteric response. Despite the nomenclature, residues in the loop form no direct interactions with the adenylate portion of the corepressor. With the exception of residue E228, the hydrophilic side chains of ABL residues interact with solvent. Hydrogen bonding interactions are observed between E228 and the R182 side chain. One striking structural feature is a hydrophobic cluster formed by side chains of three loop residues, V214, V219, and W223, which is assembled on one face of the adenine ring (Figure 9B). Given that formation of the cluster is linked to binding of the adenylate it is logical to infer that it may be integral to the disorder-to-order transition that accompanies adenylate binding. Moreover, since binding of the weak activator, biotin, is not coupled to this folding process, it is reasonable to hypothesize that the full allosteric response requires the formation of the cluster. In this study detailed thermodynamic analyses were performed to determine the contribution of the cluster to the allosteric activation process in BirA. Single amino acid replacements of residues in the hydrophobic cluster were constructed and resulting purified mutant proteins were analyzed for ligand binding and corepressor-induced dimerization. The mutant proteins were also subjected to structural probing using subtilisin-mediated partial proteolysis. The combined results indicate that disruption of the hydrophobic cluster compromises effector-induced folding of the ABL and that the folding is critical to allosteric response in the biotin repressor.

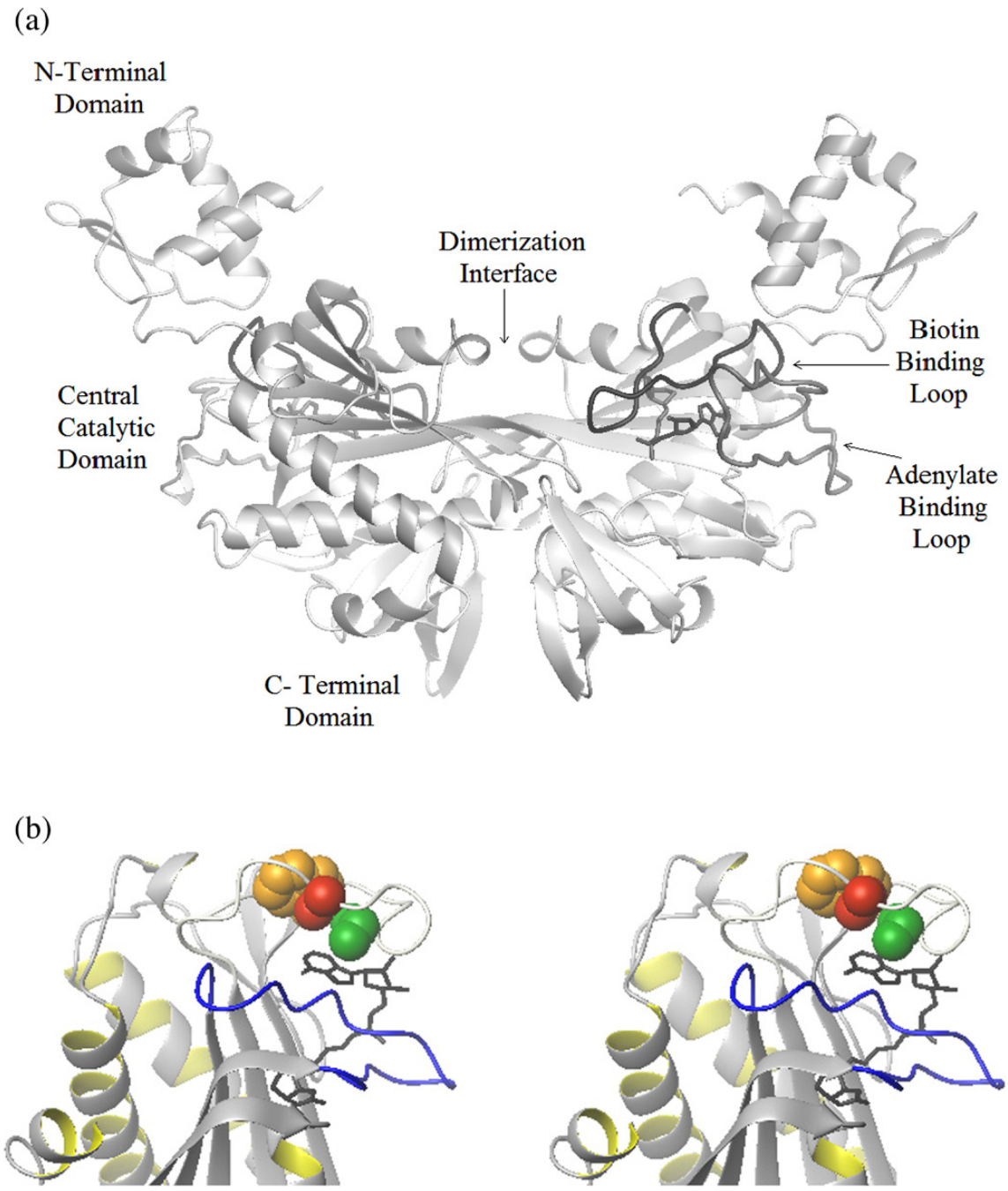

Figure 9. *(legend on next page)*

Figure 9. (A) Structure of the BirA: btnOH-AMP complex. The ligand-bound dimer complex is formed with the dimerization interface located at the central domain of each monomer. The biotin binding loop is located at the dimer interface, while the adenylate binding loop is distal to this interface and folds over the adenylate moiety of btnOH-AMP. (B) Stereo view of the ligand binding site with the hydrophobic cluster highlighted: the biotin binding loop (BBL) is shown in blue and is ordered over the biotin moiety. Represented in grey is the ABL folded over the adenylate moiety. The side chains of the hydrophobic cluster, V214 (green), V219 (red) and W223 (yellow), are shown as space filling models. The figures were generated using MolMol *(28)* with PDB file 2EWN as the input.

B. Results

1. Biotin binding to BirA variants:

Structural data indicate that the biotin binding (BBL) and the adenylate binding (ABL) loops undergo a disorder-to-order transition upon small ligand binding *(31).* Previous studies reveal that mutations in the biotin binding loop can lead to decreased affinity for both biotin and bio-5'-AMP *(32).* Isothermal titration calorimetry was used to investigate the functional effects of mutations in the adenylate binding loop on small ligand binding. Biotin binding measurements were performed to investigate the possible interaction between the BBL and ABL in substrate binding. Titrations with both bio-5'-AMP as well as its analogue btnOH-AMP were also performed. While the structural data available for the latter ligand allows correlation of functional effects with structure, the former ligand is the physiological effector.

Titrations of variant repressors with biotin were performed using the standard direct calorimetric titration method. Since dimerization of the biotin-bound repressor occurs in the millimolar range of concentration, no contribution of coupled dimerization to the measurements need be considered. Calorimetric data were obtained from titrations in which 25-10 μl injections of a 20 μM concentrated biotin stock were injected into a 2 μM protein sample. A typical ITC profile for biotin binding to BirA in standard buffer (10 mM Tris-HCl (pH 7.50 ± 0.02 at 20.0 ± 0.1 ^{o}C), 200 mM KCl, 2.5 mM $MgCl_2$) is shown in Figure 10A. Data of similar quality were obtained from titrations of each variant with biotin. The best-fit curve was

obtained from nonlinear least-squares analysis of the data using a single-site binding model (Origin 7.0). Consistent with previously published data, the equilibrium dissociation constant for the wild type BirA·biotin interaction is 4.2 (± 0.3) x 10^{-8} M *(29).* Moreover, the binding is characterized by a large favorable enthalpy and an opposing unfavorable entropy (Table 2 and Figure 11A). As shown in Figure 11A and Table 2, the biotin binding properties of the ABL variants are similar to those measured for the wild type protein.

2. Bio-5'-AMP and BtnOH-AMP Binding to the ABL Variants

Titrations of BirA variant proteins with adenylate ligands were performed to determine effects of single amino acid replacements of the hydrophobic cluster on adenylate binding. Binding of both the physiological corepressor, bio-5'-AMP, and its analogue, btnOH-AMP, was measured. Previous studies revealed that both bio-5'-AMP and btnOH-AMP bind very tightly to the wild type repressor with equilibrium dissociation constants of 4 (± 2) x 10^{-11} M and 1.5 (± 0.2) x 10^{-9} M, respectively *(104).* These tight interactions necessitated use of the displacement titration method for measurement (Sigurskjold) *(105)* in which the protein is first titrated to saturation with the weaker binding ligand, biotin, followed by its displacement with the ligand that binds more tightly, either bio-5'-AMP of btnOH-AMP. By contrast, the affinities of the ABL variants for the two adenylate ligands are sufficiently weak to allow use of the direct titration method for determining the thermodynamic parameters governing the binding processes. In all cases the protein concentration used for the titration was sufficiently low to avoid any contribution of coupled dimerization to the

binding process. A representative titration is shown in Figure 10B. The data were analyzed using a single site model and the results are shown in Table 2 and Figures 11B (btnOH-AMP) and 11C (bio-5'-AMP). Each ABL variant exhibited adenylate binding properties distinct from those measured for the wild type repressor. All three ABL variants exhibited lower affinities for the adenylate ligands than does the wild type repressor with energetic penalties ($\Delta\Delta G^o$) for btnOH-AMP binding ranging from 0.8 to 1.8 kcal/mole. By contrast, the magnitudes of the $\Delta\Delta G^o$ for bio-5'-AMP are all approximately 3 kcal/mole. Thus, while the defects measured for bio-5'-AMP and btnOH-AMP binding are not identical, they parallel one another. The partitioning of the $\Delta\Delta G^o$ into enthalpic and entropic penalties is distinct for the three variants. For W223A the less favorable free energy associated with binding either ligand reflects only a loss in binding enthalpy. Replacement of Val 214 or Val 219 with alanine resulted in more favorable binding enthalpy for each ligand and a sizable opposing entropy ($-T\Delta S^o$).

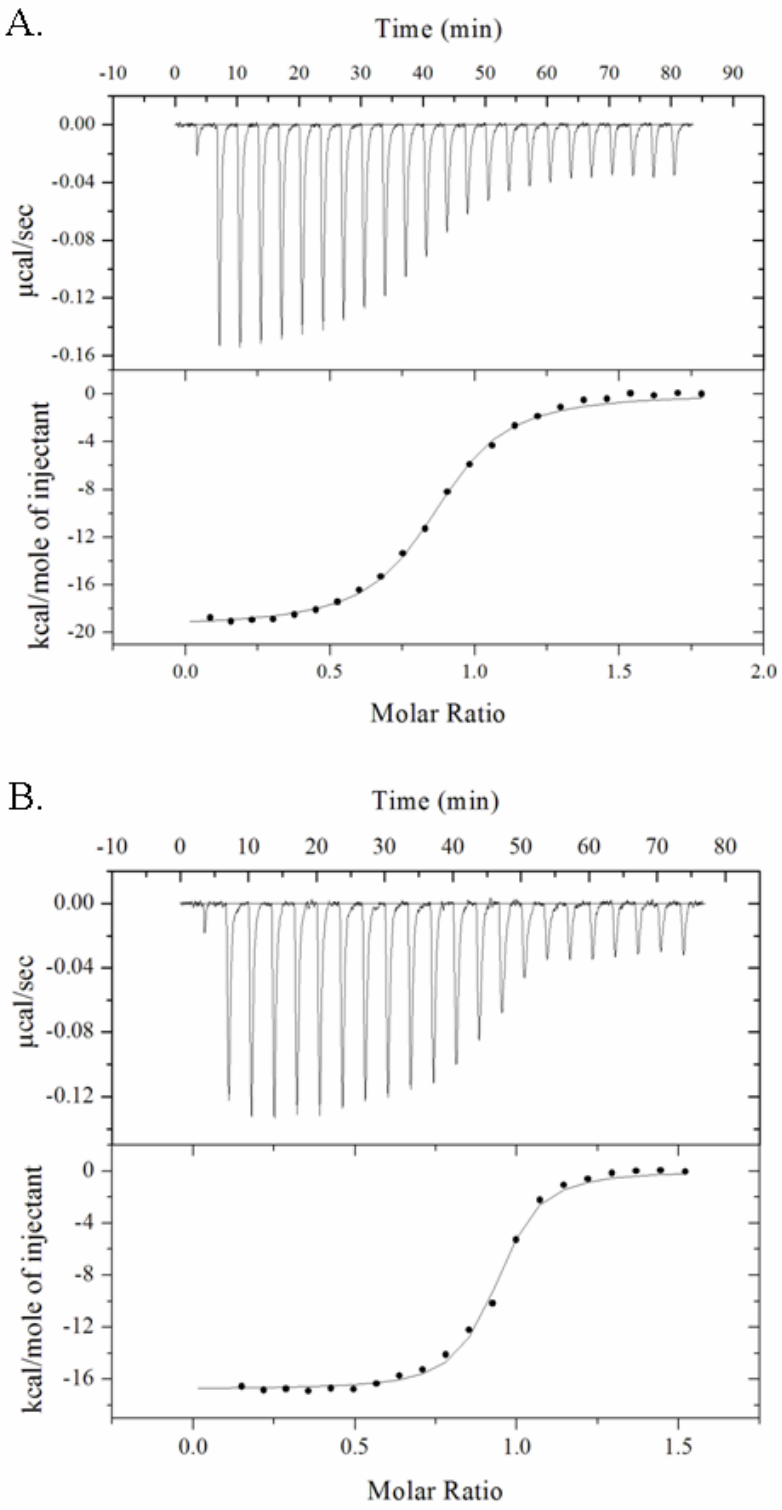

Figure 10. *(legend on next page)*

Figure 10. Calorimetric titrations of BirA.

(A) Direct titration of V214A with biotin. 25-10 µl volumes of 20 µM biotin solution were injected into 2 µM BirA. (B) Direct titration of BirA variant V214A with bio-5'-AMP. 21 10 µL volumes of 20 µM bio-5'-AMP solution is injected into 2 µM BirA variant V214A. These experiments were performed at 20 °C in standard buffer [10 mM Tris-HCl (pH 7.50 ± 0.02 at 20.0 ± 0.1 ˚C), 200 mM KCl, 2.5 mM $MgCl_2$]. The best-fit curves obtained from non-linear least-squares analysis of these data using a single-site binding model (Origin 7.0) are also shown.

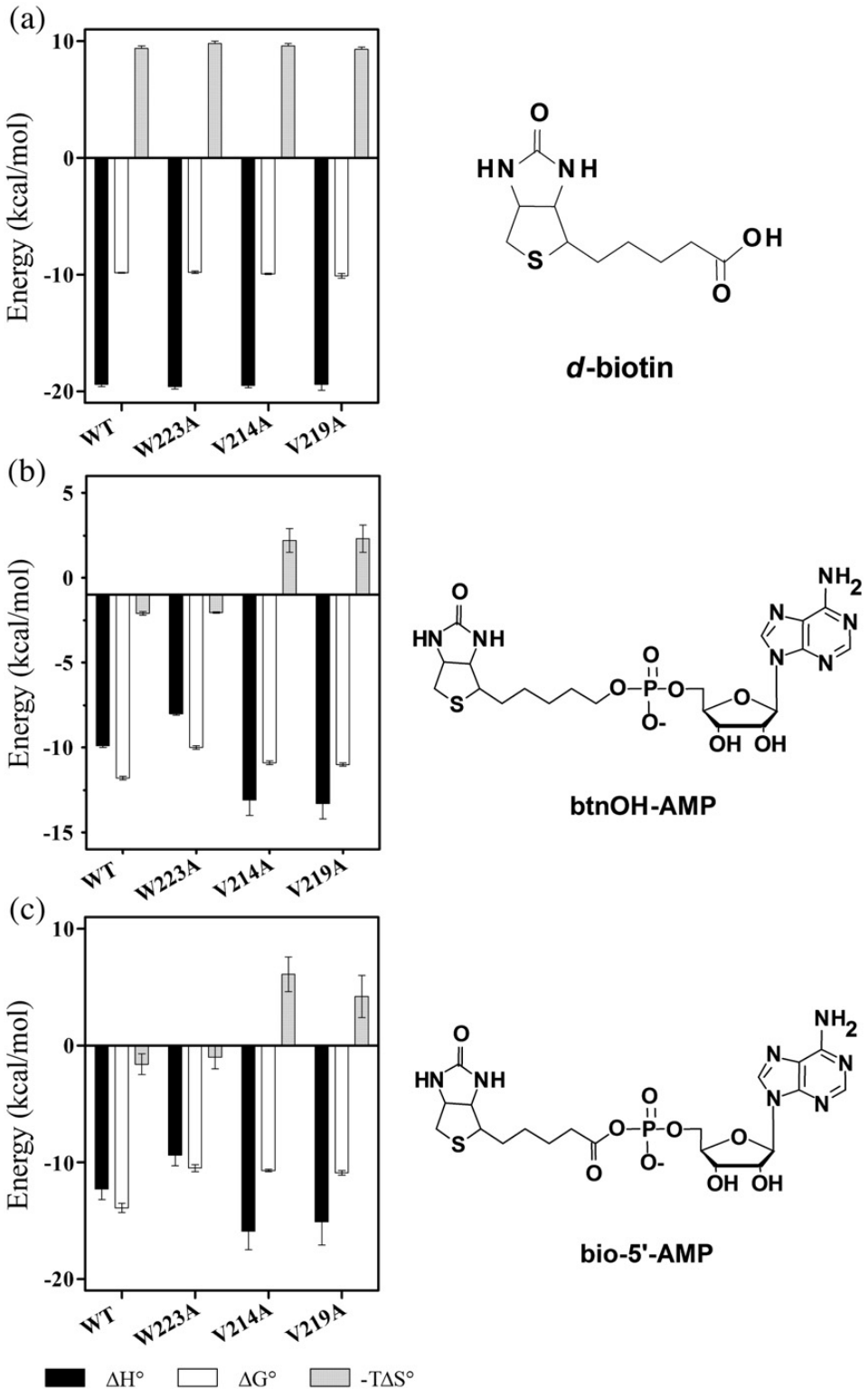

Figure 11. *(legend on next page)*

Figure 11. Thermodynamic profiles for binding of (A) biotin, (B) btnOH-AMP, and (C) bio-5'-AMP to WT-BirA and ABL variants. Each panel *(left)* shows enthalpic, ΔH°, and entropic, $-T\Delta S^{\circ}$, contributions to and Gibbs free energies of, ΔG° binding. Ligand structures are also shown *(right).* Note that the scale is different for btnOH-AMP than for the other two ligands.

Table 2. Thermodynamics of Ligand Binding to the BirA ABL Variants

Ligand	Protein	K_b (M)[a]	ΔG^o (kcal/mol)[b]	ΔH^o (kcal/mol)[a]	$-T\Delta S^o$ (kcal/mol)[b]	n[a]
Biotin	WT	4.3 (± 0.3) x 10^{-8}	-9.84 ± 0.04	-19.4 ± 0.2	9.4 ± 0.2	0.91 ± 0.01
	W223A	4.7 (± 0.4) x 10^{-8}	-9.8 ± 0.1	-19.6 ± 0.2	9.8 ± 0.2	0.83 ± 0.01
	V214A	3.8 (± 0.8) x 10^{-8}	-9.9 ± 0.1	-19.5 ± 0.2	9.6 ± 0.2	0.85 ± 0.01
	V219A	3.8 (± 1.0) x 10^{-8}	-10.0 ± 0.2	-19.4 ± 0.5	9.3 ± 0.2	0.91 ± 0.01
btnOH-AMP	WT	1.5 (± 0.2) x 10^{-9}	-11.8 ± 0.1	-9.9 ± 0.1	-2.1 ± 0.1	0.89 ± 0.01
	W223A	3.8 (± 0.6) x 10^{-8}	-10.0 ± 0.1	-8.0 ± 0.1	-2.05 ± 0.04	0.85 ± 0.01
	V214A	6.9 (± 1.1) x 10^{-9}	-10.9 ± 0.1	-13.1 ± 0.9	2.2 ± 0.7	0.88 ± 0.01
	V219A	5.8 (± 1.0) x 10^{-9}	-11.0 ± 0.1	-13.3 ± 0.9	2.3 ± 0.8	0.82 ± 0.01
bio-5'-AMP	WT	3.9 (± 1.9) x 10^{-11}	-13.9 ± 0.4	-12.3 ± 0.9	-1.6 ± 0.9	0.91 ± 0.01
	W223A	1.4 (± 0.9) x 10^{-8}	-10.5 ± 0.5	-9.4 ± 0.9	-1.0 ± 1.0	0.93 ± 0.01
	V214A	9.7 (± 1.6) x 10^{-9}	-10.7 ± 0.1	-15.9 ± 1.1	6.1 ± 1.5	0.88 ± 0.01
	V219A	6.9 (± 2.0) x 10^{-9}	-10.9 ± 0.2	-15.1 ± 2.0	4.2 ± 1.8	0.90 ± 0.01

All measurements were performed in Standard Buffer (10 mM Tris-HCl pH 7.50 ± 0.02 at 20.0 ± 0.1 ^oC. 200 mM KCl, 2.5 mM $MgCl_2$) as described in the Materials and Methods section. The reported values represent the average of at least two independent titrations with standard deviation. a. Values of K_b, ΔH^o, and n were the best-fit values obtained from nonlinear least squares analysis of the titration data to a simple binding model using Origin. b. The values of the Gibbs free energy, ΔG^o, were calculated using the expression $\Delta G^o = RT\ln K_b$ and those of $-T\Delta S^o$ were calculated using the relationship $\Delta G^o = \Delta H^o - T\Delta S^o$.

3. Heat Capacity Changes Associated with Small Ligand Binding

In order to determine the heat capacity changes associated with small ligand binding to the ABL variants, the temperature dependence of the binding enthalpy was measured. These measurements were accomplished using the Total Association at Partial Saturation (TAPS) technique in which the protein is placed in the sample cell and, following the initial 2 μL control injection, five injections of ligand are made under conditions in which all ligand associates with protein *(106)* (Figure 12). These five injections are followed by a large volume injection that is sufficient to saturate the protein with ligand. Finally, several post saturation injections are made in order to determine the heat of ligand dilution. Since the amount of ligand added in the final injections is identical to that used in the first five, subtraction of the average integrated signal associated with these final injections from the heat associated with each of the first five yields the corrected heat of binding of the ligand to the protein. These measurements were made for binding of wild type and the ABL variant proteins to biotin, biotinol-5'-AMP and bio-5'-AMP at temperatures ranging from 5-20 ^{o}C. Dimerization of holoBirA becomes more favorable with increasing temperature *(107).* Therefore, in order to avoid any contribution of protein-protein interactions to the measured enthalpy, the temperature range at the high end was limited to 20 ^{o}C. The results are shown in Figure 13 along with the best-fit lines obtained from linear regression of the dependence of the measured heat on temperature. The resolved values of the heat capacity associated with the ligand binding processes are shown in Table 3. Consistent, with the results of the full titrations, the heat capacity associated with biotin binding to the mutants is identical

to that measured for the wild type repressor (Figure 13, Table 3). However, differences are observed for the two adenylate ligands. As evidenced by the shallower slopes in the enthalpy versus temperature profiles, the negative heat capacity changes measured for btnOH-AMP binding to the BirA mutants are consistently smaller in magnitude than those measured for the wild type protein (Table 3). The results obtained for bio-5'-AMP are more complex with the enthalpy change associated with the W223A mutant binding exhibiting a nonlinear dependence on temperature (Figure 13). However, as observed with btnOH-AMP, bio-5'-AMP binding to the V214A and V219A mutants is accompanied by a negative heat capacity change that is smaller in magnitude than that measured for the wild type repressor (Figure 13, Table 3).

4. Dimerization of Adenylate-bound Repressor Variant Proteins

Bio-5'-AMP binding promotes binding of BirA to the biotin operator by enhancing repressor dimerization. Results of previous studies indicate that while apoBirA dimerizes weakly in the millimolar concentration range, the BirA-bio-5'-AMP complex exhibits relatively tight dimerization with a K_D in the micromolar range of concentration. Thus the coupling free energy for dimerization associated with bio-5'-AMP binding to apoBirA is –4.0 kcal/mole. As indicated in the Introduction, structures of both the BirA:biotin and BirA:btnOH-AMP complexes are dimeric. However, while biotin is a weak allosteric activator, btnOH-AMP is nearly equivalent to bio-5'-AMP in its ability to drive repressor dimerization. For the wild type repressor dimerization of the btnOH-AMP complex is energetically more favorable than that of the biotin complex by approximately -3 kcal/mole *(29).* Indeed,

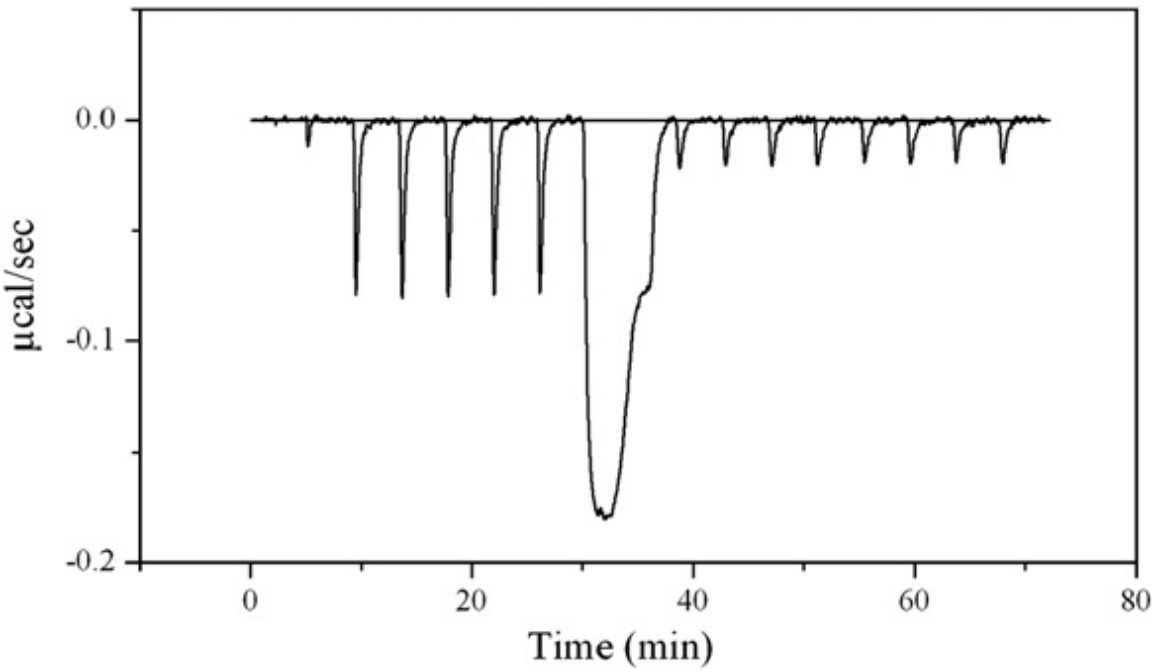

Figure 12. Titrations of BirA V214A with bio-5'-AMP under conditions of total association at partial saturation. The experiment was performed in standard buffer at 15 °C. A 2 µM protein solution was titrated with a 20 µM bio-5-AMP solution. The first 2 µL injection was followed by 5 x 5 µL injections, one 150 µL injection, and finally, 8 x 5 µL injections. The averaged integrated heat of the last eight injections provide the enthalpy of ligand dilution and was subtracted from the integrated heat of injections 2 through 6 to obtain five measures of corrected binding enthalpy of the process in a single experiment.

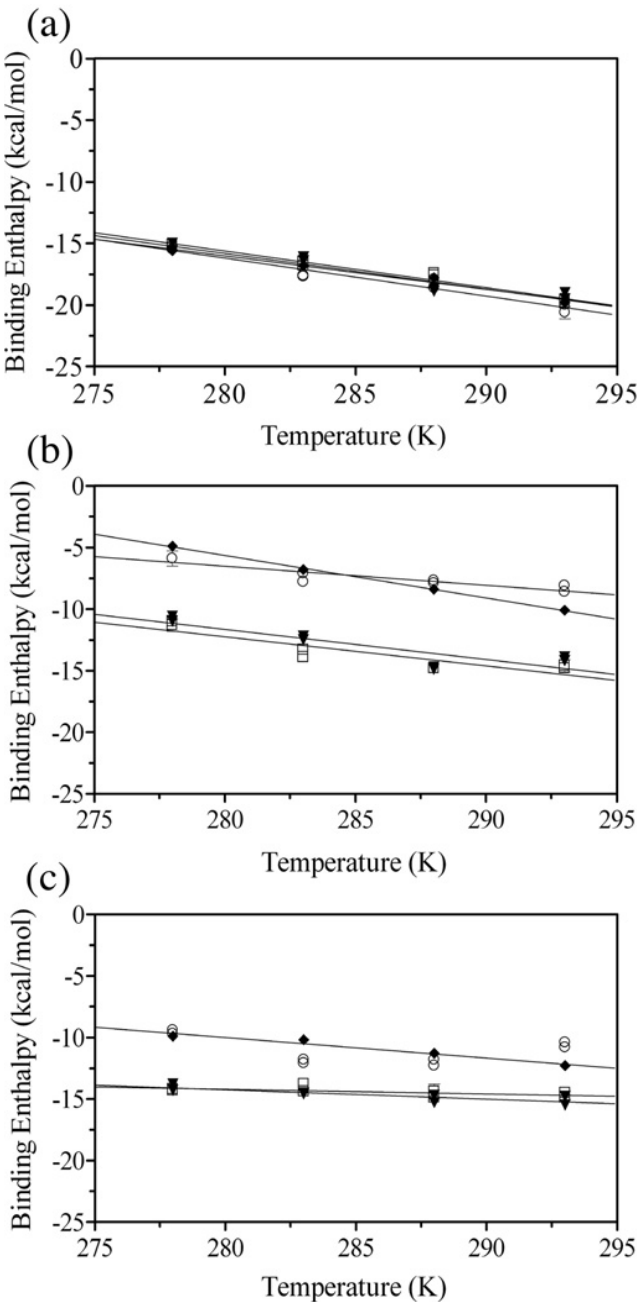

Figure 13. Heat capacity changes for binding of (A) biotin, (B) btnOH-AMP, and (C) bio-5'-AMP to WT-BirA and ABL variants. A plot of the temperature dependence of the binding enthalpy for (▼) WT-BirA, (□) V219A, (♦) V214A and (O) W223A with each ligand. Experiments were performed under conditions of total association at partial saturation as described in Figure 12.

Table 3. Heat Capacity Changes Associated with Ligand Binding to ABL Variants.

Ligand	BirA Variant	ΔC°_{p} (cal-mol/K)
Biotin	Wild Type	-270 (± 30)
	W223A	-310 (± 30)
	V214A	-290 (± 40)
	V219A	-296 (± 23)
btnOH-AMP	Wild Type	-340 (± 8)
	W223A	-150 (± 30)
	V214A	-240 (± 50)
	V219A	-240 (± 50)
bio-5'-AMP	Wild Type	-170 (± 30)
	W223A	N.D[a]
	V214A	-80 (± 20)
	V219A	-40 (± 20)

All measurements were performed using the TAPS method in Standard Buffer adjusted to pH 7.50 ± 0.02 at the working temperature. The reported heat capacity changes were obtained from linear least squares analysis of the temperature-dependence of the binding enthalpy, ΔH^{o}. a. The heat capacity change for this binding reaction was not determined (see text).

the energetic enhancement of dimerization associated with biotin binding is, within error, zero. A major difference between the two structures is the folding of the ABL around the adenylate moiety in the adenylate-bound species. The ITC results presented above indicate that all three ABL variants are defective in adenylate binding. The dimerization properties of each variant bound to btnOH-AMP and bio-5'-AMP were measured by sedimentation equilibrium in order to determine the effects of the mutations on the coupling of small ligand binding to dimerization.

Sedimentation equilibrium measurements were performed at three loading concentrations of each complex and the samples were subjected to centrifugation at three rotor speeds. In all cases the concentrations of both ligand and protein were sufficiently high to ensure saturation of the protein with ligand. Figure 14A shows results of data obtained for the BirA·btnOH-AMP complex. The data were first analyzed using a single species model in order to obtain the average molecular weight of the complex. In all cases single species analysis indicated protein self-association. The data were then subjected to global analysis using a monomer-dimer self-association model to resolve the dimerization constants. The quality of each fit was assessed from the magnitude of the square root of the variance of the fit and the residual plots. The dimerization free energy of the wild-type repressor bound to each of the adenylates is in excellent agreement with previously reported values *(17, 29).* Results obtained with the ABL variants indicate in all cases defects in dimerization relative to the wild type repressor. The resolved equilibrium dissociation constants for dimerization of the btnOH-AMP-bound variants differ from those measured for the

wild type protein by 1.8 to 2.7 fold (Table 4). Defects in dimerization of the bio-5'-AMP-bound variants are greater in magnitude and the equilibrium dissociation constants for dimerization differ from 4.7 to 10.7 fold (Table 4). As shown in Figure 14B, while the magnitude of $\Delta\Delta G_{Dim}$ for the btnOH-AMP-bound variants ranges from 0.4 to 0.6 kcal/mole, it ranges from 0.9 to 1.5 kcal/mole for the bio-5'-AMP-bound species.

5. Probing Structural Consequences of the Mutations by Partial Proteolysis

The BirA·btnOH-AMP structure reveals that the ABL undergoes a disorder-to-order transition concomitant with adenylate binding. A striking feature of the folded ABL is the hydrophobic cluster formed by residues V214, V219, and W223. We have hypothesized that folding of the ABL and the associated formation of this cluster is important for the allosteric response in BirA. Results of ligand binding and dimerization measurements performed on the ABL variants indicate functional defects. These defects in dimerization are consistent with reduced allosteric responses in the variants. Partial proteolysis measurements were performed to determine if these functional defects are correlated with defective ligand-induced folding of the ABL.

Previously, the kinetics of subtilisin-catalyzed proteolysis of WT BirA were measured in the absence and presence of ligands to investigate ligand-linked conformational changes in the adenylate binding loop. Initial subtilisin cleavage occurs between residues 217 and 218 in the ABL and gives rise to two products of 25 and 10 kDa *(108).* The time dependence of the cleavage can be measured by

subjecting the cleavage products to SDS-polyacrylamide gel electrophoresis. The amount of intact BirA present at specific time points after addition of protease is quantitated by densitometry of a Coomassie brilliant blue-stained gel as shown in Figure 15A. The apparent rate of cleavage of the protein is obtained from analysis of the densitometry data using a pseudo first-order kinetic model for the reaction. A graphical representation of the data and analysis are shown in Figure 15B. For the wild type repressor, binding of the weak activator biotin results in a 2-fold decrease in the rate of proteolysis relative to unliganded repressor, while binding of the strong activator bio-5'-AMP results in a 10-fold decrease *(108).* The apparent rates of proteolysis of each repressor ABL variant were measured in the absence of ligand and in the presence of biotin and bio-5'-AMP. The results shown in Table 5 indicate differences in the cleavage rate for each variant in the absence of ligand relative to that measured for the wild-type repressor. More significantly, replacement of residues in the hydrophobic cluster resulted in decreased levels of adenylate-linked protection of the adenylate binding loop from proteolysis.

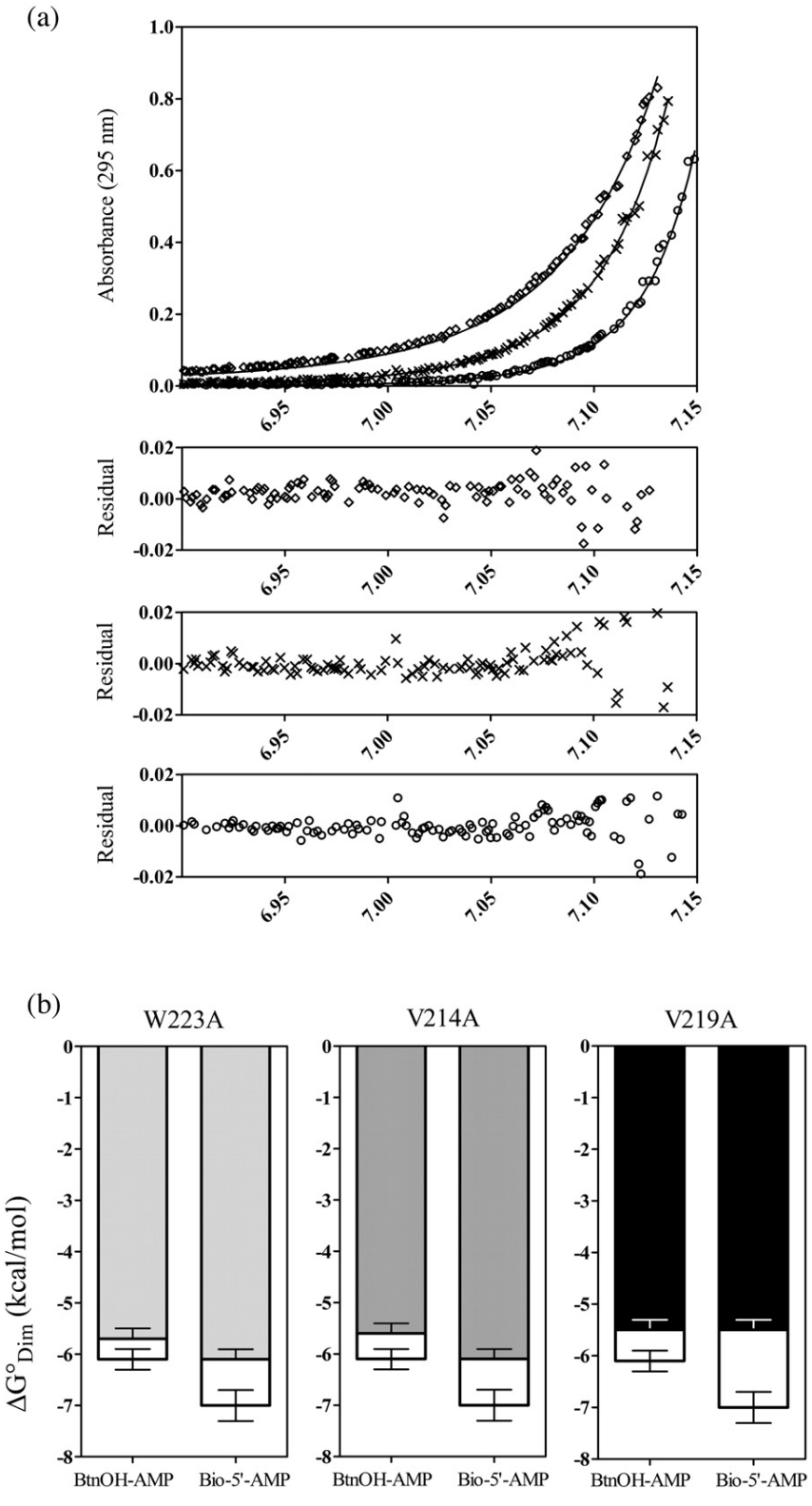

Figure 14. *(legend on next page)*

Figure 14. (A) Absorbance *versus* radial position for 45 μM W223A·btnOH-AMP at 22,000 (◊), 26,000 (x) and 30,000 (o) rpm obtained in standard buffer at 20 ˚C. The best-fit curves were generated from global analysis using a monomer-dimer model of six data sets acquired at multiple loading concentrations and spun at three speeds. The residuals of the fit for each data set shown are provided in the bottom panels. (B) Free energy of dimerization, ΔG°_{Dim}, of each ABL variant complexed with btnOH-AMP or bio-5'-AMP (dark bars) compared to that measured for the wild type repressor (white bars).

Table 4. Dimerization Properties of Complexes of the BirA ABL Variants

Ligand	**BirA Variant**	**K_{dim} (M)**	**ΔG°_{dim} (kcal/mol)**
btnOH-AMP	WT	2.7 (± 0.8) x 10^{-5}	-6.1 ± 0.2
	W223A	5 (± 1) x 10^{-5}	-5.7 ± 0.2
	V214A	6 (± 2) x 10^{-5}	-5.6 ± 0.2
	V219A	8 (± 1) x 10^{-5}	-5.5 ± 0.2
bio-5'-AMP	WT	6 (± 2) x 10^{-6}	-7.0 ± 0.3
	W223A	3 (± 1) x 10^{-5}	-6.1 ± 0.2
	V214A	3 (± 1) x 10^{-5}	-6.1 ± 0.2
	V219A	8 (± 1) x 10^{-5}	-5.5 ± 0.2

All measurements were performed in Standard Buffer (10 mM Tris-HCl pH 7.50 ± 0.02 at 20.0 ± 0.1 ^{o}C. 200 mM KCl, 2.5 mM $MgCl_2$) as described in Materials & Methods. The reported values represent the average of at least two independent measurements performed by subjecting samples prepared at multiple loading concentrations of the relevant complex and centrifuged at multiple rotor speeds. Each resulting data set was subjected to global analysis using a monomer-dimer model.

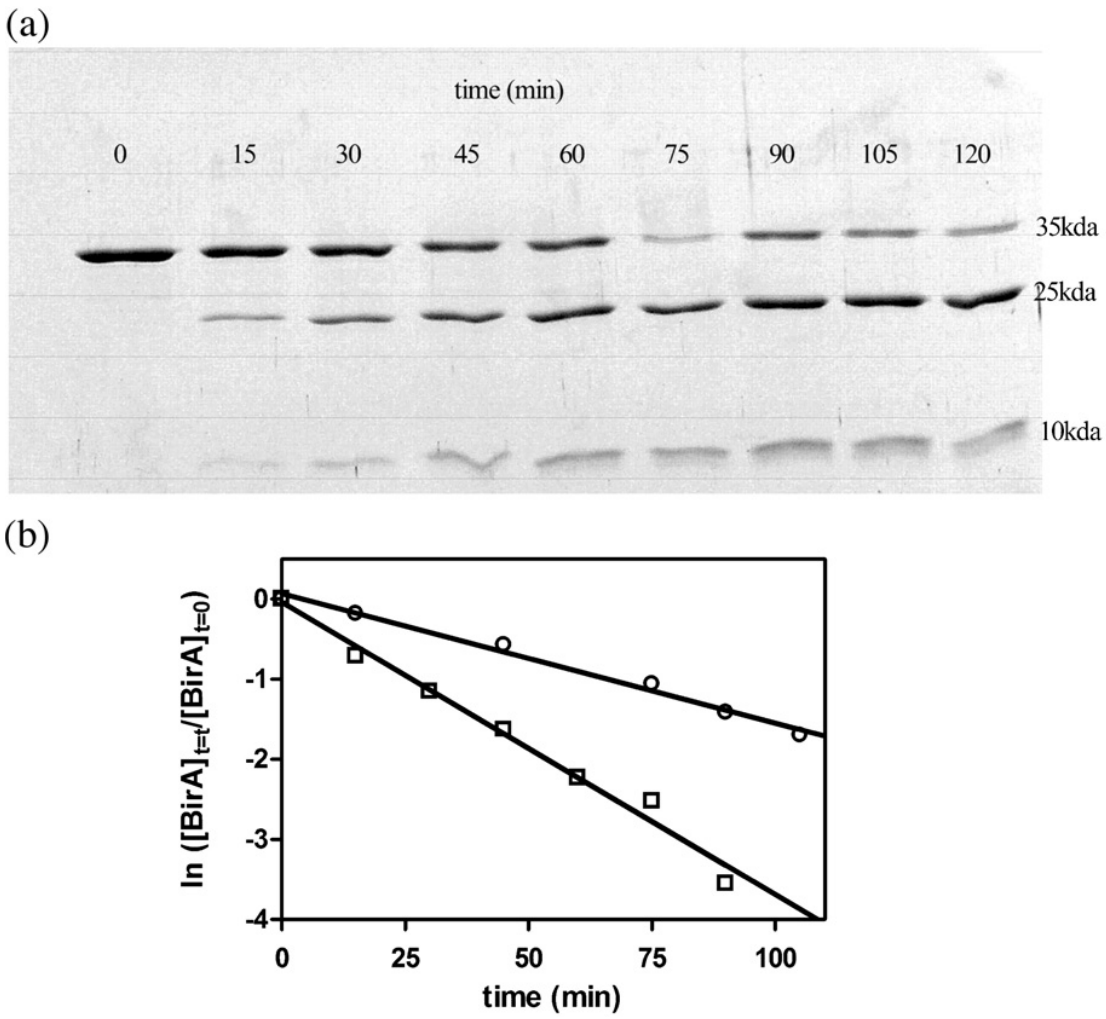

Figure 15. (A) Proteolytic time course of BirA variant V219A complexed with bio-5'-AMP shows decreasing amount of intact protein (35 KDa) as a function of time after addition of the protease subtilisin. (B) Kinetic time course of pseudo-first order cleavage of 2 μM BirA variant V219A (□) and 2 μM BirA variant V219A + 20 μM bio-5'-AMP (O). All measurements were performed in standard buffer at 20 ˚C.

Table 5. Pseudo-first Order Rates of Proteolytic Cleavage of ABL Variant Proteins

BirA variant	**No ligand (apo) (min^{-1})**	**bio-5'-AMP (holo) (min^{-1})**	**k_{apo}/ k_{holo}**
Wild Type	0.026 ± 0.003	0.004 ± 0.001	6.5 ± 0.3
V219A	0.032 ± 0.007	0.013 ± 0.004	2.5 ± 0.4
V214A	0.018 ± 0.006	0.007 ± 0.002	2.6 ± 0.4
W223A	0.041 ± 0.010	0.008 ± 0.001	5.1 ± 0.3

All measurements were performed in Standard Buffer (10 mM Tris-HCl pH 7.50 ± 0.02 at 20.0 ± 0.1 ^{o}C. 200 mM KCl, 2.5 mM $MgCl_2$) as described in Materials & Methods. The reported rates represent the average of at least two independent determinations and the errors represent the 95% confidence intervals.

C. Discussion

In the biotin regulatory system, allosteric activation occurs through ligand-linked dimerization of the biotin repressor, BirA. The repressor binds substrates biotin and ATP to catalyze synthesis of biotinyl-5'-adenylate or bio-5'-AMP *(4).* The adenylate-bound or activated holo-monomer self-associates and the resulting dimer then binds to the biotin operator sequence, bioO, to repress transcription initiation at the biotin biosynthetic operon *(5, 7).* Bio-5'-AMP binding initiates the allosteric signal that is propagated through the BirA monomer to enhance dimerization. Elucidation of the allosteric mechanism in BirA therefore requires determination of the ligand-linked structural and dynamic changes in the monomer that are important for promoting dimerization.

Combined structural and equilibrium thermodynamic data suggest the importance of folding of the adenylate binding loop for the allosteric response. High-resolution structures are available for the apoBirA monomer and two dimers in which the repressor is complexed with biotin or an analogue of bio-5'-AMP, btnOH-AMP *(30, 31).* While enhancement of dimerization energetics upon biotin binding is in effect zero, binding of btnOH-AMP results in an enhancement nearly as large as that associated with physiological corepressor binding *(29).* Comparison of the apoBirA monomer with the two ligand-bound dimer structures reveals that three loops, which are disordered in the unliganded protein, are ordered and participate directly in the intersubunit interface of each ligand-bound structure. However, although the two dimers share this structural similarity, a major difference is localized to the adenylate

binding loop. While in the biotin (weak effector)-bound structure the ABL remains disordered, in the btnOH·AMP (strong effector)-bound structure it is folded. Close inspection of this loop in the BirA-btnOH-AMP structure reveals that it is folded over the adenine ring with side chains of residues V214, V219, and W223 forming a hydrophobic cluster *(31).* While these three residues do not directly interact with the adenylate, formation of the core may be important for allosteric activation. Single amino acid substitutions of hydrophobic cluster residues were made to assess contributions of the core to the functional properties of BirA.

Biotin binding measurements indicate that all ABL variants bind the substrate with thermodynamics identical to those measured for the wild type repressor. Therefore, biotin binding is independent of perturbations in the adenylate binding loop. These results contrast with previous studies of mutations in the biotin binding loop, which result in defects in both biotin and adenylate binding. The structure of the biotin-bound dimer indicates that while the BBL is folded over the biotin molecule, the ABL is not folded. However, in the adenylate-bound dimer both loops are folded with the ABL arranged around the adenylate moiety. These structural results support the known catalytic mechanism of BirA in which an ordered mechanism operates with biotin binding first followed by ATP. Biotin binding to apo-BirA induces folding of the BBL, which creates the ATP binding site. In the absence of biotin no ATP binding site exists. Taken together these data explain the insensitivity of biotin binding to mutations in the adenylate binding loop.

Since the ABL is ordered around the adenylate moiety in the BirA:btnOH-AMP structure the consequences for adenylate binding of altering loop residues were investigated. Measurements of both bio-5'-AMP and btnOH-AMP binding were performed because, while the former is the physiological effector, structural data are available for BirA bound to the latter. Binding measurements for all ABL variants indicate the importance of the hydrophobic core residues for adenylate binding. Results indicate that both adenylate ligands bind to each variant with affinities significantly lower than they do to the wild type repressor. The energetic penalties ($\Delta\Delta G^o$) for binding btnOH-AMP ranged from +1.5 to +2 kcal/mole and those associated with bio-5'-AMP ranged from +1 to +3 kcal/mole. In addition, partitioning of the energetic penalty between enthalpy ($\Delta\Delta H^o$) and entropy ($T\Delta\Delta S^o$) differed for the mutants. While for the W223A it was centered in the binding enthalpy, for the V214A and V219A variants the energetic penalty was solely in the entropic component of binding. Finally, the effects on binding were consistently larger for the physiological effector than for the analogue. This suggests that while the analogue is a reasonable mimic of bio-5'-AMP, there are differences in the structural details of the repressor's interaction with the two ligands. In conclusion, the adenylate binding results indicate that integrity of the cluster is required for tight binding of BirA to bio-5'-AMP.

Results of sedimentation equilibrium measurements indicate that mutations in the hydrophobic cluster result in defective dimerization. In their adenylate-bound complexes the three variants exhibit less favorable dimerization energetics as

compared to the wild type repressor. The defects in dimerization can be considered in terms of the effects of the mutations on the coupling free energy associated with adenylate binding. This coupling free energy, ΔG_C, is defined as the "extra" favorable Gibbs free energy of dimerization that results from binding of the adenylate to apoBirA. As indicated previously, the magnitudes of ΔG_C for bio-5'-AMP and btnOH-AMP binding to wild type BirA are -4 and -3 kcal/mole, respectively. Assuming that dimerization of the apo-form of each ABL variant is identical to that measured for wild type BirA, the coupling free energy can be calculated for each variant. The assumption is justified by the fact that no residues that are directly involved in the monomer-monomer interface are perturbed in any of the ABL variants. Results of the calculation, which are shown in Figure 16, indicate losses in coupling free energy of +0.3 to +0.6 kcal/mole for the analogue and +0.8 to +1.4 kcal/mole for the physiological effector, bio-5'-AMP. Thus, although mutations in the hydrophobic cluster do not directly alter the dimerization interface, disruption of the cluster distal to this interface perturbs the allosteric response associated with adenylate binding.

Measurements of the heat capacity changes associated with ligand binding and the kinetics of subtilisin-mediated proteolysis are consistent with the conclusion that mutations in the hydrophobic cluster compromise ligand-linked folding of the ABL. The negative heat capacity changes associated with btnOH-AMP binding to all three mutants and bio-5'-AMP binding to V214A and V219A are smaller in magnitude than those measured for binding of wild type repressor to the two ligands *(109-111).*

These results are consistent with the burial of less hydrophobic surface area in binding of the mutants to the two ligands. Bio-5-AMP binding to the W223A mutant exhibits a nonlinear dependence of binding enthalpy on temperature. Although this phenomenology has been observed in other systems, the explanation for the observation in this instance is beyond the scope of this work *(112-115).* Partial proteolysis with subtilisin provides a low-resolution measure of the ligand-induced folding of the ABL with bio-5'-AMP binding to wild type BirA resulting in a 6.5-fold decrease in the pseudo-first order cleavage rate. By contrast, the bio-5'-AMP-linked decreases in proteolysis rates measured for the ABL variants ranged from 2.5 to 5.1 fold. This reduced level of protection observed when the hydrophobic core is altered is consistent with disruption of ligand-linked folding. These results combined with ITC measurements of ligand binding and the dimerization measurements support the conclusion that formation of the hydrophobic cluster is integral to adenylate-induced folding of the ABL and that this folding is critical for the allosteric response in BirA.

While formation of the ABL hydrophobic cluster is clearly important for the allosteric response it is likely that additional structural and dynamic changes in BirA are integral to allosteric activation. Although residues 212-223 undergo the disorder-to-order transition upon adenylate binding, ABL residues other than the hydrophobic cluster do not appear to function in the allosteric response. Site-directed mutagenesis has been employed to change residues R213, E216, E228 to alanine and none of the purified proteins are altered in ligand-linked dimerization (S. Naganathan, unpublished observations). In addition, examination of the structure of the btnOH-

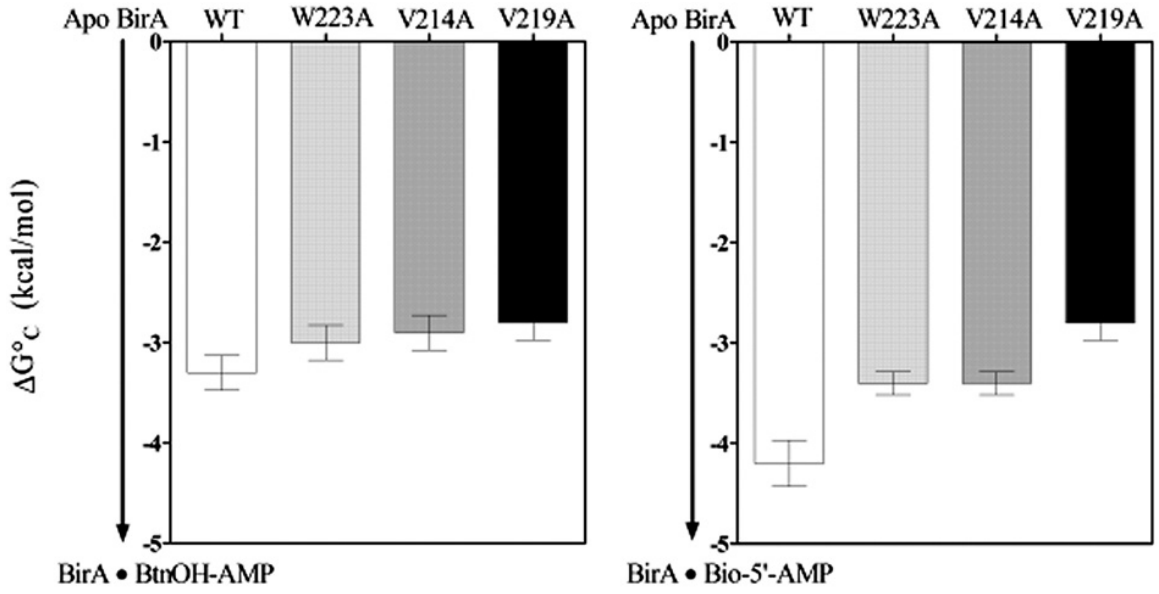

Figure 16. Coupling free energies, ΔG^{o}_{C}, for linkage of btnOH-AMP or bio-5'-AMP binding to WT BirA and each ABL variant were calculated from the difference between the free energy of apoBirA self-association and the free energy of dimerization of the ligand bound species measured for each of the proteins in the work. In this calculation the ΔG^{o}_{Dim} for all apo-species are assumed to be identical.

AMP-bound repressor reveals that the majority of the charged or polar side chains of ABL residues are projected toward solvent. Comparison of the biotin-bound and btnOH-AMP-bound dimers reveals several structural differences outside of the ABL that may be coupled to adenylate-linked folding of the loop, and thus the allosteric response. For example, in the adenylate-bound structure the dimer interface is larger and extends to the C-terminal domains of the two subunits. Comparison of the structures of the biotin-bound and adenylate-bound monomers indicates a difference in the relative orientations of the C-terminal and central domains, a difference that may be linked to adenylate-induced folding of the ABL. Additionally, in the btnOH-AMP-bound repressor monomer the N-terminal DNA binding domain is rotated closer to the central catalytic domain than it is in the biotin-bound protein. This difference may also be linked to ABL folding. Currently hydrogen-deuterium exchange coupled to mass spectrometric analysis is being employed to further investigate these corepressor-linked structural changes in the repressor monomer.

Comparison of biotin protein ligases (BPLs) from different species highlights the importance of the adenylate binding loop for bio-5'-AMP-linked dimerization associated with the transcription repression function. Biotin protein ligases all catalyze the same reaction and their sequences are highly conserved across evolution. However, sequence comparison of bacterial BPLs, including those from eubacteria and archaebacteria, reveals that only a subset are both enzymes and transcriptional repressors *(116).* For example, *Pyrococcus horikoshii* encodes a monofunctional

ligase, which does not contain an N-terminal DNA binding domain and therefore does not bind to DNA. High-resolution structures of this ligase reveal significant structural homology between it and the C-terminal and central domains of BirA *(117).* Nonetheless, two striking differences are observed. First, although the *Ph*BPL is dimeric, the interface is formed by completely different segments of the protein than those utilized by BirA for dimerization. Second, and more relevant to this study, the adenylate binding loop is significantly truncated in the *Ph*BPL relative to *Ec*BirA. Highly divergent bacteria encode bifunctional ligases, and the bifunctionality is, thus, considered an ancient feature. As such, organisms such as *Pyrococcus horikoshii* are thought to have lost the DNA binding function. The lack of the adenylate binding loop suggests that it too is dispensable because it is not required for the ligand-linked dimerization associated with repression of transcription initiation.

The role of protein dynamics in transmitting allosteric signals in proteins is well documented. One view focuses on the coupling of changes in flexibility, as determined primarily by NMR dynamics measurements, to the allosteric mechanism *(118).* For example in the transcription factor Catabolite Repressor Protein changes in dynamics, both picosecond-nanosecond and microsecond-millisecond, are correlated with the negative cooperativity associated with cAMP binding to the protein *(119).* Another view of Freire and colleagues is that low stability regions of a protein play a central role in allosteric responses. In the biotin repressor ligand-induced folding of such a low stability region appears to nucleate the allosteric response. The mechanism

by which this initial response percolates through the remainder of the protein remains to be determined.

III. A Model for the Biotin Repressor: Biotin Operator Complex Investigating the role of flexible loops in the structural mechanism of the protein:DNA interaction.

A. Introduction

Allosteric control operates in a variety of cellular processes including transcription regulation. In order to maintain cell homeostasis and viability one way that organisms respond to changes in metabolite levels is by controlling the level of transcription initiation of specific genes by allosterically regulated transcription factors. Allosteric regulation of transcription factors involves binding of an allosteric effector, with an accompanying change in conformation to influence the affinity of the transcription factor for a specific site on DNA. This chapter discusses the structural model of the complex formed between the transcription factor, BirA and its target DNA site, bioO constructed by Dr. Z.A.Wood[†]. It specifically addresses the structural mechanism by which an allosteric effector of a site-specific DNA binding protein alters its affinity for DNA.

Transcription initiation is regulated by the action of two classes of transcription factors, activators and repressors. While, activators enhance transcription initiation, repressors inhibit this process. An activator binds at a promoter that is near or overlapping an operator sequence. This leads to stabilization of the polymerase-DNA interaction and/or promotes conversion of the transcription initiation complex from the closed to open complex required for transcription

initiation. By contrast, repressors bind to operator sequences and partially block the polymerase binding site, preventing transcription initiation (Figure 17). Transcription factors typically have an effector binding domain and a DNA binding domain. The effector binding domain often also participates in oligomerization. The DNA binding domain of the transcription factor contains the DNA-recognition elements required for specific protein:DNA binding. Characteristic DNA binding motifs include leucine zippers, zinc fingers and helix-turn-helix motifs. The helix-turn-helix (HTH) DNA binding motif is most common *(120, 121).* It consists of two α helices packed against each other and linked by a four-residue turn or loop. One of these two helices is the recognition helix that binds in the major groove of DNA providing specificity at a transcription control sequence. The HTH motif typically consists of additional helices that stack against the first two to provide stability. Some HTH motifs are linked to a wing (w-HTH), that is formed by a two-stranded β sheet and a turn that extends to the minor groove to increase protein:DNA contacts (Figure 18). Transcription factors function in DNA binding as monomers *(122)* or oligomers *(15).* Many function as homodimers that bind to palindromic DNA sites *(120).* Oligomerization provides multiple DNA-recognition elements in the protein to form a more stable protein: DNA interaction.

There are several mechanisms by which the functional properties of a transcription factor are allosterically controlled by effector binding to influence the protein's affinity for site specific DNA binding. For the purpose of simplicity, the discussion here focuses only on the repressor class of transcription factors. Allosteric

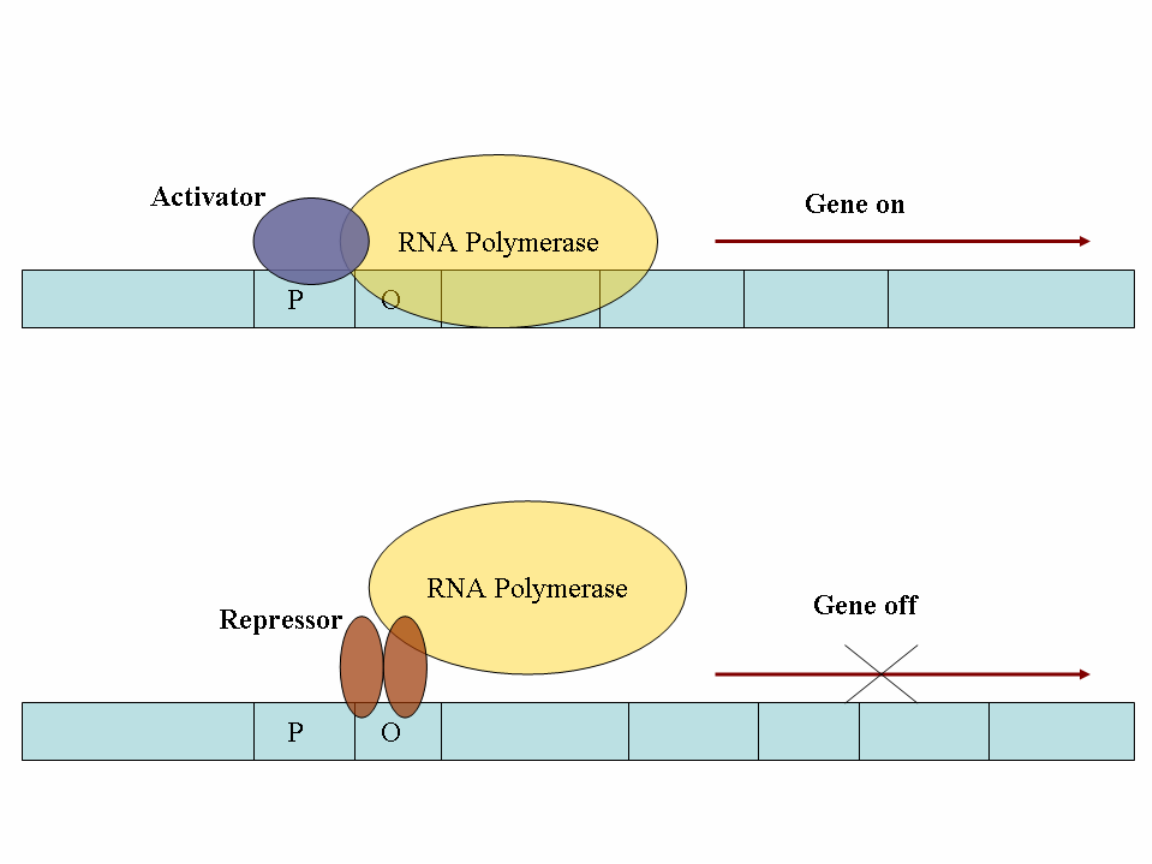

Figure 17. Regulation of Transcription Initiation

Activators bind at the promoter to enhance transcription initiation by stabilizing the RNA Polymerase-DNA interaction (top). Repressors bind the operator sequence partially blocking the binding site for RNA polymerase, hence preventing transcription initiation (bottom).

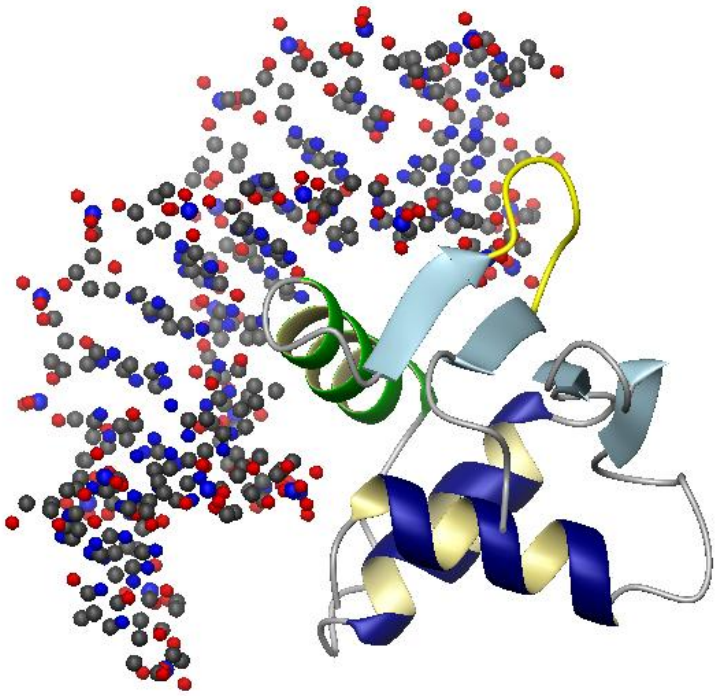

Figure 18. The winged Helix-Turn-Helix motif.

A model of the three dimensional structure of the w-HTH of the transcription factor, elk-1 complexed with DNA determined by X-ray crystallography *(123).* The recognition helix (green) contacts the major groove of the DNA and the wing (yellow) extends into the minor groove of the DNA. This model was generated using MolMol *(28)* with Protein Data Bank file 1DUX as input.

effectors that bind repressors are classified as inducers and corepressors. While inducer binding to a repressor destabilizes its interaction with DNA, corepressor binding increases the affinity of a repressor for DNA. Based on the influence of effector binding on their mechanistic properties, allosteric transcription repressors can be classified into two categories. In repressors that exist as preformed oligomers, effector binding alters the affinity for DNA by altering the conformation of the DNA recognition elements in the repressor. Some examples of this class are lactose repressor (LacR), tryptophan repressor (TrpR), purine repressor (PurR) and nickel repressor (NikR). In another class of transcriptional repressors, effector binding affects the self-assembly properties of the repressor, and the change in oligomeric state alters the affinity for DNA. The diphtheria toxin repressor (DtxR), luecine responsive element (LrpA) and the biotin repressor (BirA) belong to this class of repressors.

Allosteric effector binding elicits a change in stability of a protein:DNA complex by structurally altering the surface of the protein that interacts with DNA. In some proteins the effector binding domain is distal to the protein:DNA interface. In these cases the response accompanying effector binding takes place from a distance to affect the stability of the protein:DNA complex. Most often this effect is achieved by altering the conformation of the DNA-recognition elements of the DNA binding motifs to influence site-specific DNA binding. In other proteins, binding of the allosteric effector creates a new structural unit composed of the effector and effector binding domain that directly participates in the protein:DNA interface. As a

consequence, the interface extends beyond the characteristic DNA binding motifs, hence increasing the stability of the protein:DNA complex. An example of the former mechanism of effector action is the lactose repressor, LacR, which functions in DNA binding as a homotetramer. It is formed as a dimer of dimers, in which each dimer binds to an operator site. Structural and biochemical data indicate that effector, allolactose, binding to the LacR core domain that is distant from the DNA binding domain, results in a small hinge movement in the NH_2 subdomain of the core domain *(124)*. This displaces the hinge helices of the N-terminal domain, thereby destabilizing the repressor-DNA interaction (Figure 19). By contrast, in the tryptophan repressor, TrpR, the binding site for tryptophan is located at the repressor:operator interface in the absence and presence of effector (Figure 20) *(66).* Binding of the effector, tryptophan, serves as a switch between non-specific to specific protein:DNA recognition. Based on structural and biochemical analyses, different mechanisms have been proposed for the TrpR system *(62, 125, 126).* One model suggests that binding of L-Trp to the protein dimer acts like a wedge between the core domain and the DNA binding domain. Another proposes that tryptophan binding induces folding of portions of the helix-turn-helix domain of TrpR. In both models tryptophan directly participates in the protein:DNA interface and its binding results in positioning the recognition helix of each monomer in the proper geometry for tight operator binding. The nickel repressor, NikR, is another example in which effector binding creates a new structural unit composed of the effector and effector binding domains that interacts with DNA. NikR is a homotetramer to which binding of one nickel ion per subunit activates NikR:operator binding *(67, 69).* The crystal

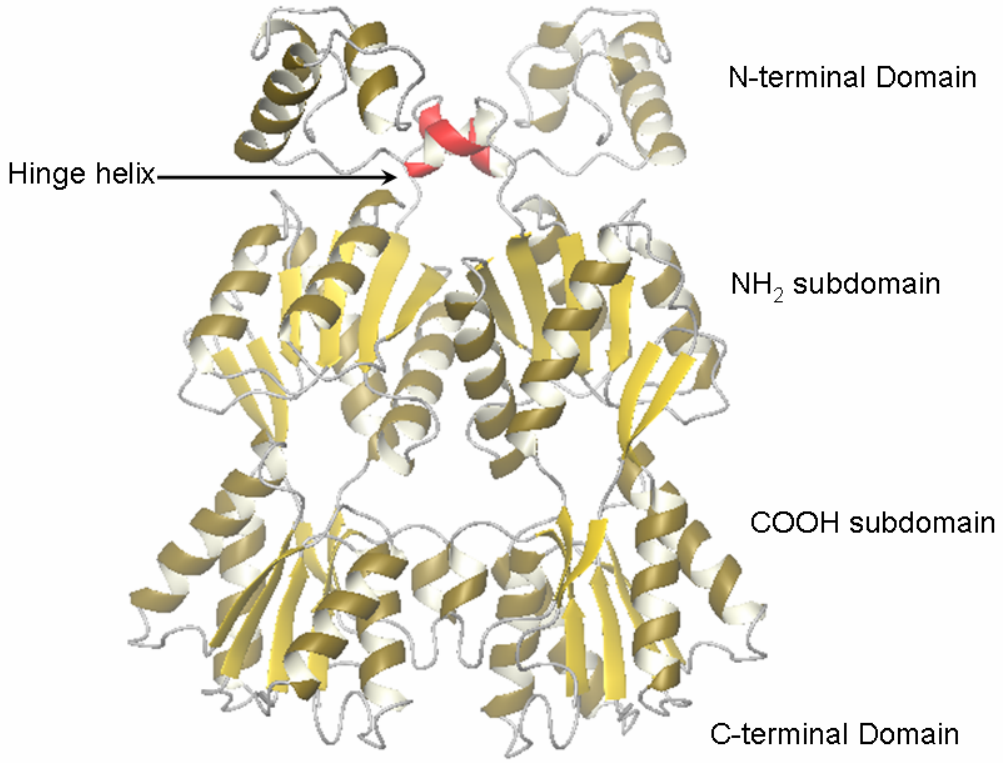

Figure 19. A model of the three dimensional structure of the LacR dimer determined by X-ray crystallography *(127).* The hinge helix (red) in each monomer, undergoes movement to destabilize the protein:DNA interaction formed *via* the N-Terminal Domains. This model was generated using MolMol *(28)* with the Protein Data Bank file 1JWL as input.

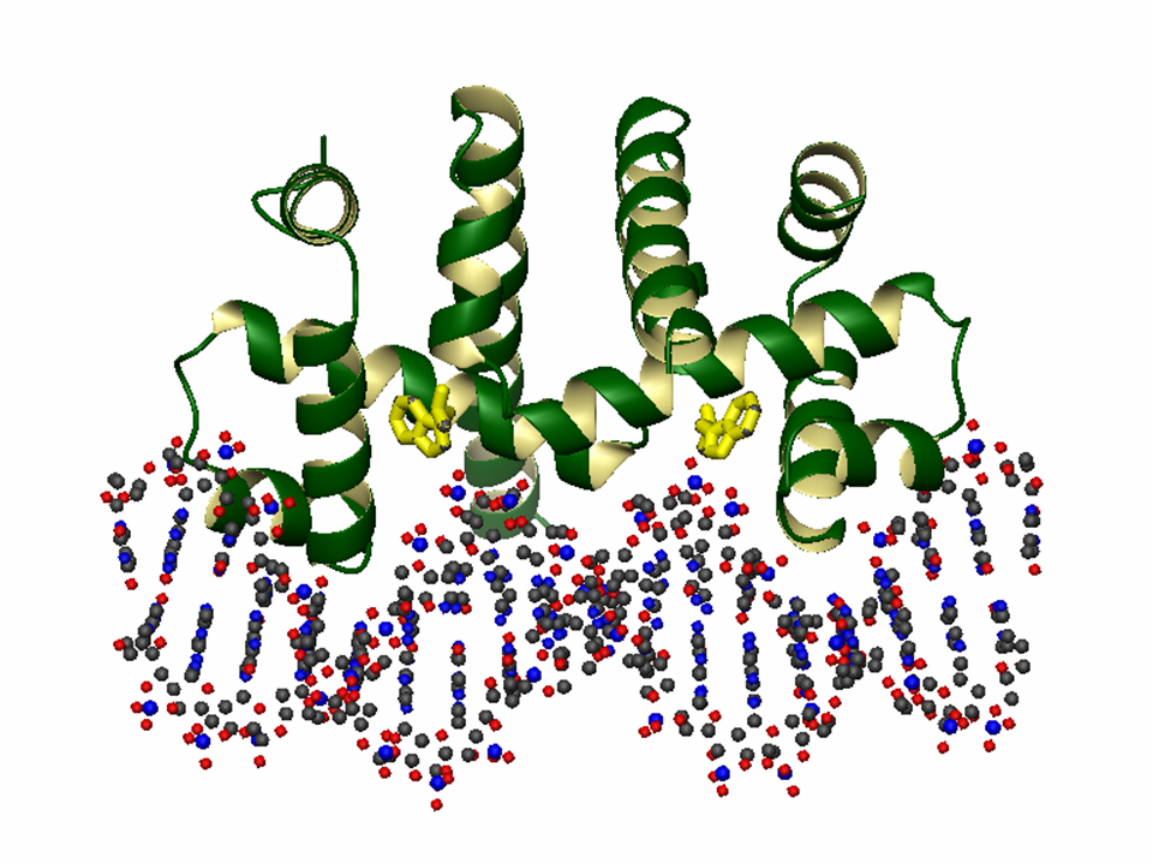

Figure 20. A model of the three dimensional structure of the holoTrpR homodimer:Operator complex determined by X-ray crystallography *(127)*. The recognition helix of the HTH domain contacts the major groove of DNA. L-trp (yellow) is located at the protein:DNA interface. This model was generated using MolMol *(28)* with the Protein Data Bank file 1TRO as input.

structure of the NikR-operator complex indicates specific and non-specific contacts. The ribbon-helix-helix (RHH) domain and repressor:operator interface as shown in Figure 21. These three systems illustrate that at a structural level the stability of the protein:DNA complex is affected by binding an allosteric effector that alters the features of the interface formed between the protein and DNA. This occurs through two general mechanisms: one involves action at a distance and the second involves a direct role for the effector and the effector binding domain in the protein:DNA interface.

The biotin repressor, BirA, is an allosteric transcription factor that binds at the biotin operon to control biotin biosynthesis *(3).* The apoBirA monomer binds biotin and ATP to synthesize its physiological corepressor, bio-5'-AMP *(4).* Corepressor binding induces dimerization of holoBirA (BirA:bio-5'-AMP) and facilitates its DNA binding. As revealed by the x-ray crystallographically determined structure of apoBirA, the protein is organized into three domains: a C-terminal domain, a central catalytic domain containing the effector binding site and four partially disordered loops, and an N-terminal DNA binding domain composed of a winged helix-turn-helix motif *(18).* Thermodynamic analyses and comparison of the structures of apoBirA, the biotin-bound and adenylate-bound dimers, has enabled an understanding of this mechanism of allosteric activation in BirA *(18, 27, 29-31).* Figure 22 provides a schematic representation of the mechanism. Allosteric effector binding induces BirA dimerization. Three of the four partially disordered loops in the apoBirA structure are ordered in the biotin-bound dimer structure and participate in the

dimerization interface. One of these loops is the biotin binding loop (BBL; residues 110-128), which folds over the biotin moiety. Adenylate binding induces folding of the fourth loop, the adenylate binding loop (ABL; residues 212-234). This disorder-to-order transition that occurs concomitant with adenylate binding nucleates the allosteric response in BirA *(128).*

The BirA homodimer binds to a 40 base-pair, inverted palindromic sequence of the biotin operator (bioO) to repress transcription initiation at the two divergent overlapping promoters, Pa and Pb of the biotin operon *(6).* As revealed by solution studies, the N-terminal DNA binding domain of each monomer of the dimer interacts with the two 12 base-pair termini of the 40 base-pair biotin operator sequence. Comparison of the biotin-bound and adenylate- bound dimer structures reveals as much as a 19º rotation of the N-terminal DNA binding domain relative to the central domain, thereby creating a change in orientation of the winged helix-turn-helix motif. This may facilitate a specific and stable protein:DNA interaction.

Extensive biochemical studies have been performed to identify regions on BirA and bioO that participate in formation of the repression complex *(35, 129).* Hydroxyl radical footprinting performed on the ligand-bound repressor dimer in the presence and absence of bioO revealed decreased reactivity/increased protection to/from hydroxyl radical cleavage of the protein backbone when complexed with DNA. Increased protection is observed in all domains of the protein structure, with the most pronounced effects in the N-terminal DNA binding domains and segments

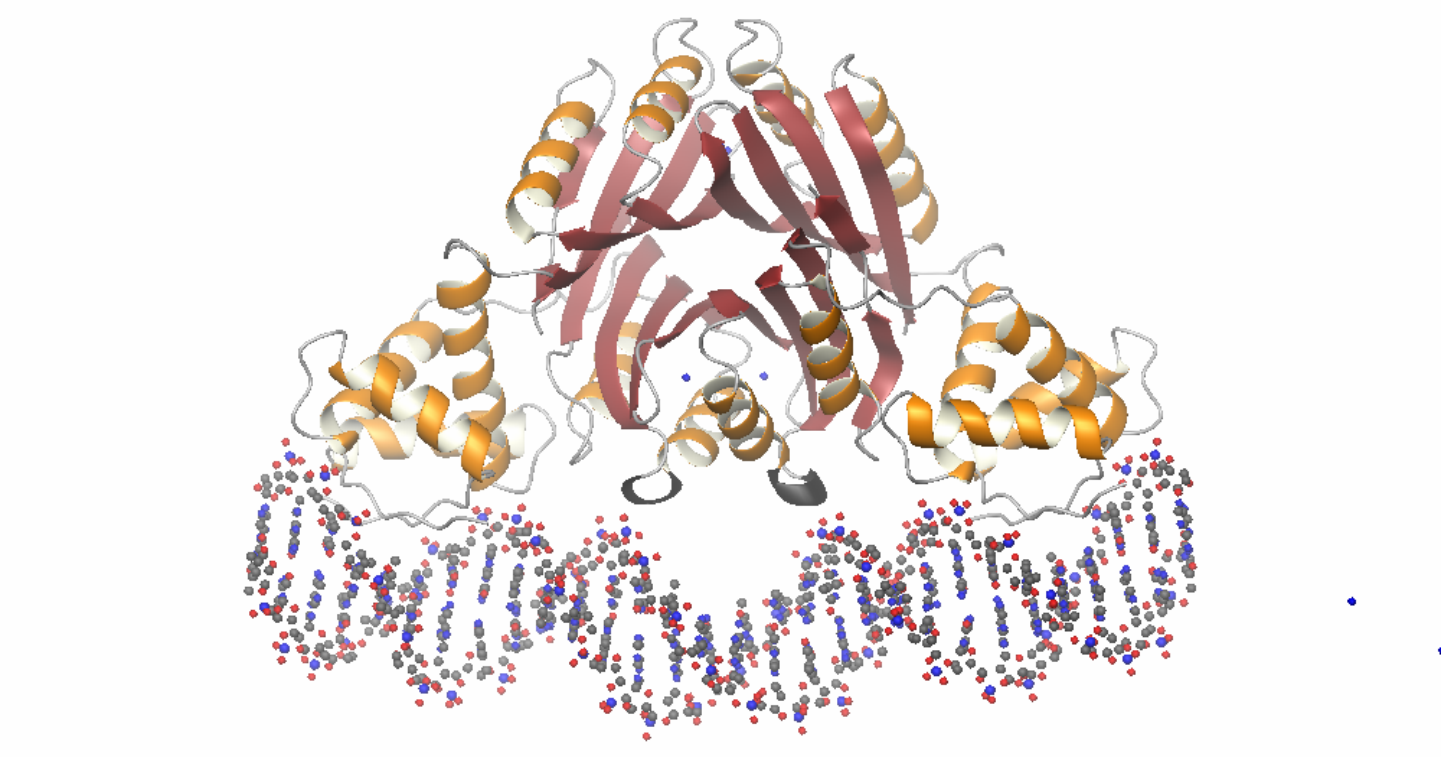

Figure 21. A model of the three dimensional structure of the NikR-operator complex determined by X-ray crystallography *(72).* The bound nickel ions are shown in blue. The Metal Binding Domain (MBD) Loops are indicated in black and point toward the phosphate backbone of the DNA. This model was generated using MolMol *(28)* with the Protein Data Bank file 2HZV as input.

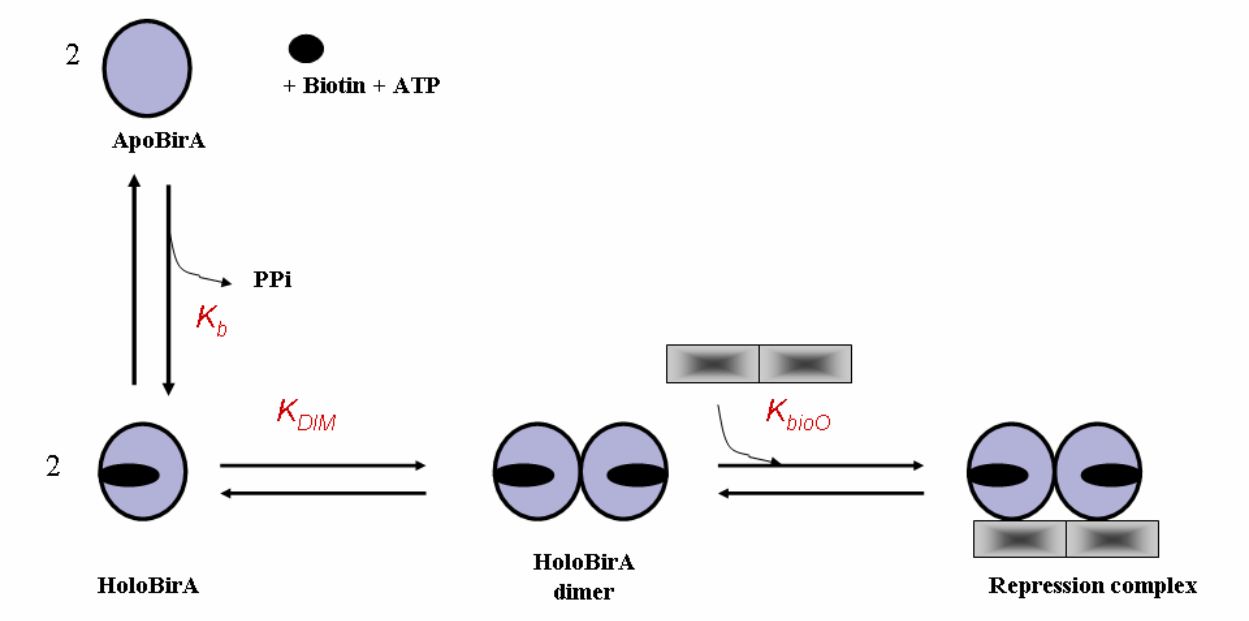

Figure 22. Allosteric Activation of the Biotin Repressor

Ligand binding is positively coupled to repressor dimerization. The thermodynamically stable dimer subsequently binds site-specifically to the biotin operator sequence, bioO. ApoBirA refers to the unliganded protein and holoBirA is the bio-5'-AMP-bound species. K_b, K_{dim}, and K_{bioO} refer to the equilibrium constants governing ligand binding, holoBirA dimerization, and holoBirA dimer binding to bioO, respectively.

of the central domain. The recognition helix and wing of the w-HTH motif of the N-terminal domain of BirA are protected, consistent with their binding in the major and minor grooves of bioO, respectively. Regions of the central domain that are protected include residues 65-170 and 187-221. These correspond to portions of the amino-terminal segment of the central domain, two β-strands, loop 194-199 involved in the dimer interface and the two effector binding loops, BBL and ABL. A similar approach was employed to probe the surface of bioO that participates in the protein:DNA interaction *(129).* This involved the use of chemical and biochemical tools that can detect the accessibility of the backbone and nucleotide bases of the DNA in the presence and absence of the holoBirA dimer. These probes include hydroxyl radical footprinting, dimethyl sulfate (DMS) protection and DNase I sensitivity and their combined results are shown in Figure 23A. The DNase I cleavage data indicate increased sensitivity in the central region of the 40 base-pair sequence and two specific positions of hypersensitivity at positions -10 and +10, at the termini of the inverted palindromic sequence, when bound by the repressor dimer. Hydroxyl radical footprinting allowed comparison of free bioO and holoBirA dimer bound bioO and revealed four regions of protection from hydroxyl radical cleavage upon dimer binding. The dimethyl sulfate protection data provide very specific detail regarding repressor contacts with the biotin operator. DMS reacts with N7 of guanine nucleotides and N3 of adenine nucleotides, which are accessible from the major and minor grooves, respectively. Probing DMS modification of the operator sequence in the absence and presence of the repressor dimer allows isolation of specific sites of contact between the winged helix-turn-helix of the repressor with DNA. These

biochemical data provide a map of the surface of bioO that contacts BirA. It indicates that BirA primarily interacts with DNA using the w-HTH motif of each monomer to bind to the termini of the biotin operator sequence, and suggests the participation of the central domain at the protein:DNA interface.

A detailed comparison of high resolution structures of apoBirA and ligand-bound dimers has provided valuable information that were used by our collaborator, Dr. Zachary Wood, to build a model of the protein:DNA interface. The biotin repressor undergoes significant structural changes as a consequence of ligand-induced dimerization. Comparison of the apoBirA and the adenylate-bound dimer structures exhibits significant differences in the structural features that correlate with the thermodynamic properties of the system *(18, 31).* The dimer structure reveals large decreases in solvent accessible surfaces as compared to apoBirA. These regions exhibit less mobility/flexibility as evidenced by their lower B-factors and show improved packing in the structure of the adenylate-bound dimer. Improved packing is observed at the dimerization interface and extends to large portions of the central and C-terminal domains, which is consistent with formation of a more thermodynamically stable homodimer. The effector binding loops, BBL and ABL, located in the central domain also display improved packing as an outcome of allosteric effector binding. A striking observation is the correlation between these regions of increased packing with those of the dimer backbone that are protected from hydroxyl radical cleavage upon allosteric effector binding. This comparison is shown in Figure 23B. Although the structure of the BirA homodimer:operator complex has not been solved, these

correlations provided a basis to systematically build a model of the holoBirA dimer:bioO complex using a combination of structural and biochemical data.

The model of the holoBirA dimer:bioO complex was preliminarily built by manual docking of the N-terminal DNA binding domains of BirA in the adenylate-bound dimer structure onto bioO, utilizing the binding relationship between winged helix-turn-helix motifs and the DNA backbone (Figure 23C). Based on the DMS modification data obtained on the nucleotide accessibility in bioO, the contacts between the BirA dimer and bioO are refined. Consequently, interactions between the N-terminal domains of the BirA dimer and bioO are off the center axis of the duplex, to form the protein:DNA interaction. The Adaptive Poisson-Boltzmann Solver allows efficient calculation of electrostatic properties of protein structures. Such calculations performed on the adenylate-bound dimer structure reveal multiple exposed charges on the surface of BirA. In addition to the concentration of positive charges observed at the N-terminal DNA binding domains, is the large span of positive charges located in the effector binding loops of the repressor's central domain as demonstrated in Figure 23D. Based on this prominent feature, the central catalytic domain was lowered onto the DNA backbone in the model in order to accommodate possible electrostatic interactions between the positive charges on the protein surface and the negative backbone of the DNA. This was made possible by allowing for a minor conformational change at the linker region between the N-terminal domain and the catalytic domain, which, based on the adenylate-bound dimer structure, is considered highly mobile. Lowering the central domain onto the DNA backbone also accounts

for the regions of contact at the protein:DNA interface revealed by the hydroxyl radical footprinting data obtained on the repressor and bioO. Overall, the model displays a new structural element composed of the effector and effector binding domain at the protein:DNA interface (Figure 24).

Based on the holoBirA dimer:bioO model, it is anticipated that the effector binding loops and the DNA backbone interact *via* salt bridges. These contacts predominate between positively charged residues, Arg116 and Lys122 of the BBL and Arg212 and Arg213 of the ABL and the DNA backbone (Figure 25). It is noteworthy that these positively charged residues are located in the sequences 65-170 and 187-221 that were protected from hydroxyl radical cleavage in the ternary complex. This model of the holoBirA dimer:bioO complex suggests another example of an allosteric transcription repressor in which the effector binding region forms part of an extended interface between the repressor dimer and DNA to form a stable repression complex.

In this chapter a site-directed mutagenesis approach is employed to test the proposed model. Single, double and quadruple amino acid replacements of residues R116, K122, R212, and R213 to alanine were constructed. The DNA binding properties of these variant repressor proteins were evaluated using the DNase I footprinting technique. This approach enables assessment of the effect of disrupting putative electrostatic contacts between the effector binding loops of the repressor dimer and bioO phosphate backbone on the total assembly properties of the ternary

complex. Overall, the results of this study reveal no significant differences in the total assembly energetics of the repression complex, even upon total abolition of all four positively charged residues. These results indicate that the effector binding loops do not contribute significantly to stabilizing the transcription repression complex through electrostatic interactions with the DNA.

---

† *The model presented in this chapter of the holoBirA dimer:bioO complex was entirely constructed and proposed by Dr. Zachary A. Wood, an x-ray crystallography collaborator at University of Georgia. Figures 23-25 used to describe the model were his creation. I thank him for his contribution to this study.*

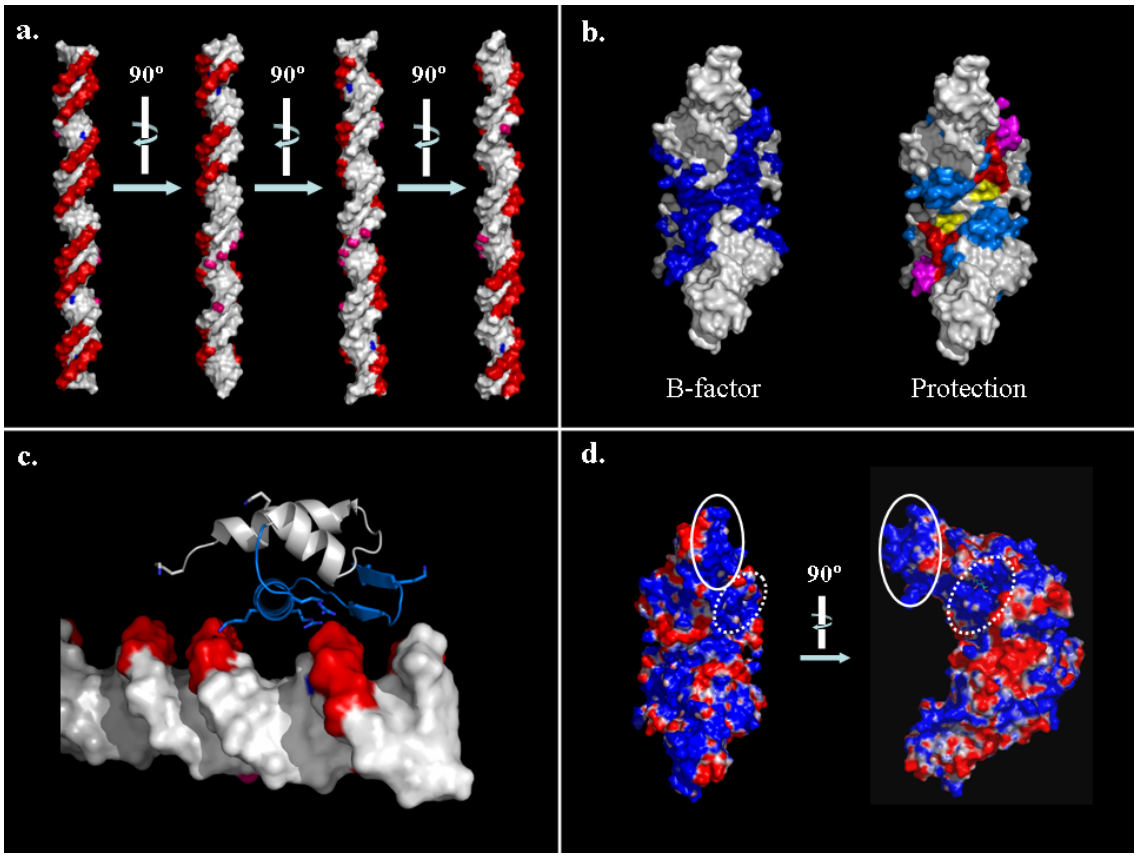

Figure 23. *(legend on next page)*

Figure 23. Construction of the hypothetical model of the holoBirA dimer:bioO complex. (a.) Solution structural probing of bioO bound by the repressor dimer. Regions of protection of bioO against hydroxyl radical agent (red), DNase I (pink) and dimethyl sulfate (blue). (b.) Comparison of packing interactions determined from structural data (left) and protection from hydroxyl radical cleavage data (right). Both images are generated by comparing apo and corepressor bound dimer. Colored regions represent increased packing/protection upon binding the corepressor. Images are bottom views of the dimer. (c.) Manual docking of the winged-helix-turn-helix motif of BirA onto the DNA backbone. (d.) APBS calculated electrostatic surface of BirA. Depicted are the positive (blue), negative (red) and neutral (white) charges on the surface of BirA. The DNA binding domain (bold) and effector binding domain (dotted) are highlighted on the bottom (left) and side (right) views of the repressor dimer.

This figure was created by Dr. Z.A.Wood.

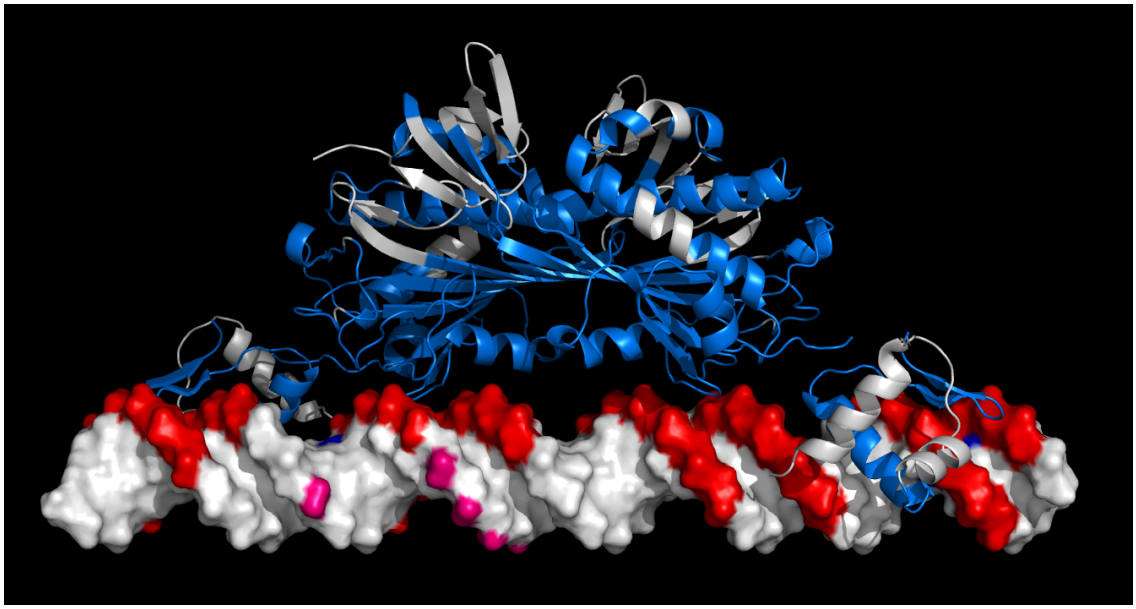

Figure 24. A hypothetical structural model of the holoBirA dimer:bioO complex. The N-terminal domains are bound at the termini of the DNA and off the center of axis of the DNA duplex. The central region of the repressor dimer is lowered. *This figure was created by Dr. Z.A.Wood.*

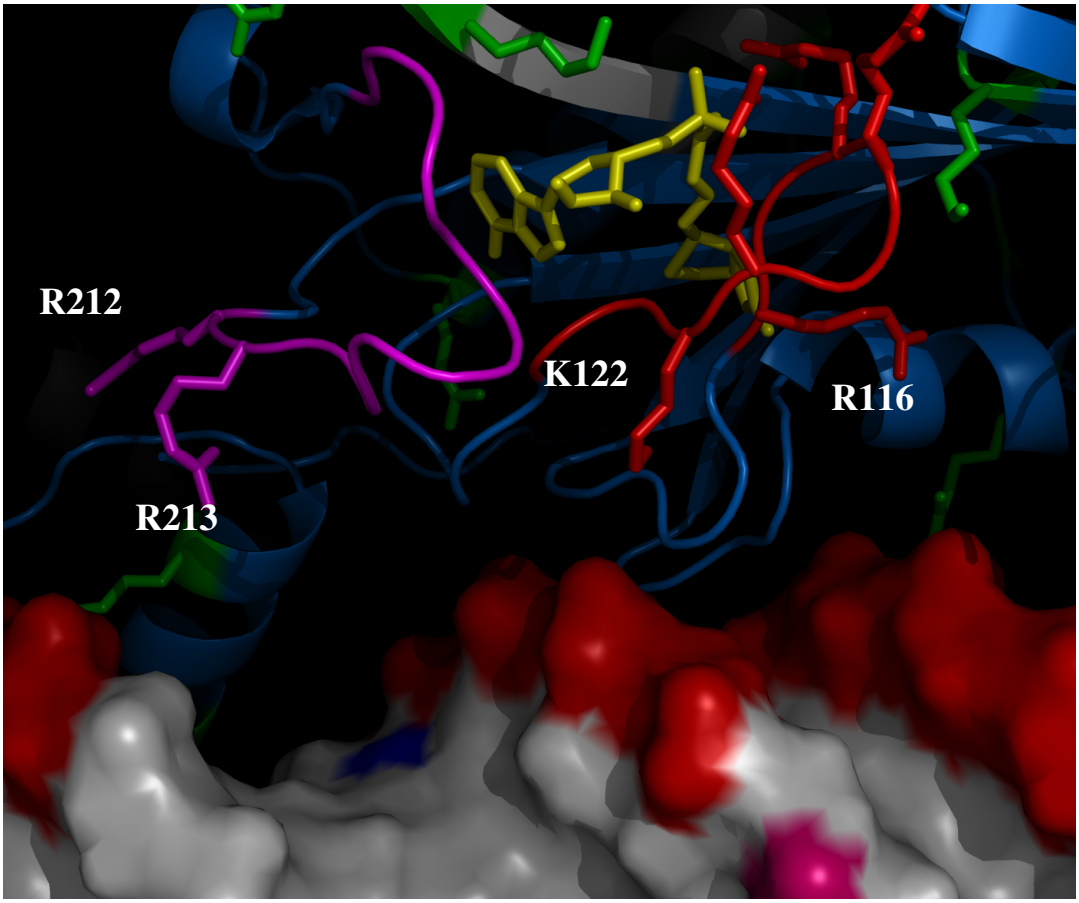

Figure 25. Effector binding loops extend towards the bioO backbone

Positively charged residues of the effector binding loops of BirA extend toward the phosphate backbone of bioO. Residues R212 and R213 of the ABL (magenta) and R116 and K122 of the BBL (red) are labeled. *This figure was created by Dr. Z.A.Wood.*

B. Results

A model for the holoBirA dimer:bioO complex was built using structural and biochemical data and described in the Introduction to this chapter. The model proposes that the structural mechanism of corepressor function involves creating a new structural module for interaction between the protein and DNA *via* the effector binding loops of the central domain. It is postulated that the positively charged residues in the effector binding loops interact directly with the DNA backbone by forming salt bridges. The focus of this chapter is to test the effect of disrupting these putative electrostatic interactions at the protein:DNA interface on ternary complex assembly. The BirA variant proteins R116A and K122A of the BBL, and R212A and R213A of the ABL, the double mutants: $R_{116}A/K_{122}A$, $R_{212}A/R_{213}A$ and the quadruple mutant repressor, $R_{116}A/K_{122}A/R_{212}A/R_{213}A$ were constructed. These variant proteins were subjected to quantitative DNase I footprinting measurements to evaluate their effects on the energetics of total assembly of the repression complex.

1. Bio-5'-AMP Binding to BirA Variant Proteins

Corepressor, bio-5'-AMP binding to BirA induces its dimerization and subsequent DNA binding. Thus in this system, ligand binding is positively coupled to the assembly of the repression complex. The DNase I footprinting technique was utilized to determine the DNA binding and total repression complex assembly properties of the BirA variants. In order to design the measurements using saturating concentration of corepressor, the bio-5'-AMP binding affinities of the variants proteins were first determined by equilibrium titration methods using isothermal

titration calorimetry and steady-state fluorescence measurements as described in the Materials and Methods section. All experiments were performed at sufficiently low protein concentration to eliminate any contribution of coupled dimerization to the binding process. Representative data are shown in Figure 26A-C. The thermodynamics of bio-5'-AMP binding to the variant proteins are shown in Table 6. BirA variant K122A and all variant proteins containing the Arg116Ala mutation exhibited significantly weaker affinities for the ligand.

2. Dimerization Properties of bio-5'-AMP bound Repressor Variants

Assembly of the repression complex occurs by coupled dimerization and DNA binding. Solution studies have shown that repressor dimerization precedes DNA binding in formation of the repression complex *(16).* Therefore, the total assembly energetics of the repression complex represents the sum of the energetics of dimerization and that of DNA binding by the dimer. In order to deconvolute these two processes and determine defects in DNA binding alone, it is critical to measure the dimerization properties of the repressor variants. The dimerization energetics were measured for the single mutant BirA proteins under standard buffer conditions by sedimentation equilibrium. Figure 27 shows results of data obtained for the BirA-bio-5'-AMP complex. The results indicated moderate to no significant differences in the dimerization properties of these variants as compared to the wild-type repressor (Table 7). BirA variants K122A and R212A exhibit moderate defects in dimerization energetics of +0.5 and +0.9 kcal/mol, respectively.

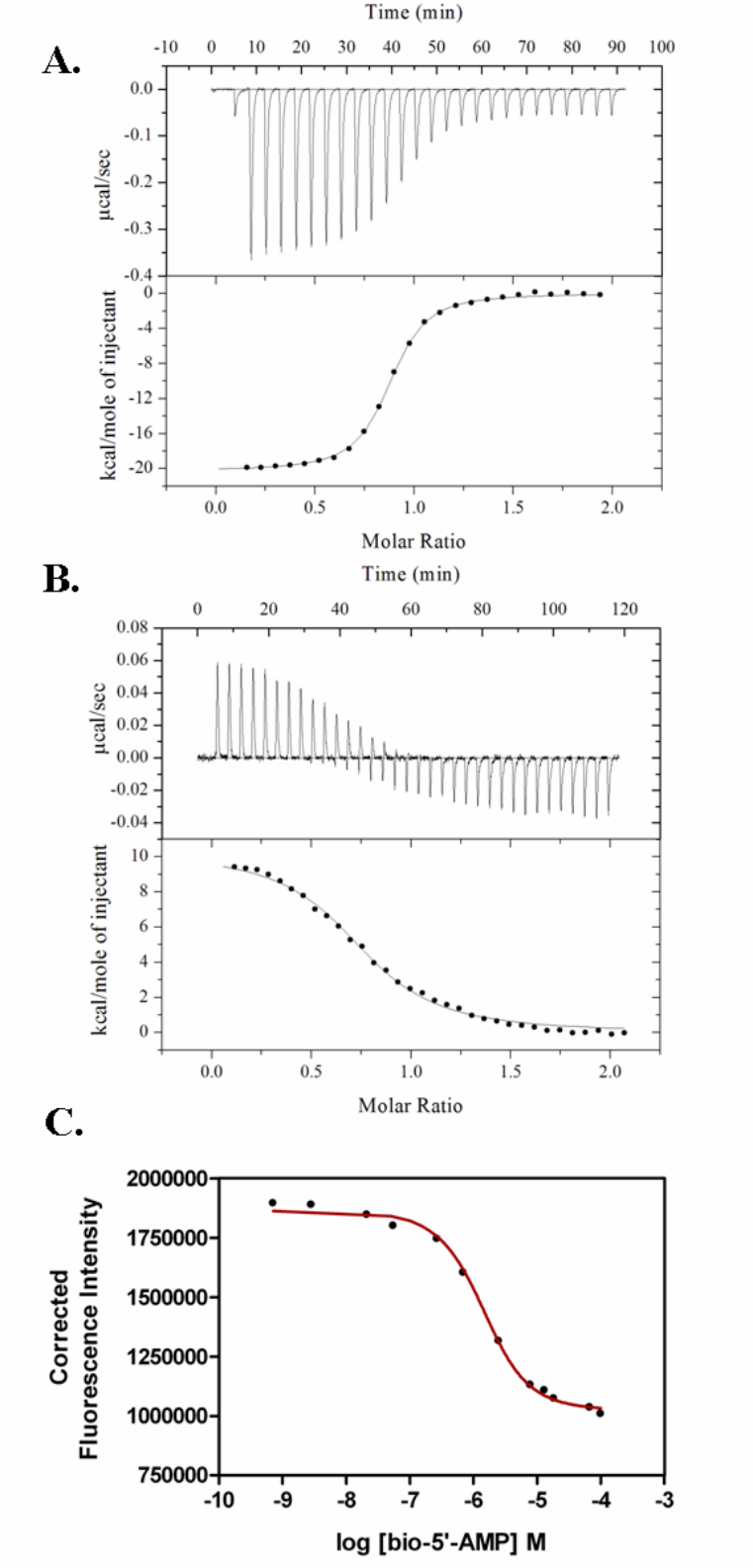

Figure 26. *(legend on next page)*

Figure 26. Bio-5'-AMP Binding to BirA Variant Proteins

(A) Direct equilibrium titration of biotin binding R213A. (B) Displacement titration of bio-5'-AMP binding R213A saturated with biotin. (C) Equilibrium binding titration obtained by steady-state fluorescence measurement of bio-5'-AMP binding $R_{116}A/K_{122}A/R_{212}A/R_{213}A$. Data were fit as described in the Materials and Methods section. All measurements were performed in Standard Buffer (10 mM Tris-HCl pH 7.50 ± 0.02 at 20.0 ± 0.1 ^{o}C. 200 mM KCl, 2.5 mM $MgCl_2$) as described in Materials & Methods.

Table 6. Thermodynamics of Bio-5'-AMP Binding to BirA Variant Proteins:

BirA Variant	K_b (M)[a]	ΔG^o (kcal/mol)[b]
WT	3.9 (± 1.9) x 10^{-11}	-13.9 ± 0.4
R116A	2.2 (± 0.3) x 10^{-7}	-8.9 ± 0.1
K122A	1.8 (± 0.4) x 10^{-8}	-9.0 ± 0.2
R212A	3.3 (± 1.0) x 10^{-11}	-14.0 ± 0.2
R213A	2.8 (± 1.5) x 10^{-11}	-14.0 ± 0.3
R116A/K122A	9.5 (± 1.3) x 10^{-7}	-8.0 ± 0.3
R212A/R213A	6.5 (± 1.1) x 10^{-10}	-12.3 ± 0.2
Quadruple	4.7 (± 1.0) x 10^{-7}	-8.5 ± 0.2

All measurements were performed in Standard Buffer (10 mM Tris-HCl pH 7.50 ± 0.02 at 20.0 ± 0.1 ^oC. 200 mM KCl, 2.5 mM $MgCl_2$) as described in the Materials and Methods section. The reported values represent the average of at least two independent titrations with standard deviation. a. Values of K_b are the best-fit values obtained from nonlinear least squares analysis of the titration data to a simple one-site binding model using Origin or GraphPad Prism 4. b. The values of the Gibbs free energy, ΔG^o, were calculated using the expression $\Delta G^o = RT\ln K_b$. Equilibrium binding measurements by steady-state fluorescence were performed for bio-5'-AMP binding to the BirA R116A variants, both double mutants, and the quadruple. All other measurements were made using ITC employing the displacement titration method as discussed in Materials and Methods. Bio-5'-AMP binding to BirA variant K122A was measured by the direct equilibrium titration method.

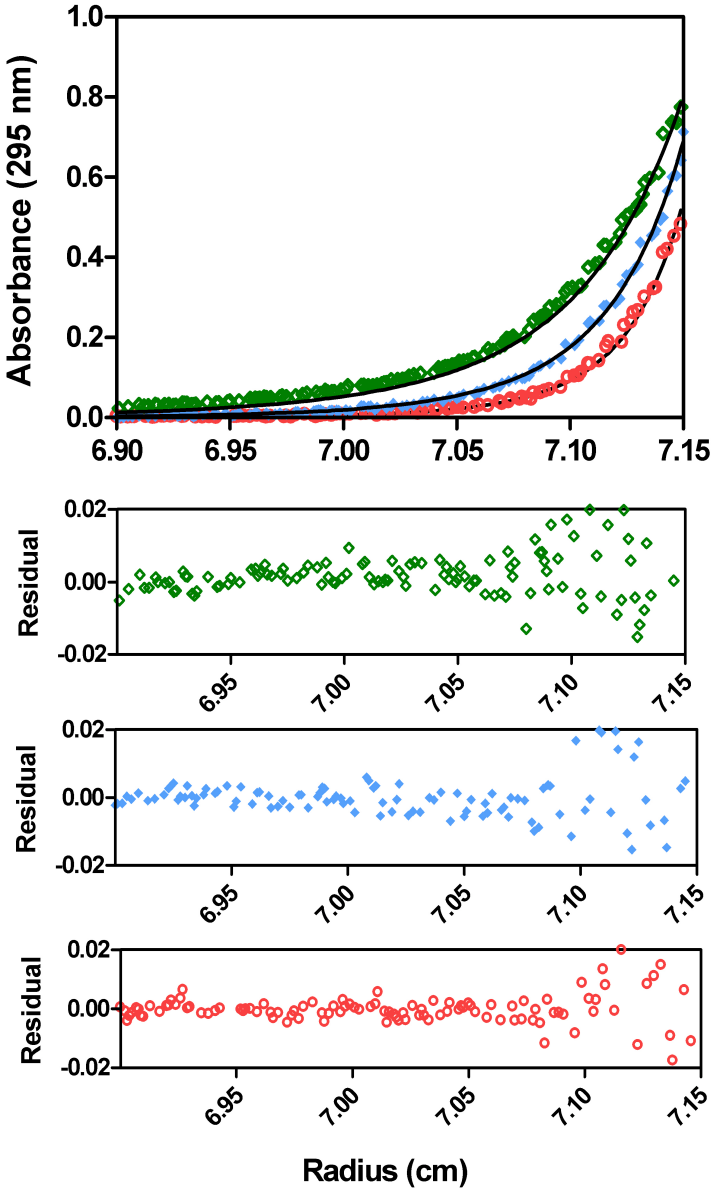

Figure 27. Absorbance *versus* radial position for 45 μM R212A·bio-5'-AMP at 22,000 (◊), 26,000 (♦) and 30,000 (o) rpm obtained in standard buffer at 20 ˚C. The best-fit curves were generated from global analysis using a monomer-dimer model of six data sets acquired at multiple loading concentrations and spun at three speeds. The residuals of the fit for each data set shown are provided in the bottom panels.

Table 7. Dimerization Properties of BirA Variant- bio-5'-AMP Complexes

BirA Variant	K_{dim} (M)	ΔG^{o}_{DIM} (kcal/mol)
WT	6 (± 2) x 10^{-6}	-7.0 ± 0.3
R116A	5 (± 2) x 10^{-6}	-7.1 ± 0.3
K122A	2.1 (± 0.6) x 10^{-5}	-6.2 ± 0.2
R212A	1.5 (± 0.6) x 10^{-5}	- 6.4 ± 0.3
R213A	5 (± 2) x 10^{-6}	-6.9 ± 0.3

All measurements were performed in Standard Buffer (10 mM Tris-HCl pH 7.50 ± 0.02 at 20.0 ± 0.1 ^{o}C. 200 mM KCl, 2.5 mM $MgCl_2$) as described in Materials & Methods. The reported values represent the average of at least two independent sedimentation equilibrium measurements performed by subjecting samples prepared at multiple loading concentrations of the variant-bio-5'-AMP complex to centrifugation at multiple rotor speeds. Reported errors represent 95% confidence intervals. The resulting data sets were subjected to global analysis using a monomer-dimer model to determine K_{DIM}.

3. Binding of BirA Variant Proteins to bioO

DNase I footprints of holoBirA wild-type and variant proteins binding to bioO were performed under standard buffer conditions (10 mM Tris-HCl (pH 7.50 ± 0.02 at 20.0 ± 0.1 ^{o}C), 200 mM KCl, 2.5 mM $MgCl_2$) and were all qualitatively similar. A representative footprint of BirA variant R213A binding to bioO is shown in Figure 28. Binding isotherms obtained from quantification of the footprints reflect both dimerization and DNA binding processes. The data were subject to non-linear least squares analysis using the following equation:

$$\overline{Y} = \frac{K_{DIM} K_{bioO} [holoBirA]^2}{1 + K_{DIM} K_{bioO} [holoBirA]^2} \qquad \text{.....(1)}$$

The expression relates the fractional occupancy, $\overline{Y}$, to the holoBirA concentration. K_{DIM} is the equilibrium association constant for repressor dimerization and K_{bioO} is the equilibrium association constant for dimer binding to bioO. This model is used in non-linear least-squares analysis of the data to obtain the K_{bioO}. The K_{DIM} was fixed at the value resolved from sedimentation equilibrium measurements. The results of free energies of the variant repressor dimers binding to bioO are shown in Table 8. The free energy of total repression complex assembly, ΔG°_{TOT}, can be calculated using the equations: $\Delta G^{\circ}_{TOT} = -RT\ln(K_{bioO}K_{DIM})$ or $\Delta G^{\circ}_{TOT} = \Delta G^{\circ}_{DIM} + \Delta G^{\circ}_{bioO}$.

Alternatively, the model

$$\overline{Y} = \frac{K_{TOT} [holoBirA]^2}{1 + K_{TOT} [holoBirA]^2} \qquad \text{.....(2)}$$

is used to fit the data to obtain K_{TOT}, the equilibrium association constant for total assembly of the holoBirA dimer:bioO complex, which is the product of K_{DIM} *and*

K_{bioO}. The free energy of total repression complex assembly, ΔG°_{TOT}, can be calculated using the equation $\Delta G^{\circ}_{TOT} = -RT\ln K_{TOT}$.

The binding isotherms and best fit curves of each variant repressor protein binding to bioO compared with that of the wild-type repressor are displayed in Figure 29. Resolved parameters shown in Table 8 indicate that the total free energies of assembly of the repression complex for the variant repressor proteins are not significantly different from that of wild-type BirA. As compared to the ΔG°_{TOT} for wild-type holoBirA dimer:bioO assembly which is -19.7 ± 0.4 kcal/mol, the variant proteins exhibit only about ± 1 kcal/mol differences. Additionally, the total assembly energetics resolved using models (1) and (2) for the single mutation repressor variants were in agreement with each other.

C. Discussion

Transcription regulation involves binding of transcription factors to specific sites on DNA. The affinity of protein-DNA interactions can be modulated by binding of an allosteric effector to the transcription factor. Effector binding is accompanied by conformational changes that alter the structural features of the protein's surface that interacts with DNA. The aim of this chapter was to investigate the role of the effector in influencing the structural features of the protein:DNA interface of the complex formed between the *E. coli* biotin repressor dimer and its DNA target, bioO.

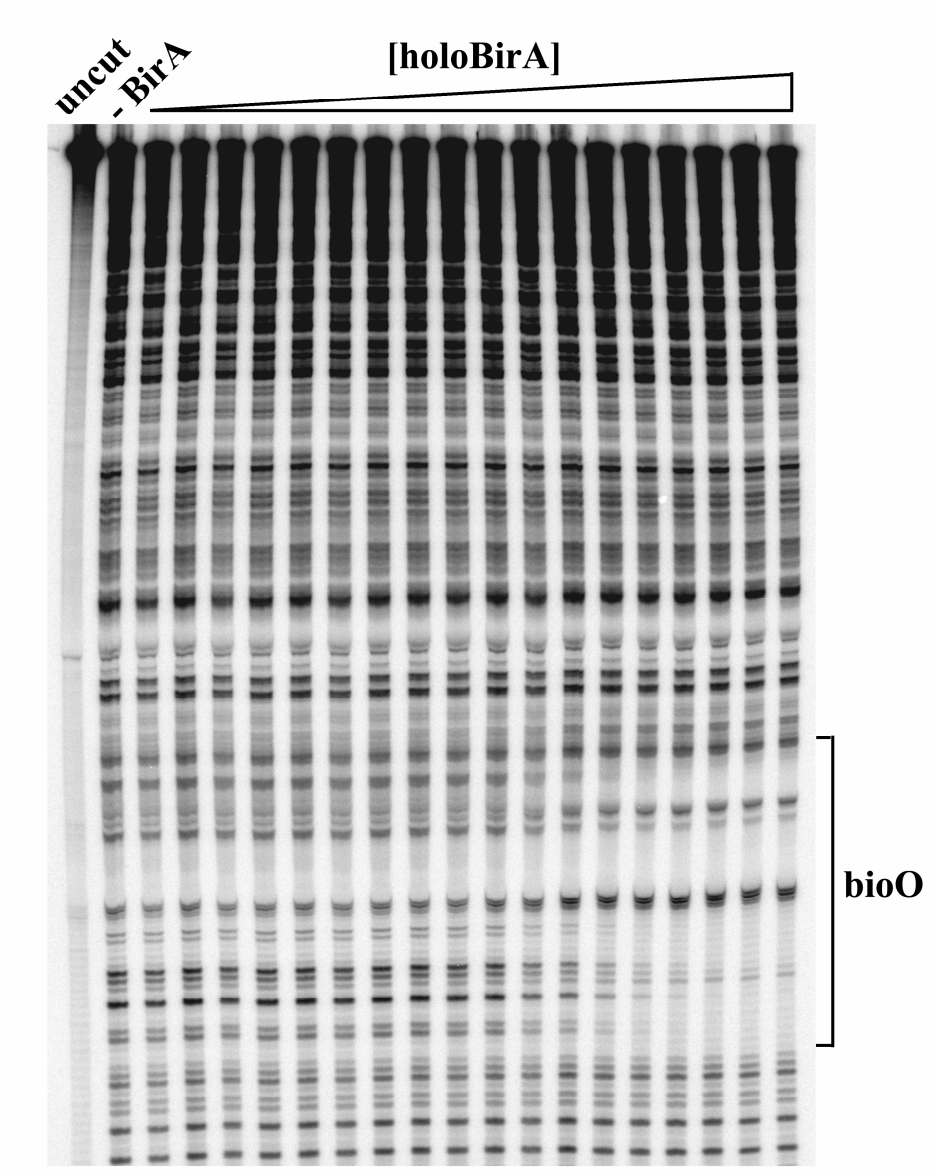

Figure 28. DNase I Footprinting of BirA variant R213A-bio-5'-AMP with bioO

The footprint was obtained in buffer containing 10 mM Tris-HCl (pH 7.50 ± 0.02 at 20.0 ± 0.1 °C), 200 mM KCl, 2.5 mM $MgCl_2$, 1 mM $CaCl_2$, 2 µg/mL sonicated calf thymus DNA, and 100 µg/ml BSA.

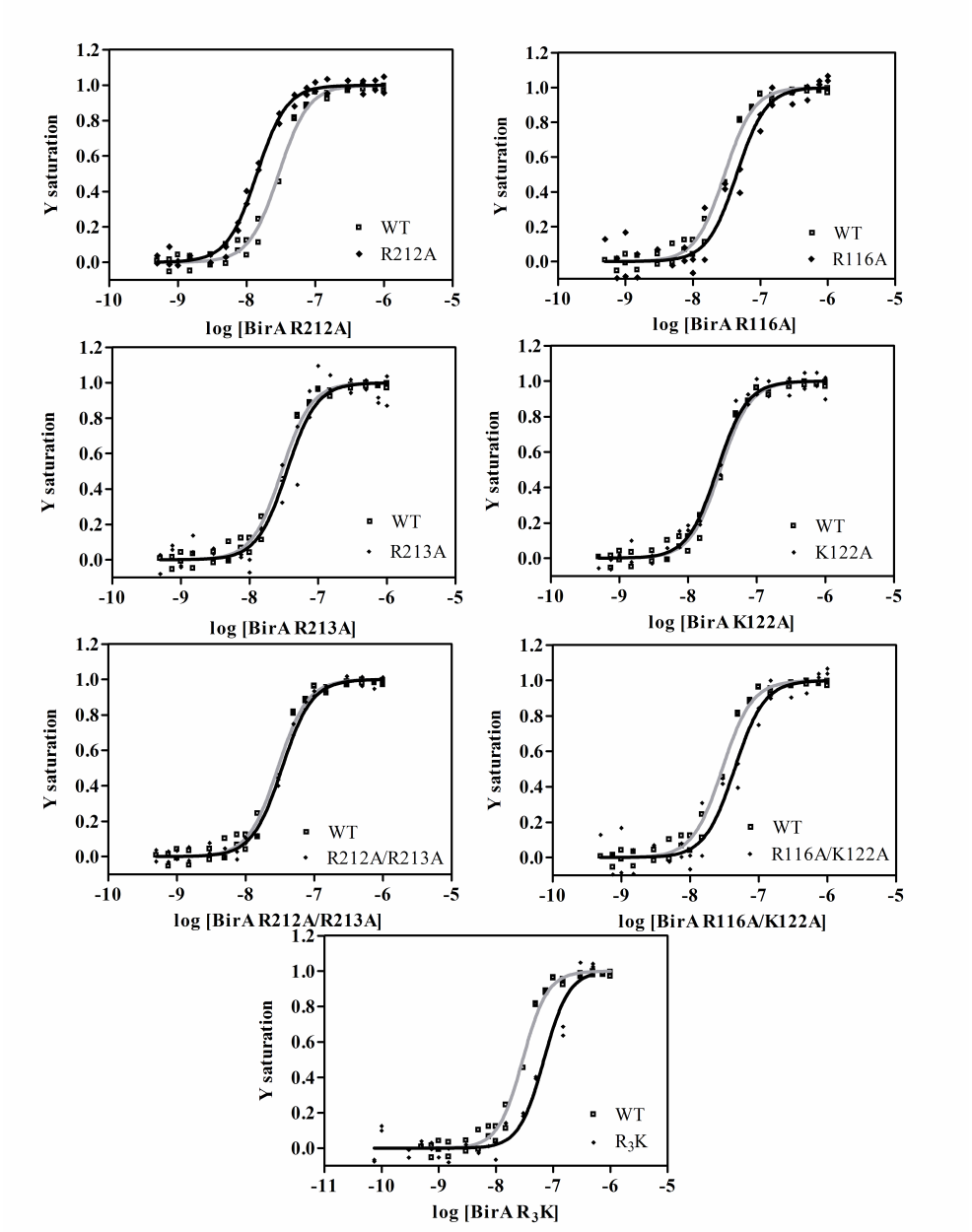

Figure 29. DNA binding isotherm of holoBirA Variant Repressors to bioO

Each panel represents the variant repressor binding to bioO, superimposed with that of wild-type BirA. (■) correspond to wild-type and (◊) to BirA variant data obtained from quantitation of footprinting gels. The best fit curves are from fitting data to equation (2) are represented (grey) for wild-type and (black) variant repressor. R_3K represents the quadruple variant repressor, BirA variant $R_{116}A/K_{122}A/R_{212}A/R_{213}A$.

Table 8. Energetics for Total Assembly of the Repression Complex

BirA Variant	ΔG^{o}_{bioO} (kcal/mol)[a]	ΔG^{o}_{TOT} (kcal/mol)[b]
WT	-12.7 ± 0.3	-19.7 ± 0.4
R116A	-13.1 ± 0.2	-20.0 ± 0.1
K122A	-14.0 ± 0.2	-20.2 ± 0.2
R212A	-14.5 ± 0.2	-20.9 ± 0.2
R213A	-12.9 ± 0.2	-19.8 ± 0.1
R116A/K122A	n.d.	-19.9 ± 0.2
R212A/R213A	n.d.	-19.6 ± 0.2
Quadruple	n.d.	-19.1 ± 0.1

All measurements were performed in Standard Buffer (10 mM Tris-HCl pH 7.50 ± 0.02 at 20.0 ± 0.1 ^{o}C. 200 mM KCl, 2.5 mM $MgCl_2$) as described in Materials & Methods.

(a.) Footprinting data were fit by fixing the K_{DIM} obtained from sedimentation equilibrium measurements to equation (1) to determine K_{bioO}. (b.) Footprinting data were fit to obtain K_{TOT} using equation (2). All reported values represent the average of two independent measurements. Free energies are calculated using the equation $\Delta G^{o} = -RT\ln K$.

Detailed solution studies and structural data obtained on the biotin repressor have enabled an understanding of the mechanism of allosteric activation in BirA. This mechanism involves binding of the corepressor, bio-5'-AMP, which enhances holoBirA dimerization, and subsequent biotin operator binding. Although a structure of the repression complex has not yet been solved, chemical and biochemical probing combined with structural data have provided insight into the interface formed in holoBirA dimer: bioO complex *(35, 129).* Based on these data, a model for the interaction between the dimer and DNA was predicted. Dimethyl sulfate (DMS) protection data provided very specific detail regarding repressor contacts with the biotin operator. The wHTH motif of BirA is expected to contact the 12 base pair termini of the 40 base pair bioO sequence *via* the recognition helix in the major groove and wing extending into the minor groove. This interaction produces a 40 degree bend in the central region of the DNA, distorting it toward the dimer in the repression complex, as evidenced from circular permutation analysis *(129).* While these data provided a preliminary understanding of the protein:DNA interaction, this study presents a combination of modeling and experimental measurements to dissect the participation of the effector binding region at the protein:DNA interface.

Combining the data summarized in the previous paragraph with calculations of the surface electrostatics of BirA obtained from structural data, our x-ray crystallography collaborator, Dr. Zachary A. Wood constructed a model for the dimer:DNA complex. The model was used to postulate the structural mechanism by which allosteric effector-induced alteration in BirA affects its surface of interaction

with bioO. It suggested direct contact between the effector binding region of BirA and central region of bioO. Electrostatic interactions are predicted between the effector binding loops located in the central domains of the repressor dimer and the DNA backbone. Direct participation of the loops in DNA binding would raise an interesting structural mechanism in the context of allosteric activation in BirA. These loops are also involved in allosteric effector binding and in the allosteric activation mechanism of BirA. In this study, mutations of positively charged residues that should abolish the putative electrostatic interactions were constructed to test the predictions of the model. Mutant repressor proteins were subjected to thermodynamic characterization of their ligand binding, dimerization and repression complex assembly properties.

Since ligand binding is positively coupled to repression complex assembly, the bio-5'-AMP binding properties of the BirA variants were determined. Measurements indicate that BirA variants R212A and R213A bind the effector with affinities identical to that measured for the wild-type repressor. However, bio-5'-AMP binds to BirA variants K122A and all variants containing the mutation R116A with affinities significantly lower than for the wild type repressor. The energetic penalties ($\Delta\Delta G^o$) for these variants ranged from +4.1 to +5.9 kcal/mol. Inspection of the effector-bound dimer structure of BirA indicate that biotin binding is accompanied by folding of the BBL, thereby creating the binding site for ATP. Folding of the biotin binding loop contributes two hydrogen bonds from the main-chain atoms of R116 to the ureido ring of biotin and additional packing interactions to

create the adenylate binding pocket *(31).* It is conceivable that disruption of K122 and R116 affects folding of the BBL required to make these contacts.

Sedimentation equilibrium measurements were performed to determine defects in dimerization properties of the variant proteins. The dimerization energetics measured for the single mutation BirA variants indicate that while R116A and R213A are unaffected, variants K122A and R212A exhibit defects of +0.6 to +0.8 kcal/mol as compared to the wild-type repressor. Structural data indicate that none of these residues participate directly at the dimerization interface. Moreover, based on ligand binding and dimerization measurements, it is evident that defects in ligand binding do not directly correlate with defects in dimerization for these variant repressors.

DNA binding and repression complex assembly properties of the variant repressors were measured by the DNase I footprinting technique. The energetics of total assembly of the repression complex was used to test the validity of the structural model. Results indicated only a moderate 0.9 kcal/mol loss in total repression complex assembly energetics, even with the quadruple mutant. This result is contradictory to predictions based on the model that eight putative electrostatic interactions (four for each monomer) exist between the effector binding loops of the dimer and the bioO backbone. The discrepancies between the predictions from the model and experimental results are addressed below.

Assembly of the repression complex occurs by coupled dimerization and DNA binding *(16)*. The energetics of bioO binding were measured for the single mutation BirA variants. The total free energy of repression complex assembly was calculated for these variants from the sum of their dimerization and bioO binding energetics. These values agreed well with that obtained from fitting DNase I footprinting data to obtain their energetics of total assembly. However, the results raised an interesting observation with variants K122A and R212A. Although these variants were moderately defective in dimerization, their total assembly energetics were unaffected. Defects in dimerization energetics were compensated by the energetics of bioO binding. The contributions to the compensatory energetics are presently unclear and will require further investigation.

The electrostatic contributions to protein:DNA interactions have been evaluated in several protein:DNA complexes through extensive experimental measurements. For example, solution studies performed on the LacR:operator binding process has revealed release of 8 cations upon binding of the homotetramer, LacR, to its operator sequence. This stoichiometry of ion release is consistent with structural data on the repressor:DNA complex, which indicates eight electrostatic interactions between the protein and phosphates of the DNA backbone *(114, 130, 131)*. The model of the holoBirA dimer:bioO complex predicts eight electrostatic interactions between the effector binding loops and the DNA backbone, in addition to those formed *via* the DNA binding motifs of the protein with the DNA backbone. The combined electrostatics should be revealed by measuring the salt dependence of DNA

binding. However, measurements performed by DNase I footprinting to determine the electrostatic contribution to the BirA dimer binding to bioO and to total assembly of the dimer-DNA complex, indicated only a modest release of 2.5 ± 0.3 ions *(107).* This surprisingly low apparent stoichiometry of ion release for this process could be a consequence of ion uptake by the DNA or by the protein in the coupled process of dimerization and DNA binding. The experimentally determined small number of ions released does not correlate with the large number of putative electrostatic interactions predicted by the model.

The moderate loss in total assembly properties of BirA variants in the effector binding loops and the modest number of ions released in the dimer-DNA binding process is inconsistent with formation of multiple electrostatic interactions at the protein:DNA interface. In view of these discrepancies between the proposed model and experimental results, a critical analysis of the construction of the structural model revealed several oversights. First, comparison of the hydroxyl radical footprinting data obtained on the corepressor-bound dimer and the complete repression complex suggested that the dimer:DNA complex assembly involves formation of an extended surface of interaction at the protein:DNA interface. This was based on the increased protection from cleavage accompanied by formation of the repression complex. In the corepressor-bound dimer the BBL and ABL undergo 90% and 50% increased protection respectively, from cleavage as compared to apoBirA monomer. However, while formation of the repression complex results in a 90% increased protection in regions of the N-terminal segment of the central domain, the ABL undergoes only a

40% greater protection and the BBL undergoes no significant change. These observations highlight that interaction between the dimer and bioO offers only minor changes in the accessibility of effector binding loops to hydroxyl radical cleavage. Therefore, it is conceivable that while formation of the repression complex could be accompanied by increased contacts between the central domains of the dimer and DNA backbone, the effector binding loops do not play a critical role in the interaction. Formation of the repression complex merely increases the packing interactions at the protein:DNA interface and is not supplemented by electrostatic contacts as proposed by the model. Moreover, changes in reactivity to hydroxyl radical could be a representation of a global change in the protein instead of specific conformational rearrangements. It has been suggested that in cAMP receptor protein (CRP) binding to DNA, the sensitivity to hydroxyl radical cleavage reflects a combination of solvent accessibility, charge and hydrophobicity *(132).* Therefore, the hydroxyl radical cleavage data are not comprehensive in the context of constructing this model. Second, the model for the holoBirA dimer:bioO was constructed with the omission of a valuable experimental result. Use of the circular permutation analysis technique on bioO in the holoBirAdimer-bio complex, indicated that the DNA deviated from linearity in the order of 40 degrees toward the dimer. Although this assay provided information on a global level rather than identification of a local point, extensive mapping of the DNA in the repression complex enabled isolation of three loci of bending. These correlate with the three DNase I hypersensitive sites: two at the 12 base-pair termini that interact with the wHTH motifs of the repressor dimer, and one in the central region of the 40 base-pair bioO sequence. The structural model

of the holoBirA dimer:bioO complex was constructed without consideration of the bend angle in the central region of the DNA. Collectively, these oversights of experimental data could have resulted in an inaccurate representation of the protein:DNA complex.

The model of the holoBirA dimer:bioO complex provided a preliminary assessment of the structural features of the protein- DNA interface. However, this chapter has presented a good example of making too many inferences about functional features of a system based on structural modeling. Several attempts have been made to crystallize the holoBirA dimer-bioO complex but have proven unfruitful. Thus, in absence of an experimentally determined structure, refinement of the existing model with the inclusion of the DNA bend angle could provide a more accurate representation of the repressor dimer:DNA complex. In recent years, several computational approaches have been taken to predict electrostatics, solvation, and hydrogen bonding in protein-DNA interactions. Models developed to efficiently calculate such factors important in predicting specific and non-specific protein-DNA interactions have shown excellent correlation with experimental measurements *(133).* In future work a refined model of the biotin repression complex could be subjected to computational and experimental analyses to better dissect the structural mechanism of allosteric effector-induced protein-DNA interaction in the BirA system.

IV. The Roles of Flexible loops in BirA in Alternative Protein:Protein Interactions.

A. Introduction

A protein's functional properties are regulated in response to cellular requirements. One common mode of regulation of protein function is through interaction with another protein partner. For example, some enzymes can control gene expression in response to the availability of their substrates. These enzymes by forming specific protein:protein interaction with transcription factors control their ability to regulate transcription initiation *(134)*. In other systems alternate distinct functions of a protein are modulated *via* exchange of one protein partner for another. This class of multi-functional proteins contributes to important biological processes and an understanding of their mechanisms of regulation requires elucidation of the structural, kinetic and thermodynamic rules that govern acquisition of different partners.

The structural features by which a single protein forms specific interactions with different protein partners to control biological function is not well understood. However, one of the best studied is β-catenin which functions in transcriptional activation and in cell-cell adhesion *(89)* As a coactivator of transcription initiation β-catenin interacts with members of the T-cell factor (Tcf)/ lymphoid enhancer factor (LEF) family of transcription factors. Alternatively, β-catenin interacts with cadherins in its cell adhesion function. Structural data indicate that the same β-catenin surface is

used to form complexes with its two partners, and that the chemistries of the two interfaces are very similar *(91, 92)*. In this system the utilization of a single protein surface in alternative protein:protein interactions makes the distinct functions mutually exclusive. The ability of a single protein to be both promiscuous and specific in interaction with two different protein partners is crucial to functional switching. In this study we examine the physical-chemical and structural features important to formation of alternative protein:protein interactions of a bifunctional protein.

The *Escherichia coli* Biotin Regulatory System provides an example of a protein for which binding partner decides functional fate. The central component of the system, BirA, the biotin repressor/biotin protein ligase functions as a transcriptional repressor and a metabolic enzyme *(2, 3)* (Figure 30). As an enzyme BirA catalyzes biotin linkage to the biotin carboxyl carrier protein (apoBCCP), a subunit of the acetyl-CoA carboxylase enzyme (ACC). In this two-step reaction the apoBirA monomer first binds to biotin and ATP to catalyze synthesis of the intermediate, bio-5'-AMP *(4)*. The resulting bio-5'-AMP bound form of BirA, holoBirA, then transfers biotin to the BCCP subunit of ACC, which catalyzes the first committed step of fatty acid synthesis. As a transcriptional repressor BirA binds specifically to the 40-base pair biotin operator sequence (bioO) to repress transcription of the biotin biosynthetic operon *(5, 6)*. The intermediate in biotin transfer, bio-5'-AMP, also induces BirA homodimerization, thereby facilitating repression complex assembly. Thus the activated monomer, holoBirA, serves as an

obligate species in both functions. Moreover, the functional switch between metabolism and transcription repression occurs by alternative protein:protein interactions in which holoBirA forms a homodimer or a heterodimer with apoBCCP.

Structurally, the functional switch in BirA reflects formation of two mutually exclusive protein:protein interfaces. The structure of the BirA homodimer bound to effector has been solved by x-ray crystallography *(30, 31).* The homodimer interface is formed through side by side anti-parallel alignment of the β-strand, composed of residues 188-196 of each holoBirA monomer's central domain to form an extended β-sheet. Additionally, three loops located in the central domain participate at the dimerization interface. While the structure of the BirA:apoBCCP complex has not been determined, a model has been proposed *(97).* The model was generated by docking a holoBirA monomer from the homodimer structure with the experimentally determined structure of apoBCCP87 *(135).* BCCP87 is the C-terminal fragment of BCCP that is functionally identical to intact BCCP in biotin transfer *(136).* As observed in the homodimer structure, the heterodimer interface is formed by aligning the same β-strand (residues 188-196) of the holoBirA monomer used in homodimerization with a β-strand, composed of residues 122-128, of apoBCCP in a parallel orientation. The model is supported by combined structural and mutagenesis studies *(93).* Moreover, the general features of the model were confirmed in an experimentally determined structure of the BirA paralog, *Pyrococcus horikoshii* biotin protein ligase, bound to its acceptor protein *(137).* Based on the experimentally determined and modeled structures of the homodimer and heterodimer, respectively

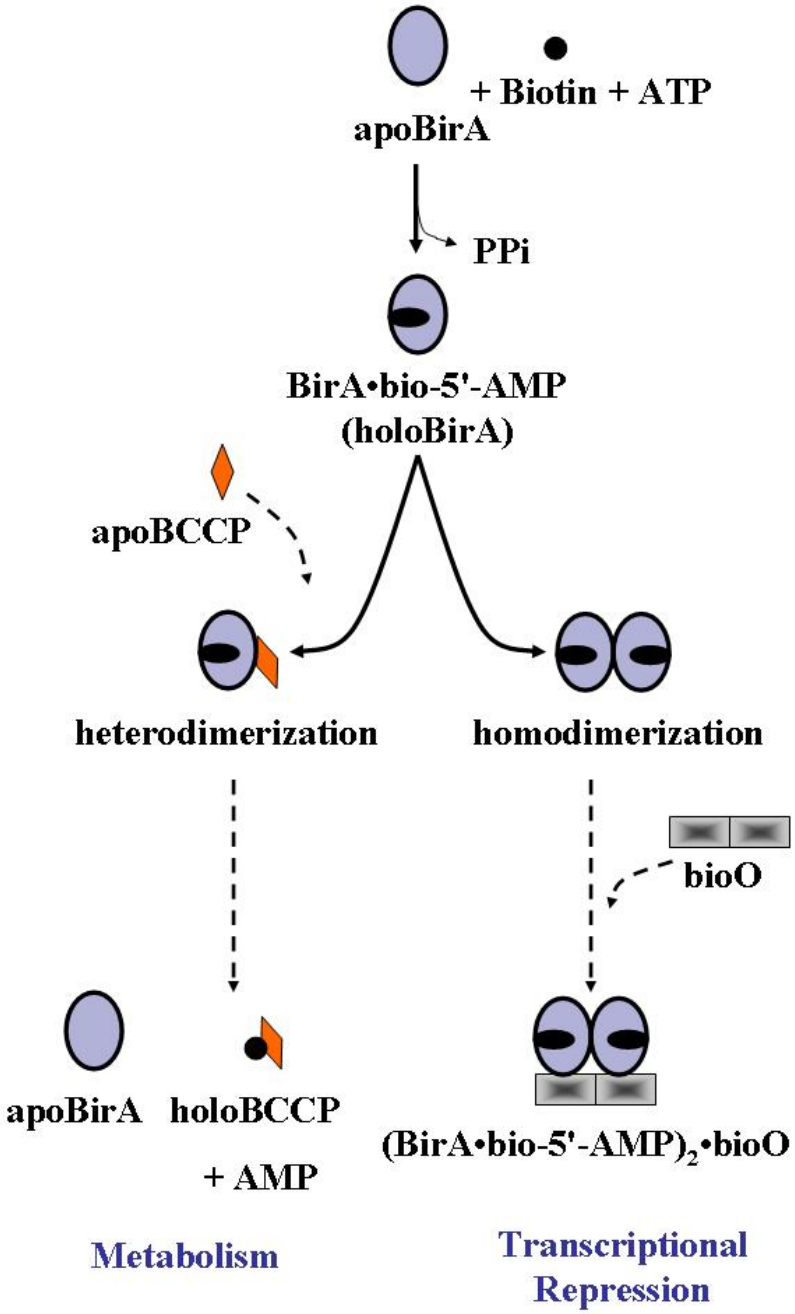

Figure 30. A schematic representation of the biotin regulatory system.

The activated protein, BirA-bio-5'-AMP, switches between functioning as a biotin ligase and a transcriptional repressor.

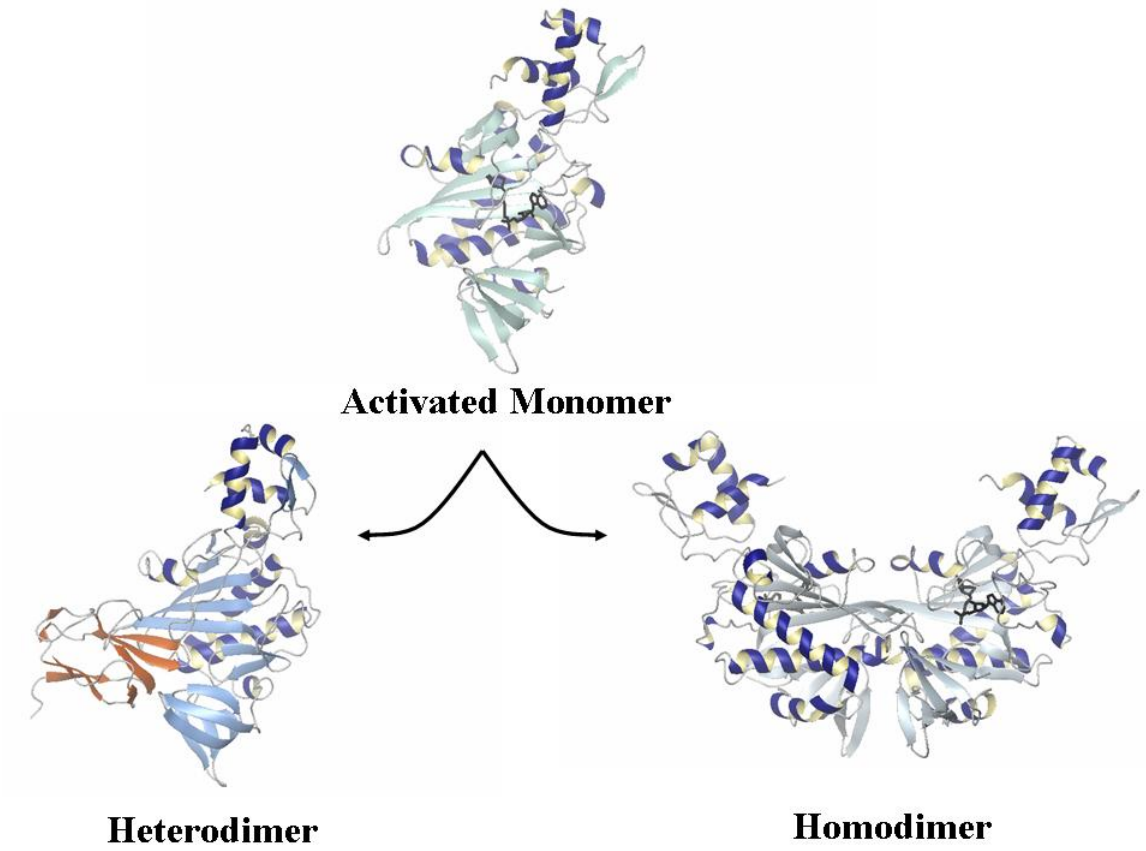

Figure 31. Structural Models of the Homodimer and Heterodimer

Structural models of the BirA-apoBCCP heterodimer and holoBirA homodimer. The activated holoBirA monomer switches between two mutually exclusive protein:protein interactions. Models were constructed using the program MolMol *(28)* with Protein Data Bank files 2EWN for the homodimer and 1K67 for the heterodimer (hypothetical model) as input. The activated monomer was constructed using one subunit of the homodimer.

(Figure 31), it is evident the two interactions use the same BirA surface for dimerization, thus rendering them mutually exclusive.

In vivo and *in vitro* approaches have been employed to determine the mechanism of functional switching of BirA between metabolism and transcription repression. ApoBCCP production is controlled by growth rate *(138).* In rapidly dividing cells, apoBCCP concentration increases in response to requirement for fatty acids. It has also been shown that the intracellular apoBCCP concentration influences transcription repression at the biotin biosynthetic operon. In bacterial cultures in which transcription initiation at the biotin operon is repressed, induction of apoBCCP synthesis results in derepression *(93, 94).* A reasonable interpretation of these results is that apoBCCP engages holoBirA, thereby depleting the holoBirA pool available for homodimerization. Since dimerization is a prerequisite of biotin operator binding, derepression occurs.

The biological and structural features of the biotin regulatory system are consistent with control of BirA function by competitive and mutually exclusive interactions. In theory, the control can occur at either an equilibrium or kinetic level. The equilibrium dimerization constant, K_D, of holoBirA homodimerization measured by sedimentation equilibrium is 6 ± 2 μM *(27).* Direct measurements of the heterodimer binding interaction are prohibited by the chemistry that follows association of holoBirA with apoBCCP. However, measurement of the interaction could be accomplished by an indirect method. The holoBirA-apoBCCP interaction

was monitored through perturbation of holoBirA homodimer occupancy of the biotin operator using the inhibition DNase I footprinting technique *(96).* The inhibition data obtained over a range of apoBCCP concentrations revealed an inhibition constant for apoBCCP of 2 ± 1 μM. This value agreed well with measurements of partitioning between the two interactions by sedimentation velocity *(95).* Overall, the similar equilibrium constants for formation of the homodimer and heterodimer are consistent with kinetic rather than thermodynamic control of the functional switch in BirA. Moreover, sedimentation velocity measurements employed to investigate the kinetics of holoBirA dimerization indicate that the process is characterized by unusually slow kinetics *(95)*, thus lending further support to a kinetically controlled switch.

Results of combined structural and biochemical studies indicate that the two dimerization processes dictating the functional switch in BirA are energetically equivalent yet structurally distinct. The detailed physical basis of formation of these two distinct interactions using a single holoBirA surface remains unclear. Although they are isoenergetic, preliminary evidence suggests that the detailed chemistries of the two interactions are not equivalent. For example, bio-5'-AMP and its non-hydrolyzable analogs, btnSA (5'-O-[N-(biotinyl) sulfamoyl] adenosine) and btnOH-AMP (biotinol-adenylate) are structurally similar. Like bio-5'-AMP, binding of these analogs to BirA promotes homodimerization, albeit to lesser extents than does the physiological effector *(29).* By contrast, complexes of holoBirA bound to these analogs do not interact with apoBCCP. The ability of apoBCCP to discriminate between the dimerization surfaces of the different holoBirA monomers suggests

distinct dimerization chemistries. Moreover, while homodimerization is characterized by large temperature dependence with an enthalpy of + 41 kcal/mol, preliminary measurements performed at two temperatures indicate that the enthalpy associated with heterodimerization is negligible *(107).* These results prompt further investigation of the detailed structural elements required for the two dimerization interfaces.

Previous studies of BirA mutants that are perturbed in homodimerization have revealed two classes of defects, including those that directly disrupt the protein:protein interface and those that perturb allosteric activation of dimerization by bio-5'-AMP. Single site mutations of residues R118 and R119 located in a flexible loop that participates at the dimerization interface are severely defective in homodimerization *(32).* These residues are part of a glycine rich sequence that is conserved in all biotin ligases. Moreover, deletion of residue A146 and mutation of residue D197 located in two other loops that participate at the dimer interface results in dramatic defects in homodimerization *(32).* Mutations of residues located in a flexible loop distal to the dimerization interface have also shown defective homodimerization properties and belong to the class of allosteric mutants. In the structure of the adenylate-bound BirA residues V219, V214 and W223 form a hydrophobic cluster over the adenine ring of the ligand *(31).* Single site mutations of these residues moderately perturb the homodimerization energetics *(128).* Furthermore, formation of the cluster is integral to the disorder-to-order transition of the flexible loop involved in allosteric signal transmission. These combined mutants

provide tools to investigate the structural requirements for heterodimer formation between holoBirA and apoBCCP.

The focus of this study is to investigate the physical-chemical and the structural determinants of homo- and hetero-dimerization of BirA. Both the salt and temperature dependence of heterodimerization were measured by sedimentation equilibrium. Results of these studies indicate modest dependence of the interaction on both solution variables. The mutants described above that are defective in homodimerization and additional mutants subjected to analysis of homodimerization in this work, are examined for their effects on heterodimerization (Figure 32). Heterodimerization properties of variant proteins were probed using two techniques. In one, the process was assessed by monitoring inhibition of homodimerization of wild-type and mutant holoBirA proteins. This inhibition was detected by its effect on bioO occupancy. In the second assay, the heterodimerization interaction was measured by determining the kinetics of BirA-catalyzed transfer of biotin to apoBCCP. The combined results indicate that, consistent with the results of homodimerization measurements, the BirA variants exhibit a range of defects in heterodimerization. Results of measurements on the mutants that are defective in the allosteric response indicate that the same allosteric mechanism extends to the heterodimerization process. By contrast, measurements performed on mutants that perturb the homodimerization interface indicate that while some structural determinants are important for both interactions, select residues are exclusively critical for one but not the other. Overall these results indicate that against a backdrop

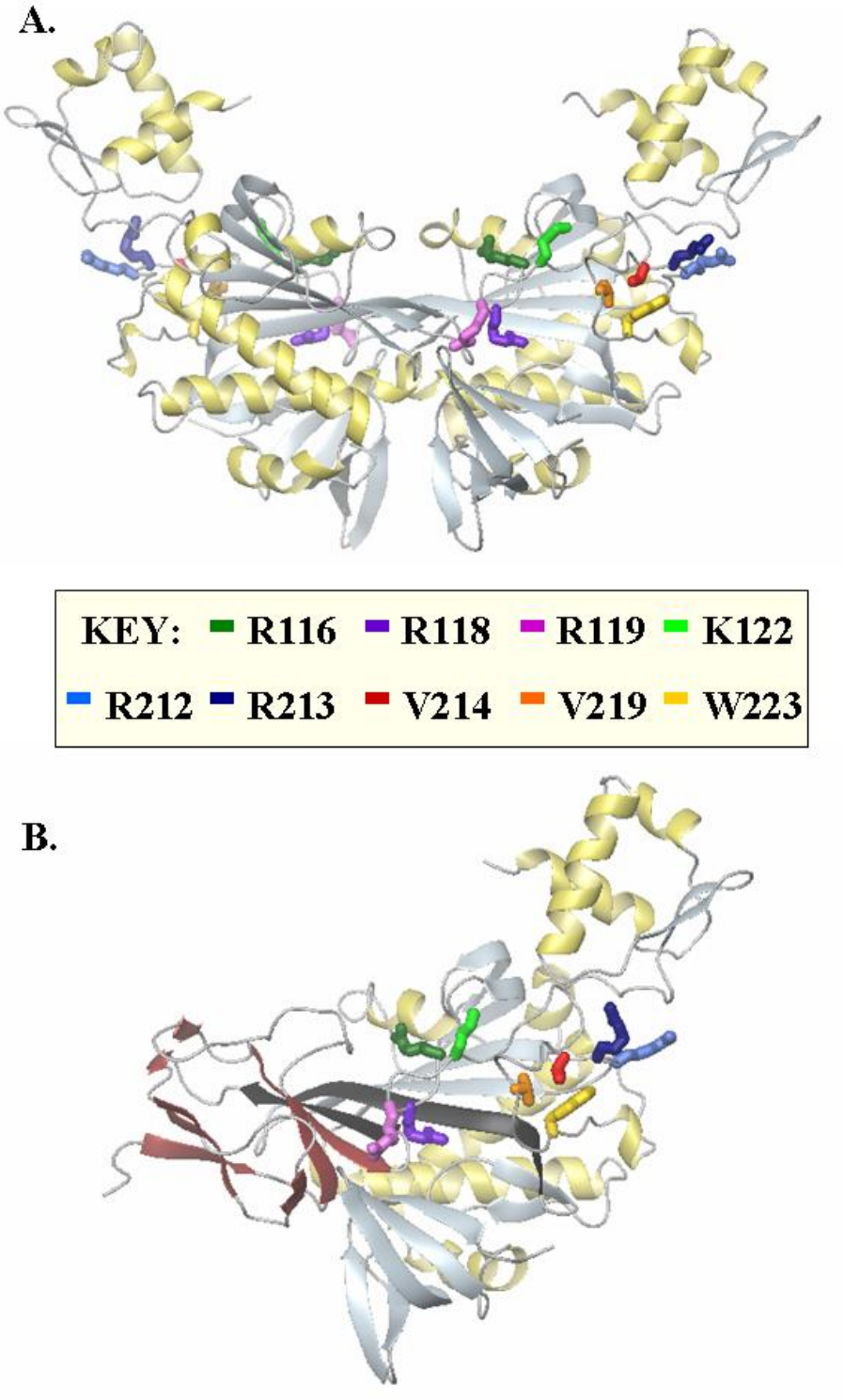

Figure 32. *(legend on next page)*

Figure 32. Residues investigated in Homodimerization and Heterodimerization

The residues investigated are displayed on (A) experimentally determined structure of the homodimer *(31)* and (B) hypothetical structural model of the heterodimer *(97)*. The β-sheet at the dimerization interface of both structures is highlighted in black. Figures were constructed using MolMol *(28)* with Protein Data Bank code 2EWN for (A) and 1K67 for (B).

of significant overlap of structural features that contribute equally to the two alternative protein:protein interactions, "hotspots" have evolved that are exclusive to one but not the other.

B. Results

1. Homodimerization of Mutant Repressor Proteins

The transcriptional repression function of BirA occurs through regulation of homodimerization. Bio-5'-AMP binding promotes biotin operator occupancy by enhancing repressor homodimerization. Results of previous studies indicate that while apoBirA dimerizes weakly in the millimolar concentration range, the BirA-bio-5'-AMP complex exhibits relatively tight dimerization with a K_D in the micromolar range of concentration of 6 ± 2 μM *(17, 27).* Thus the coupling free energy for dimerization associated with bio-5'-AMP binding is –4.0 kcal/mole. Solution studies and x-ray crystallographically determined structures have indicated that the BirA homodimerization interface is formed *via* a β-sheet in the central domain of each holoBirA monomer *(30, 31).* Moreover, the same surface on BirA is used in its interaction with apoBCCP *(97).* The purpose of this study is to investigate the overlap in structural determinants critical to both protein:protein interactions. Previous analysis of the self-assembly properties of a pool of mutants provided information about the structural features important for homodimer interaction (see below). In this study we characterize the homodimerization properties of four additional mutants.

Analysis of the self-assembly properties of BirA mutants has revealed two classes of defects, including mutations that perturb the protein:protein interface and those that disrupt the coupling between bio-5'-AMP binding and dimerization. Among the BirA mutants at the homodimer interface are R118G and R119W. Sedimentation equilibrium measurements performed on the two proteins at saturating bio-5'-AMP concentrations revealed that they are characterized by very weak dimerization *(32).* Indeed, at concentrations at which the wild-type holoBirA is predominantly a dimer the two proteins were monomeric. However, measurements of total assembly of these mutants on bioO by DNase I footprint titrations allows estimation of their dimerization properties. As discussed in the introduction, the total assembly of holoBirA on bioO reflects dimerization followed by DNA binding. Assuming that for these mutants the energetic penalties associated with the total assembly reflect only the decreased dimerization energetics, the dimerization free energies for R118G and R119W are -3.4 and -2.2 kcal/mol, respectively (Table 9). Another mutant at the homodimer interface is A146Δ which exhibits defective dimerization energetics of -5.8 kcal/mol. Mutations in the adenylate binding loop, which is distal to the dimerization interface disrupt the coupling between bio-5'-AMP binding and dimerization. These allosteric mutants are at residues V214, V219 and W223 that form a hydrophobic cluster around the adenine ring of the adenylate ligand. Mutation of these residues to alanine results in energetic penalties for dimerization ($\Delta\Delta G^{\circ}_{dim)}$ of + 1 to +1.5 kcal/mol relative to the wild-type repressor *(128)* (Table 9).

In this work sedimentation equilibrium measurements were performed on four additional BirA mutants, two of which are in the BBL and two in the ABL. While these mutants were originally constructed for an unrelated study, they proved useful for these investigations. Residues R116 and K122 of the BBL are located in close proximity to the dimerization interface, and R212 and R213 of the ABL are positioned distal to the interface. All sedimentation equilibrium measurements were performed at three loading concentrations of each complex and the samples were subjected to centrifugation at three rotor speeds. In all cases the bio-5'-AMP concentration was sufficiently high to ensure saturation of the protein with ligand. The data obtained for R212A (Figure 33) was first analyzed using a single species model in order to obtain the average molecular mass of the complex. The data were then subjected to global analysis using a monomer-dimer association model to resolve the dimerization constants. The quality of the fit was assessed from the magnitude of the square root of the variance of the fit and the distributions of the residuals. Single species analyses indicated protein assembly for all proteins. The resolved equilibrium dissociation constants for the holoBirA variant complexes are shown in Table 9, indicate that BirA variant R116A and R213A exhibit dimerization energetics identical to the wild-type repressor. By contrast, BirA variants K122A and R212A demonstrate moderate defects in dimerization energetics ($\Delta\Delta G^{\circ}_{dim}$ of +0.6 to +0.8kcal/mol).

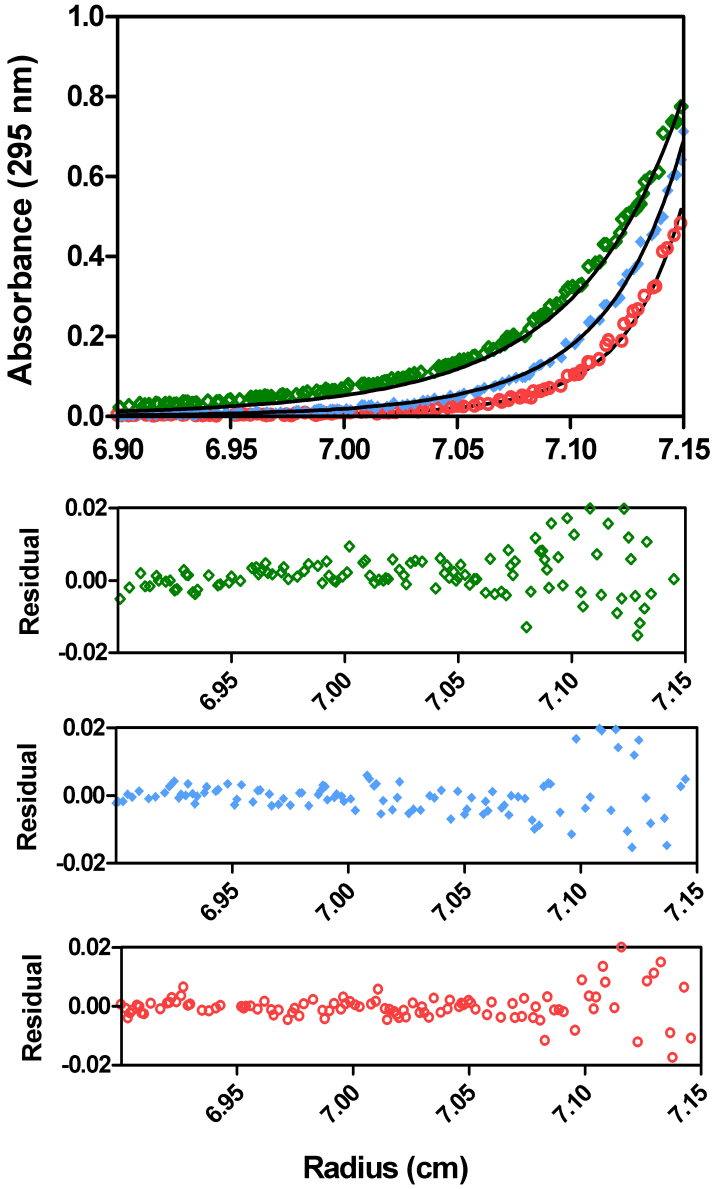

Figure 33. Absorbance *versus* radial position for 45 μM R212A·bio-5'-AMP at 22,000 (◊), 26,000 (♦) and 30,000 (o) rpm obtained in standard buffer at 20 ˚C. The best-fit curves were generated from global analysis using a monomer-dimer model of six data sets acquired at multiple loading concentrations and spun at three speeds. The residuals of the fit for each data set shown are provided in the bottom panels.

Table 9. Homodimerization Properties of the BirA Variant – bio-5'-AMP Complexes

BirA Variant	K_{dim} (M)	ΔG°_{dim} (kcal/mol)
WT	$6 (\pm 2) \times 10^{-6}$	-7.0 ± 0.3
R119W †	2.2×10^{-2}	-2.2
R118G †	2.5×10^{-3}	-3.4
V219A *	$8 (\pm 1) \times 10^{-5}$	-5.5 ± 0.2
V214A *	$3 (\pm 1) \times 10^{-5}$	-6.1 ± 0.2
W223A *	$3 (\pm 1) \times 10^{-5}$	-6.1 ± 0.2
K122A	$2.1 (\pm 0.6) \times 10^{-5}$	-6.2 ± 0.2
R212A	$1.5 (\pm 0.6) \times 10^{-5}$	-6.4 ± 0.3
R213A	$7 (\pm 4) \times 10^{-6}$	-6.9 ± 0.3
R116A	$5 (\pm 2) \times 10^{-6}$	-7.1 ± 0.3

All measurements were performed in Standard Buffer (10 mM Tris-HCl pH 7.50 ± 0.02 at 20.0 ± 0.1 ^{o}C. 200 mM KCl, 2.5 mM $MgCl_2$) as described in Materials & Methods. The reported values represent the average of at least two independent sedimentation equilibrium measurements performed by subjecting samples prepared at multiple loading concentrations of the variant-bio-5'-AMP complex to centrifugation at multiple rotor speeds. Each resulting data set was subjected to global analysis using a monomer-dimer model to determine K_{DIM}. † Self-association properties for these variants were determined previously *(32).* ΔG°_{dim} values were estimated from total assembly energetics and do not have errors (see text for details). * Dimerization properties for these variants were previously reported *(128).*

2. Heterodimerization Properties of holoBirA Variant-apoBCCP Complexes

The mutants described above, (Figure 35A), were investigated for their abilities to form the heterodimer with apoBCCP. Direct measurement of heterodimerization in this system is not possible because interaction between holoBirA and apoBCCP results in chemical transfer of biotin to apoBCCP, a reaction that results in dissociation of the complex and conversion of holoBirA to apoBirA. Due to these limitations alternative methods for measuring heterodimerization have been developed. In the first method the heterodimer interaction is indirectly detected by monitoring the effect of apoBCCP on binding of holoBirA dimer to bioO. In the second method direct measurement of BirA-catalyzed biotin transfer to apoBCCP is used to assess the heterodimerization process. All of the mutants that were assessed for their homodimerization properties were subjected to these two measurements. The acceptor protein utilized in both measurements corresponds to a fragment of the acceptor protein, apoBCCP87, that is known to function identically to the intact protein in BirA-catalyzed biotin transfer *(136).*

a. Inhibition DNase I footprinting Titrations:

The heterodimerization interaction was measured using inhibition DNase I footprint titrations. Addition of apoBCCP87 to a mixture of holoBirA and bioO results in perturbation of holoBirA homodimerization required for bioO occupancy. As the concentration of apoBCCP87 is increased, the level of holoBirA dimer decreases, thus decreasing the fractional occupancy of bioO. Inhibition data obtained over a range of apoBCCP87 concentrations enables measurement of the equilibrium

inhibition constant for apoBCCP87. Previous studies reveal that the results obtained with this assay are in excellent agreement with those obtained from direct measurement of inhibition of holoBirA dimerization by apoBCCP *(95).*

Design and analysis of the inhibition footprints required initial assessment of bioO binding by all the mutants using direct DNase I footprinting. Due to defects in catalysis of adenylate synthesis by some, these experiments were performed with preformed complexes of each mutant protein bound to chemically synthesized bio-5'-AMP. Direct DNase I footprint titrations were first performed to determine the optimal holoBirA concentration for use in inhibition footprints. This holoBirA concentration, which corresponds to a value just below saturation of bioO, renders the system poised for perturbation by apoBCCP87 in the inhibition measurements. A representative footprint of BirA variant R213A binding to bioO is shown in Figure 34A. Quantification of footprints yielded isotherms of fractional occupancy versus [holoBirA] that were subjected to non-linear least squares analysis using the following equation:

$$\overline{Y} = \frac{K_{TOT}[holoBirA]^2}{1 + K_{TOT}[holoBirA]^2} \qquad \text{.....(1)}$$

to obtain K_{TOT}, the equilibrium association constant for total assembly of the holoBirA dimer:bioO complex from holoBirA monomer and bioO. $\overline{Y}$ is the fractional saturation of bioO, and K_{TOT} is the product of equilibrium dimerization and bioO binding constants ($K_{DIM}K_{bioO}$). Figure 34B displays the binding isotherms and best-fit curve for BirA variant R213A. The K_{TOT} determined for each mutant was used in analysis of the relevant inhibition footprint (see below).

The inhibition DNase I footprint is performed to measure the dependence of fractional saturation of bioO by holoBirA dimer on apoBCCP concentration. In these measurements the fractional occupancy of bioO is perturbed by an interaction between apoBCCP and a certain fraction of holoBirA. The holoBirA concentration is maintained at a single value and the apoBCCP concentration is increased. The mixtures are incubated for a short time of 60-80 second, and the DNA is then probed with DNaseI for occupancy by holoBirA. The short incubation time is used to avoid complications that would arise if the holoBirA were released from bioO and provided a second opportunity to interact with apoBCCP. The inhibition footprint obtained for K122A binding to bioO is shown in Figure 34C. Inspection of the gel image reveals a loss of the footprint with increasing apoBCCP concentration. Quantification of the footprint reveals an inhibition of fractional occupancy of bioO versus apoBCCP concentration. These data were subjected to non-linear least squares analysis using the following equation:

$$\overline{Y} = \frac{K_{TOT}([holoBirA](1-\frac{(K_I[apoBCCP])}{1+K_I[apoBCCP]}))^2}{1+K_{TOT}([holoBirA](1-\frac{(K_I[apoBCCP])}{1+K_I[apoBCCP]}))^2} \quad \ldots\ldots\ldots\ldots\ldots\ldots(2)$$

Where K_{TOT} is the equilibrium association constant for total assembly of the holoBirA dimer:bioO complex from holoBirA monomer and bioO and K_I, the inhibition constant for apoBCCP and $\overline{Y}$, the fractional saturation of bioO by holoBirA. Inspection of the equation the fractional occupancy of bioO decreases with increasing apoBCCP concentration. The inhibition constant, K_I, provides a quantitative measure of the holoBirA and apoBCCP interaction (Figure 34D).

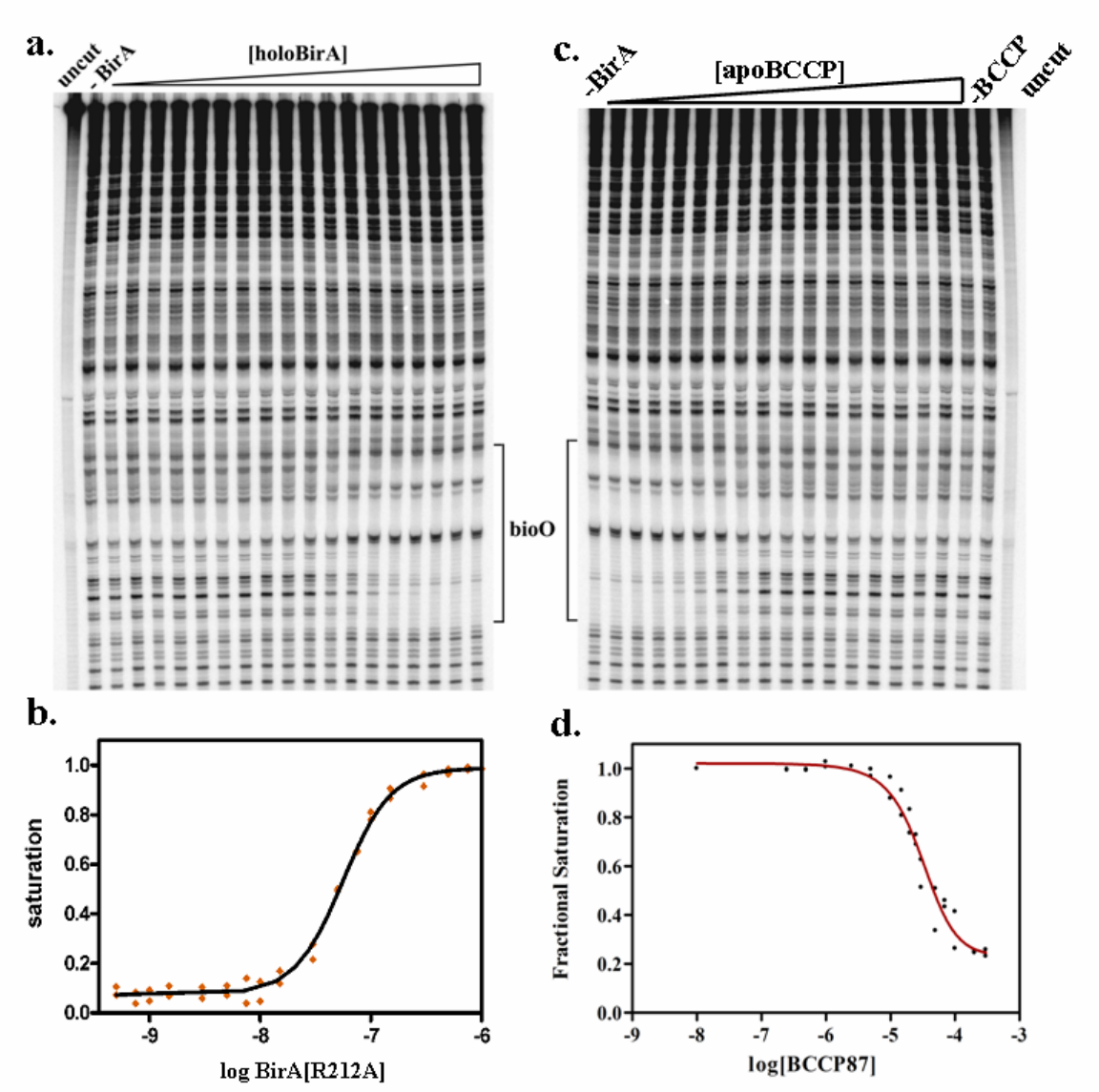

Figure 34. Direct and Inhibition DNase I Footprinting (a) Image of the gel obtained for DNase I footprinting of R212A with bioO. (b) Isotherm obtained from quantification of the data. The curve was generated from non-linear least squares analysis of data to equation (1) in text. (c) Image of the gel obtained for inhibition DNase I footprinting of K122A with bioO as a function of apoBCCP87 concentration. (d) Isotherm obtained from quantification of the data. The curve was generated from non-linear least squares analysis of data to equation (2) in text.

Table 10. Inhibition of HoloBirA Variants Binding to bioO by ApoBCCP87

BirA Variant	K_I (μM)[a]	ΔG°_I (kcal/mol)
WT	2 (± 1)	-7.6 ± 0.4
R119W	> 200	< -4.9
R118G	14 (± 3)	-6.5 ± 0.1
V219A	26 (± 4)	-6.1 ± 0.1
V214A	10 (± 1)	-6.7 ± 0.1
W223A	8 (± 1)	-6.8 ± 0.1
K122A	12 (± 3)	-6.6 ± 0.2
R212A	7 (± 1)	-6.9 ± 0.1
R213A	7 (± 2)	-6.9 ± 0.2
R116A	> 400	< -4.5

All measurements were performed in Standard Buffer (10 mM Tris-HCl pH 7.50 ± 0.02 at 20.0 ± 0.1 ^oC. 200 mM KCl, 2.5 mM $MgCl_2$) as described in the Materials and Methods section, with the exception of BirA variant R119W which was performed under the same buffer conditions with 50 mM KCl. (a.) Footprinting data were fit to equation (2) In all analyses to determine K_I the parameter, K_{TOT} obtained from direct DNase I footprinting data, was fixed. All reported values represent the average of two independent measurements and errors represent 95% confidence intervals. Values for R119W and R116A are estimates and do not have errors because they were beyond the concentration regime used in these measurements.

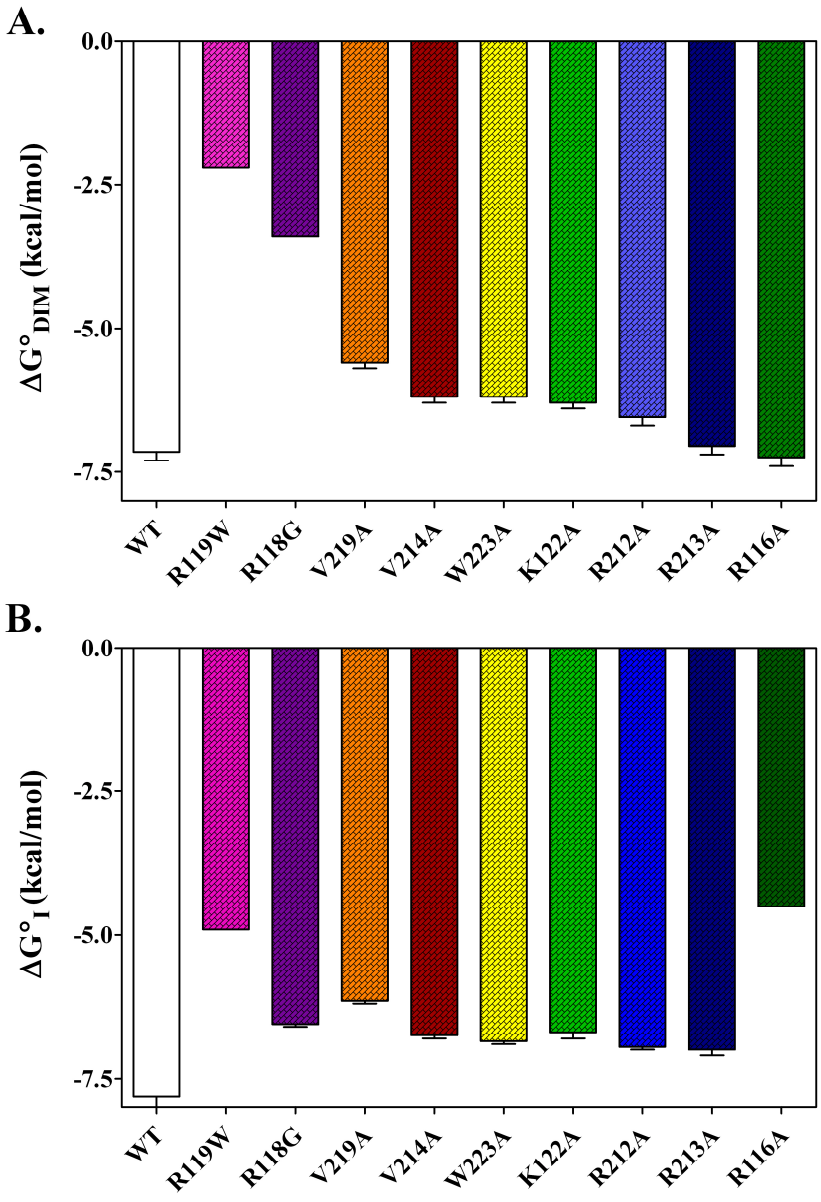

Figure 35. Free energies of Homodimerization and Heterodimerization

(A) ΔG°_{Dim} and (B) ΔG°_{I} of each holoBirA variant in colored bars, compared to that measured for the wild type repressor in white bar. Each variant is color coded as displayed in Figure 32. The reported values represent the average of at least two independent measurements and errors represent 95% confidence intervals.

Based on the results of inhibition titrations, the mutant repressors exhibit a range of affinities for apoBCCP87 (Table 10, Figure 35B). Data acquired for the wild-type is in excellent agreement with that previously reported. The K_I values for the BirA variants range from 3 - 200 fold weaker than that determined for the wild-type protein. The most striking results were obtained for BirA variants R119W and R116A, both of which showed no chamge in the level of bioO occupancy at apoBCCP concentrations as high as 300 μM.

b. BirA-catalyzed biotin transfer to apoBCCP87:

The interaction between holoBirA and apoBCCP results in BirA-catalyzed chemical transfer of biotin from bio-5'-AMP to a specific lysine residue, K122, of apoBCCP. Time courses of this reaction can be monitored by measuring the time-dependent incorporation of ^{14}C-biotin into apoBCCP. Measurement of the initial rates of incorporation versus apoBCCP concentration allows Michaelis-Menten analysis to yield the Michaelis constant, $K_{M,}$ for the acceptor protein. However, in order to measure the apoBCCP-concentration dependence of biotin transfer, the other substrates, biotin and ATP should be at concentrations of maximal velocity. Therefore, biotin binding affinities and ATP-dependence of BirA-catalyzed syntheses of bio-5'-AMP were determined for all mutants prior to performing the kinetics analyses.

(i) Biotin Binding to BirA Variant Proteins

Biotin binding affinities of variant proteins were determined by equilibrium titration methods using isothermal titration calorimetry and steady-state fluorescence measurements as described in the Materials and Methods section. Representative data shown in Figure 36 were subjected to nonlinear least squares analysis using a single site binding model to obtain the equilibrium association constant, K_a for the process. The thermodynamics of biotin binding to the variant proteins are shown in Table 11. With the exception of BirA variant R116A, all BirA variants exhibited biotin binding thermodynamics identical to wild-type. This mutant exhibited 100 fold weaker binding affinity relative to the wild-type protein. The binding parameters for R118G and R119W, which were previously reported *(139),* are also shown in Table 11.

(ii) ATP- dependence of BirA-catalyzed synthesis of Bio-5'-AMP

The initial rates of BirA-catalyzed synthesis as a function of ATP concentration was measured in order to determine the catalytic efficiency of bio-5'-AMP synthesis from biotin and ATP. Synthesis of bio-5'-AMP follows an ordered kinetic mechanism, in which biotin binds and creates the ATP binding pocket. Biotin-saturated BirA is mixed with ATP to produce BirA-bio-5'-AMP. Since the intrinsic fluorescence signal for the protein bound bio-5'-AMP is lower than that of the protein bound to biotin, the time-dependent decrease in fluorescence can be used to monitor the time course of adenylate synthesis *(140).* Figure 37A shows the stopped- flow

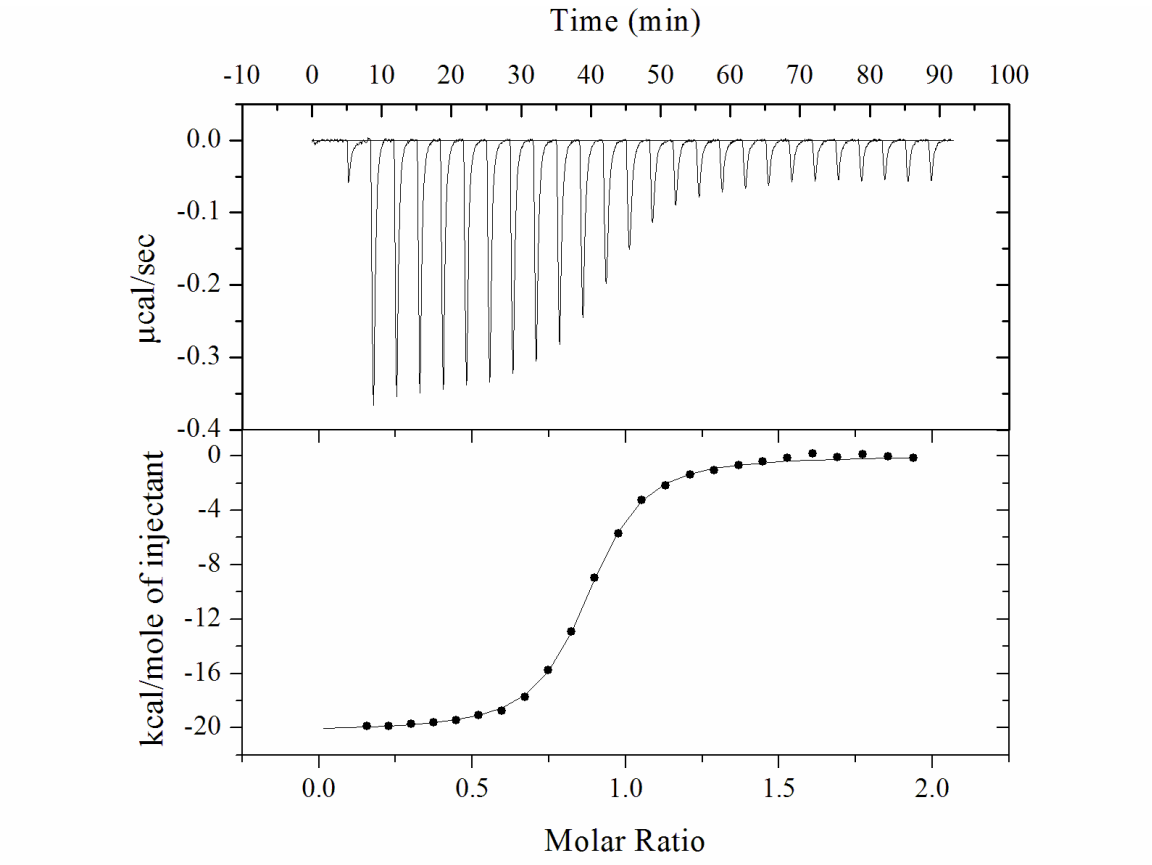

Figure 36. Biotin Binding to BirA Variant R213A.

Equilibrium titration ITC raw data (top panel) and isotherm (bottom panel) of biotin binding to BirA variant R213A. Measurement was performed in Standard Buffer (10 mM Tris-HCl pH 7.50 ± 0.02 at 20.0 ± 0.1 ^{o}C. 200 mM KCl, 2.5 mM $MgCl_2$) as described in Materials & Methods.

Table 11. Thermodynamics of Biotin Binding to the BirA Variant Proteins

BirA Variant	K_b (M)[a]	ΔG^o (kcal/mol)[b]
WT	4.3 (± 0.3) x 10^{-8}	-9.84 ± 0.04
R119W †	2.5 (± 0.3) x 10^{-7}	-8.9 ± 0.1
R118G †	1.8 (± 0.4) x 10^{-6}	-7.7 ± 0.1
V219A *	3.8 (± 1.0) x 10^{-8}	-10.0 ± 0.2
V214A *	3.8 (± 0.8) x 10^{-8}	-9.9 ± 0.1
W223A *	4.7 (± 0.4) x 10^{-8}	-9.8 ± 0.1
R116A ^	1.4 (± 0.4) x 10^{-6}	-7.8 ± 0.2
K122A	4.4 (± 0.8) x 10^{-8}	-9.8 ± 0.1
R212A	3.9 (± 0.3) x 10^{-8}	-9.89 ± 0.04
R213A	4.1 (± 0.3) x 10^{-8}	-9.9 ± 0.1

Measurements were performed in Standard Buffer (10 mM Tris-HCl pH 7.50 ± 0.02 at 20.0 ± 0.1 ^oC. 200 mM KCl, 2.5 mM $MgCl_2$) as described in the Materials and Methods section. The reported values represent the average of at least two independent titrations with standard deviation. a. Values of K_b are the best-fit values obtained from nonlinear least squares analysis of the titration data to a simple binding model using Origin or GraphPad Prism 4. b. The values of the Gibbs free energy, ΔG^o, were calculated using the expression $\Delta G^o = RT\ln K_b$. † Biotin binding thermodynamics for these variants were reported *(139).* * Biotin binding thermodynamics for these variants were reported in *(128).* ^ The equilibrium dissociation constant for binding biotin to R116A was determined from direct equilibrium fluorescence titrations.

trace obtained for BirA variant R212A synthesis of bio-5'-AMP at 500 μM ATP. This time-dependent fluorescence decrease could be analyzed using a single exponential model to obtain the initial rate of adenylate synthesis. The process monitored follows the mechanism:

$$\text{BirA•biotin + ATP} \underset{k_{-1}}{\overset{k_1}{\rightleftharpoons}} \text{BirA• biotin• ATP} \xrightarrow{k_2} \text{BirA•bio-5'-AMP + PPi}$$

in which the holo BirA•biotin complex is in rapid equilibrium with the ternary complex of the enzyme bound to both substrates. Assuming that pyrophosphate release is very fast, the chemical step is described by k_2. The initial rate increases with increasing ATP concentration. The dependence of the initial rate of bio-5'-AMP synthesis on ATP concentration is provided by the modified Michaelis-Menten equation:

$$\upsilon_o = \frac{[BirA \bullet biotin]_0 k_2 [ATP]}{[ATP] + K_{M(ATP)}} \qquad \text{.....(3)}$$

Where υ_o is the initial velocity, the maximal velocity is given by the expression, $[BirA \bullet biotin]_0 k_2$ and the $K_{M(ATP)}$ is equal to $(k_2 + k_{-1})/k_1$. Measurements are performed over a range of ATP concentrations at which [ATP] << K_M. The dependence of the initial rate on ATP concentration is analyzed using a linear equation. The slope reflects the catalytic efficiency, k_{cat}/K_M or k_2/K_M for BirA-catalyzed bio-5'-AMP synthesis as a function of ATP concentration. The data obtained for each variant is shown in Figure 37B. Due to the exceedingly slow rate with which they catalyzed adenylate synthesis, values for BirA variants V219A and W223A were not determined. The values for the other variants, which are shown in Table 12 reveal that

they are similar to wild-type BirA in their abilities to catalyze synthesis of bio-5'-AMP from biotin and ATP. Making the assumption that the k_{cat} for each variant is similar to that of the wild-type protein, the K_M for ATP is also considered similar to wild-type. The K_M for ATP for the entire reaction for the wild-type is 400μM measured by the Michaelis-Menten kinetics assay described below. In this measurement the time-dependent ^{14}C-biotin incorporation into apoBCCP is obtained at a saturation acceptor concentration over a range of ATP concentrations. The conditions used to measure K_M for apoBCCP for the variants were performed at a concentration of 1mM ATP.

(iii) Michaelis-Menten kinetics of biotin transfer to apoBCCP87:

Direct measurement of the Michaelis-Menten kinetics of BirA-catalyzed biotin transfer to apoBCCP is performed to assess the heterodimerization process. The time course of this reaction is monitored by measuring the time-dependent ^{14}C-biotin incorporation into apoBCCP. Biotin-saturated BirA was mixed with ATP and apoBCCP87 and the reaction was quenched at specific time intervals. Unincorporated ^{14}C-biotin was separated from biotinylated-BCCP87 (holoBCCP87) on a low molecular weight SDS-polyacrylamide gel. A representative image of a gel obtained from a time course carried at a single apoBCCP87 concentration is shown in Figure 38A. The time-dependence of biotinylation is determined by quantification of the band corresponding to ^{14}C-biotin-BCCP87 as a function of time. The data in the linear portion of the curve were subjected to linear least squares regression to obtain the initial velocity of BirA- catalyzed ^{14}C-biotin transfer to apoBCCP87 at each

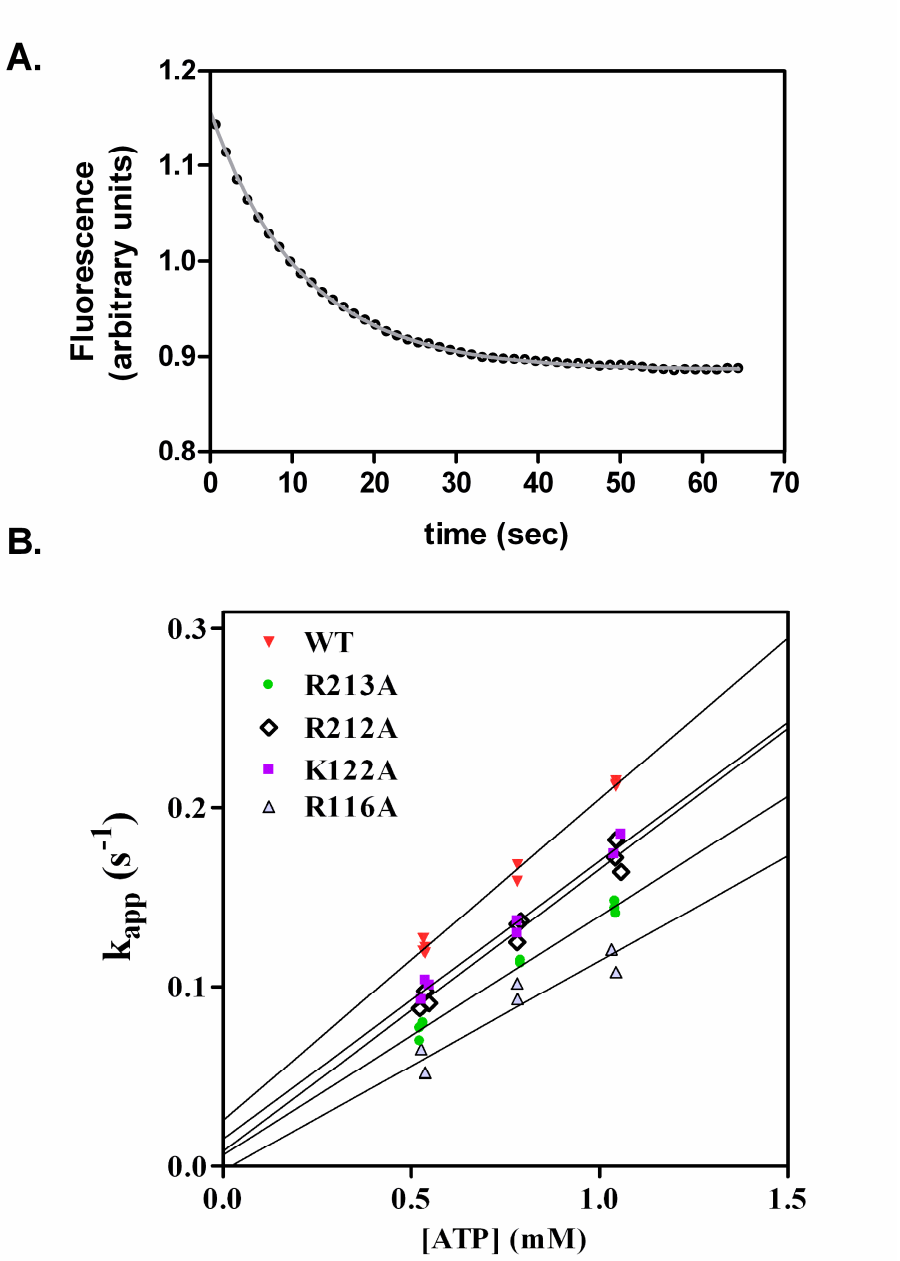

Figure 38. Stopped-flow fluorescence trace obtained for measuring BirA-catalyzed synthesis of bio-5'-AMP from biotin and ATP. (A) bio-5'-AMP synthesis by biotin-bound BirA Variant K122A monitored by stopped-flow fluorescence. (b) The ATP dependence of BirA-catalyzed synthesis of bio-5'-AMP for BirA WT and variants.

Table 12. ATP-dependence of BirA catalyzed synthesis of bio-5'-AMP

BirA Variant	k_{cat}/K_M ($M^{-1}s^{-1}$)
WT	180 ± 10
R116A	120 ± 10
K122A	160 ± 10
R212A	160 ± 10
R213A	130 ± 10

All measurements were performed in Standard Buffer (10 mM Tris-HCl pH 7.50 ± 0.02 at 20.0 ± 0.1 ^{o}C. 200 mM KCl, 2.5 mM $MgCl_2$) as described in the Materials and Methods section. The reported values represent the average of at least two independent measurements and errors represent 95 % confidence intervals.

concentration of acceptor protein. Similarly, the initial rates were obtained over a range of apoBCCP87 concentrations.The dependenceof initial rate on [apoBCCP87] was used to build a Michaelis-Menten plot as shown in Figure 38B. These data were subjected to non-linear least squares analysis using the Michaelis-Menten equation:

$$v_{\circ} = \frac{V_{MAX}[S]}{K_M + [S]} \qquad \text{.....(4)}$$

to obtain the Michaelis constant, $K_{M,}$ for apoBCCP87.

The K_M values for BCCP87 determined for wild-type BirA and variants are shown in Table 13. Due to their inability to catalyze bio-5'-AMP synthesis at a reasonable rate, the K_M values for BirA variants V219A and W223A were not determined. The K_M for BCCP87 for the wild-type protein is 12 ± 5 μM. With the exception of R119W and R116A which exhibit K_M values 12 to 14 fold higher, all variants are similar to the wild-type protein in biotin transfer to apoBCCP.

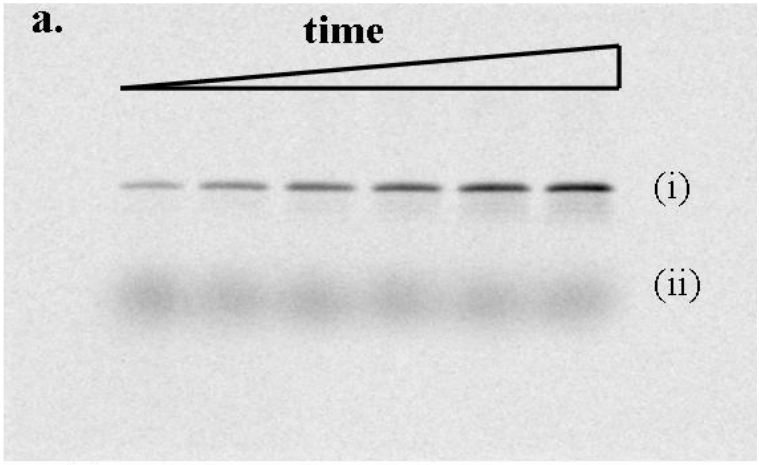

(i) ^{14}C-biotin-BCCP

(ii) Unincorporated ^{14}C-biotin

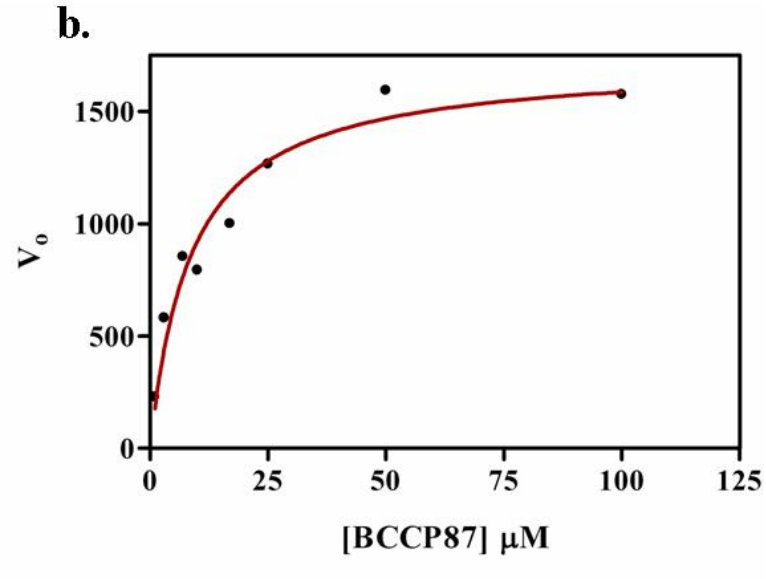

Figure 38. BirA-catalyzed ^{14}C-biotinylation of apoBCCP87

(a.) Representative gel of ^{14}C-biotinylation of 10 µM apoBCCP87 as a function of time. (b.) Michaelis-Menten plot for biotinylation of apoBCCP87. V_o represents counts of ^{14}C-biotin/second. The data were acquired at 150 µM BirA variant R212A, 1 mM ATP, and 10 µM ^{14}C-biotin in standard buffer conditions as described in the Materials and Methods section.

Table 13. Michaelis-Menten Kinetics of BirA catalyzed biotin transfer to apoBCCP87

BirA Variant	K_M (μM)[a]
WT	12 ± 5
R119W	165 ± 30
R118G	6 ± 3
V219A	n.d.*
V214A	7 ± 2
W223A	n.d.*
K122A	6 ± 2
R212A	9 ± 2
R213A	7 ± 3
R116A	150 ± 25

All measurements were performed in Standard Buffer (10 mM Tris-HCl pH 7.50 ± 0.02 at 20.0 ± 0.1 ^{o}C. 200 mM KCl, 2.5 mM $MgCl_2$) as described in Materials & Methods. The reported errors represent 95% confidence intervals of the fit, except the reported value for BirA wild-type which is the average of two independent measurements. (a) K_M values are obtained from non-linear least squares fits of the data to equation (3) * K_M for BCCP87 for BirA variants V219A and W223A were not determined (See text for details).

C. Discussion

The *E.coli* Biotin Regulatory System provides an excellent model for investigating how the functional fate of a single protein is regulated by formation of alternative protein:protein interactions. The central component of this system, BirA, funnels biotin into metabolism or regulates biotin biosynthesis by switching between two alternate interactions *(2, 3).* It can homodimerize or form a heterodimer with apoBCCP, a subunit of the acetyl-CoA carboxylase (ACC) enzyme. While the former process results in transcription repression the latter results in biotin transfer to ACC, the enzyme that catalyzes the first committed step of fatty acid synthesis. Thermodynamic analyses indicate that the two processes are iso-energetic and that the functional switch in BirA is kinetically controlled *(27, 95, 96).* Structural data indicate that a single surface on BirA is used for both homo- and heterodimerization *(30, 31, 97).* Thus the two protein:protein interactions are mutually exclusive. While both interactions use the same BirA surface and are isoenergetic, the different response of the two interactions to bio-5'-AMP analogues and change in temperature provide preliminary evidence that the detailed chemistries of the interactions differ *(29, 107).* In this study, comparison of the two interactions using wild type and single site mutants of BirA reveal that significant overlap in the structural requirements of the two interactions exists.

Structural elements on BirA required for wild type homodimerization energetics were previously studied by thermodynamic characterization of BirA mutants. The results revealed two classes of mutants, including those that directly

disrupt the protein:protein interface and those that perturb the thermodynamic coupling between bio-5'-AMP binding and dimerization. Structures of BirA indicate that three of the loops located in the central domain of BirA participate directly at the dimerization interface. One of the loops at the interface is the biotin binding loop (BBL), which contains a five residue glycine/arginine rich sequence that is conserved in all biotin holoenzyme ligases thus far sequenced. Mutants R118G and R119W in this loop exhibit defects of +3.6 and +4.8 kcal/mol. In addition to the BBL, loops composed of residues 193-199 and 140-146 are located at the homodimer interface. The two mutants D197A and A146Δ exhibit defects in dimerization of +4.5 and +2.2 kcal/mol. A fourth loop, the adenylate binding loop (ABL) is distal to the dimerization interface. Structural data indicate that the loop folds around the adenylate moiety of the adenylate ligand and that the residues V219, V214 and W223 form a hydrophobic cluster over the adenine ring of the ligand *(31).* Thermodynamic analyses of variant proteins V214A, V219A and W223A, indicate that disruption of this hydrophobic cluster moderately compromises dimerization energetics *(128).* In this study the homodimerization properties of four additional variants in the ABL and BBL are presented. Relative to the wild-type protein, mutation of residues R212 and K122 to alanines results in +0.6 kcal/mol and +0.8 kcal/mol defect in free energy of dimerization, respectively. By contrast, BirA variants R116A and R213A exhibit wild-type dimerization energetics. These measurements of the self-assembly properties of this pool of mutants provide information about the structural determinants required for both direct formation of the protein:protein interface and allosteric activation of the dimerization process. The mutants also provide a means of

investigating the structural determinants on BirA required for heterodimerization with apoBCCP.

Heterodimerization properties of BirA variants were probed by two methods. The first employs the inhibition DNase I footprint titration technique, in which the apoBCCP87 concentration dependence of inhibition of occupancy of the biotin operator by holoBirA reveals an inhibition constant, K_I, for apoBCCP87. This inhibition constant provides information about the strength of the interaction between holoBirA and apoBCCP87. The wild-type protein exhibits a K_I of 2 ± 1 μM. In the second method the kinetics of BirA-catalyzed linkage of biotin to apoBCCP are measured. The incorporation of ^{14}C-biotin into apoBCCP87 is monitored as a function of time over a range acceptor protein concentration to generate a Michaelis-Menten plot. The Michaelis constant, K_M for apoBCCP87, provides information about the affinity of holoBirA for apoBCCP assuming that formation of the product is the rate-limiting step. The K_M value determined for the reaction catalyzed by wild-type BirA is 12 ± 5 μM. While both methods provide valuable information, the K_I value obtained from the inhibition experiment is in excellent agreement with that determined by another indirect measurement of the heterodimer interaction. This method utilized sedimentation velocity to measure the perturbation of holoBirA self-association by apoBCCP *(95).* The assumptions made in the analysis of both methods are similar. Moreover, the K_I value is representative of the perturbation of homodimerization by apoBCCP, while the K_M represents the entire chemical reaction that involves bio-5'-AMP synthesis and subsequent transfer of biotin to apoBCCP87.

The Michaelis constant for apoBCCP has been measured previously by stopped-flow fluorescence *(136).* These measurements revealed a K_M for apoBCCP of 300 μM, a value approximately 30 times higher than that reported in this work. The former method measures the K_M for the entire reaction that includes two half reactions; bio-5'-AMP synthesis and subsequent biotin transfer from holoBirA to apoBCCP. By contrast, since measurements are performed with BirA preloaded with bio-5'-AMP, the latter measures only the second half reaction. The stopped-flow measurements revealed biphasic kinetics of biotin transfer, in which the first phase is dependent on apoBCCP87 concentration and the second is concentration independent. The first phase reflects substrate binding and subsequent biotin transfer and the second reflects product release. At low apoBCCP87 concentrations, the rate of the apoBCCP concentration dependent phase overlaps with that of the concentration independent phase. Since the rates cannot be deconvoluted, the dependence of initial velocity on apoBCCP concentration at low [apoBCCP] in the Michaelis-Menten plot is absent. As a consequence, the K_M for apoBCCP obtained from fitting Michaelis-Menten data is over estimated. Overall, it is evident that the ^{14}C-biotin assay utilized in this study provides an accurate K_M for apoBCCP and is in reasonable agreement with reported K_I values, in measuring the heterodimer interaction. However, defective bio-5'-AMP synthesis properties for some of the mutants precluded measurement of the K_M for apoBCCP by this kinetic assay.

BirA mutants investigated for homodimerization properties were examined for their effects on heterodimerization. Based on the results of the inhibition experiment,

the variants V214A, V219A, W223A exhibited defects of 4- 13 fold in K_I values and are thus moderately defective in heterodimerization. BirA variants R212A and R213A of the ABL are characterized by K_Is approximately 3.5 fold greater than wild-type BirA and are modestly defective. Mutation of residues K122 and R118 of the BBL result in 6 and 7 fold defects in heterodimerization, respectively. However, the most dramatic defects are observed with the BirA variants R119W and R116A. For both variants concentration as high as 200 μM apoBCCP87 did not perturb the equilibrium occupancy level of bioO. Results of the ^{14}C-biotin assay revealed that all BirA variants exhibited similar K_M values as that of the wild-type protein, with the exception of BirA variants R119W and R116A. These variants indicate 12-14 fold higher K_M values in comparison to wild-type. While these values do not directly correlate in magnitude with defects in heterodimerization observed by the inhibition experiment, it is noteworthy that both assays indicate that the most pronounced defects are observed with variants R119W and R116A. Taken together, results indicate a range of defects in heterodimerization properties of variant proteins and provide information on the structural determinants integral to the interaction between holoBirA and apoBCCP.

Residues located distal to the dimerization interface contribute important structural determinants to both dimerization interactions. These include residues of the hydrophobic cluster (V214, V219, W223) in the ABL and K122 located in the biotin binding loop. Disruption of K122 affects both dimerization interactions to similar extents. While homodimerization of K122A is characterized by 3.8-fold

higher K_D, the K_I for apoBCCP87 is 6 fold higher than that measured for the wild-type protein. Structural data suggest that K122 may contribute to stacking interactions that accompany folding of the biotin binding loop *(31).* Mutations of the hydrophobic cluster of the ABL perturb the allosteric activation of homodimerization by bio-5'-AMP. Measurements of the heterodimerization interaction were limited to the inhibition DNase I footprinting technique. Nevertheless, the determined inhibition constants indicated a striking correlation in the involvement of these residues in both protein:protein interactions. Relative to the wild-type protein, variants V214A, V219A and W223A exhibited 5-14 fold higher K_D values for homodimerization. The magnitudes of defects in homodimerization were mirrored in those of heterodimerization, represented by 4-13 fold higher K_I values for apoBCCP87. These results lead to the conclusion that the allosteric signal in BirA associated with bio-5'-AMP binding is positively coupled not only to homodimerization but also to heterodimerization.

The most striking structural features important to both protein:protein interactions are contributed by residues located at or close to the dimerization interface. These residues are part of the glycine rich sequence, ^{115}GRGRXG^{120} in BirA, conserved in all biotin holoenzyme ligases *(141).* Phenotypic analysis of *E. coli* strains that carry mutations in this sequence, G115S and R118G, indicate that they require higher biotin concentrations for survival *(3, 142).* Biochemical studies on BirA variants R116A, R118G and R119W have demonstrated over one thousand fold defects in biotin binding affinities relative to the wild-type repressor *(33).*

Additionally, the structure of the ligand-bound dimer indicates that these residues are located in the biotin binding loop that orders over the biotin moiety. These data support a uniformly integral role for the residues of this sequence in biotin binding. However, despite their close proximity to the interface their involvement in alternative dimerization interactions is diverse. While residues R118 and R119 participate directly at the homodimer interface, R116 contributes main-chain hydrogen bonds to the ureido ring of the biotin moiety. Although R118 is located at both protein:protein interfaces, it is selectively integral to the homodimerization interaction. By contrast, R116 is critical only for the apoBCCP87:holoBirA interaction. It is noteworthy, that both residues are conserved in the glycine rich sequences of all ligases. Residue R119 is not conserved within the sequence, yet is integral to both protein:protein interactions. Single site replacement of R119 with tryptophan severely disrupts both homo- and hetero-dimerization. These biochemical measurements are supported by structural data. Inspection of the dimer interface of the homodimer reveals an intermolecular salt bridge between R119 of one holoBirA monomer and D197 of the other. Previously solution studies have shown that mutation of either of these residues dramatically disrupts homodimerization *(32).* Furthermore, the model of the heterodimer indicates interaction between R119 of holoBirA and residue E169 of apoBCCP87. Thus R119 serves as an essential "hotspot" in both protein:protein interfaces.

There are many biological processes in which a single protein participates in functional switching *via* alternative protein:protein interactions. In a subset of these

systems structural data indicate use of one surface on one of the partners for both interactions, thus rendering the processes mutually exclusive. Amongst others, many transcriptional regulators posses an additional biological function regulated through interaction with another protein partner. In this study we have addressed one such transcription factor, the *E. coli* biotin repressor, BirA. The primary focus was to determine the structural features important for its alternative protein:protein interactions. Biochemical characterization of mutant proteins has provided a map of residues on BirA that are important for hetero- and homo-dimerization processes. The results indicated a range of defects in both dimerization properties for the variants (Figure 39). While there is significant structural overlap in both protein:protein interactions, residues exclusively critical to a one but not the other dimerization process have been identified. Those structural features that function in allosteric activation of homodimerization by bio-5'-AMP also extend to heterodimerization. By contrast, measurements performed on mutants that perturb the homodimerization interface indicate that while some structural determinants are important for both interactions, select residues are exclusively critical for one but not the other. Overall these results indicate that against a backdrop of significant overlap of structural features that contribute equally to the two alternative protein:protein interactions, "hotspots" have evolved that are exclusive to one but not the other.

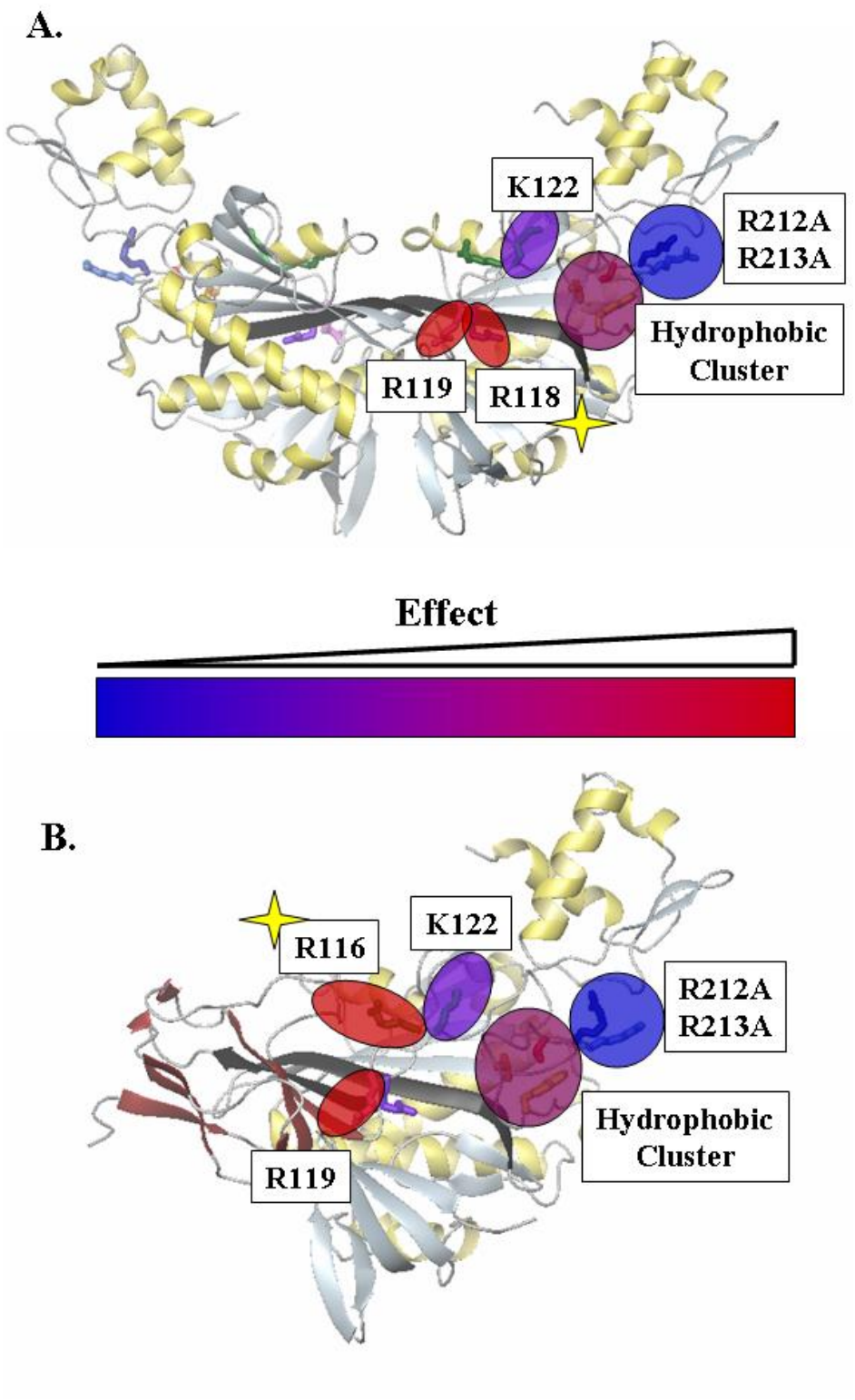

Figure 39. *(legend on next page)*

Figure 39. Overlap in Structural Determinants important to Homodimerization and Heterodimerization. The defects observed upon mutation of depicted residues on (A) homodimerization and (B) heterodimerization range from modest (blue) to dramatic (red). Residues marked with a yellow star are exclusive to one but not the other dimerization process.

VI. Materials and Methods

A. Chemicals and Biochemicals

All chemicals used in the preparation of buffers were obtained commercially and were at least reagent grade. The *d*-biotin, isopropyl β-D-thiogalactoside (IPTG), polyethyleneimine (PEI), adenosine triphosphate (ATP), DNase I, and subtilisin A were purchased from Sigma. The Klenow fragment of DNA Polymerase I and restriction enzymes, *Hind III* and *Pst I* were from Promega. The α^{32}P dATP and dGTP used for radioactive labeling of DNA, and the ^{14}C-biotin were obtained from GE Healthcare or Perkin Elmer. The bio-5'-AMP was synthesized and purified in the laboratory using a published procedure *(5)*. The biotinol- adenylate (btnOH-AMP) was synthesized as described in Brown *et al (29).* The truncated biotin carboxyl carrier protein (apoBCCP) was purified as described in Nenortas and Beckett *(136)*, with the exception of an additional chromatography step at the end, on a Hydroxyapatite ULTROL (PALL). This was performed to remove trace quantities of the DNase I that were introduced during purification. BCCP87, the C-terminal domain of BCCP, has been shown to function as the intact protein in biotin transfer in Nenortas and Beckett *(136).*

B. Expression and Purification of BirA variants

The BirA variants were expressed in the *E. coli* strain JM109 transformed with the plasmid pBtac2 carrying the *E. coli birA* gene (wild type or mutant) under transcriptional control of the *tac* promoter. The gene was altered to encode a C-

terminal $(His)_6$ tag, which does not interfere with the protein's function *(32)*. Cells were grown at 30°C in LB media and protein expression was induced by addition of IPTG at $O.D._{600nm}$ of 0.6-0.9 for 3 hours. The cells were harvested by centrifugation and lysed by sonication. After separation of the cell debris from the lysate by centrifugation, nucleic acids were removed by addition of PEI to a final concentration of 0.2% (vol/vol). The separation and purification of BirA from other cellular proteins was carried out in two chromatography steps. The protein mixture was applied to a NiNTA (Qiagen) column (150 mm x 15 mm) equilibrated with 20 mM imidazole, 50 mM $(NaH)PO_4$, 300 mM NaCl, 5% glycerol, 0.1 mM DTT, pH 8.0 and eluted with a step gradient of increasing imidazole concentration from 20 mM to 175 mM in the same buffer. With the exception of BirA V219A, K122A, R212A and double mutant R212A/R213A, fractions containing BirA were pooled and dialyzed against SP-Sepharose Starting Buffer (50 mM Tris-HCl (pH 7.5 at 4 °C), 50 mM KCl, 5% glycerol, 0.1 mM DTT) and loaded onto a SP-Sepharose (GE Healthcare) column (150 mm x 15 mm) equilibrated with the same buffer. Protein was eluted in a linear KCl gradient (0.05 M to 0.8 M) in 50 mM Tris-HCl (pH 7.5 at 4 °C), 5% glycerol, 0.1 mM DTT. The fractions containing pure BirA were pooled and dialyzed against Storage Buffer (50 mM Tris-HCl (pH 7.5 at 4 °C), 200 mM KCl, 5% glycerol) and stored at –70 °C. Fractions containing BirA for purification of variants V219A, K122A, R212A and double mutant R212A/R213A were pooled, dialyzed against SP-Sepharose Starting Buffer and loaded onto a Q-Sepharose (GE Healthcare) column (150 mm x 15 mm) and flow through containing the protein was collected. The pure protein was exchanged into Storage Buffer and stored at –70 °C. The yield for each

protein was > 12 mg/L of culture. The concentration of each protein stock was determined spectrophotometrically using a molar extinction coefficient at 280 nm calculated for each BirA histag variant using the method by Gill and von Hippel *(143)*. The pooled protein sample for each BirA histag variant was >95% pure as judged by 12.5 % SDS-PAGE followed by Coomassie brilliant blue staining. Binding activity was >90% for all variants as determined by stoichiometric titrations with bio-5'-AMP monitored by fluorescence spectroscopy *(5)* and described under the section on steady-state fluorescence measurements.

C. Isothermal Titration Calorimetry

All titrations were performed using a VP-ITC microcalorimeter with a 1.44 mL sample cell volume, a 250 μL syringe, and equipped with a thermovac degasser (MicroCal, Inc., Northampton, MA.). The protein sample was dialyzed several times against standard buffer (10 mM Tris-HCl (pH 7.50 ± 0.02 at 20.0 ± 0.1 ^{o}C), 200 mM KCl, 2.5 mM $MgCl_2$). The sample was filtered through a 0.22 μm PTFE syringe filter and the concentration determined spectrophotometrically using the ε_{280nm} calculated for each variant. The dialysis buffer was filtered and used for protein and ligand sample preparation and degassed prior to use in the calorimeter. Titrations were performed by addition of ligand to protein in the sample cell. The heat of binding for each injection was obtained after subtracting the average heat of dilution obtained from multiple injections after the saturation of protein. The binding data were analyzed using Origin 7.0 software to obtain binding isotherms and thermodynamic parameters.

1. Equilibrium Binding Titrations

a. Direct Titrations:

The biotin binding thermodynamics of wild type and all variant proteins was determined by direct titration. With the exception of bio-5'-AMP and btnOH-AMP binding to wild type BirA, variants K122A, R212A, and R213A, direct titrations were employed for measurement of ligand binding to all other variant proteins. A 2 μM BirA (wild type or variant) solution was titrated with 25 10 μl injections of 20 μM ligand (biotin, bio-5'-AMP or btnOH-AMP) in standard buffer at 20.0 ± 0.1 ^{o}C. In all titrations the c values ($KM_{tot}n$ where K is the equilibrium association constant for the binding processes, M_{tot} is the total molar protein concentration in monomer units, and n is the stoichiometry of the binding interaction) fall within the range of 100-330. This range is below the upper limit of 500 recommended for measuring equilibrium constants. The signals were integrated and non-linear least squares analysis of binding data was performed using a single site binding model to obtain the equilibrium association constant, K_a, the binding enthalpy, ΔH^{o}, the stoichiometry, n.

The data are fit to the model:

$$Q = \frac{nM_t \Delta H V_o}{2}\left[1 + \frac{X_t}{nM_t} + \frac{1}{nK_a M_t} - \sqrt{\left(1 + \frac{X_t}{nM_t} + \frac{1}{nKM_t}\right)^2 - \frac{4X_t}{nM_t}}\right] \qquad \text{(i)}$$

in which, Q is the total heat content after the ith injection, X_t is the total ligand concentration, M_t is the total protein concentration, V_o is the reaction volume. The total heat content is corrected for the change in reaction volume after each injection.

The Gibbs free energy, ΔG^o and entropic contribution to each binding process, $-T\Delta S^o$, were calculated using these relationships,

$$\Delta G^o = -RT\ln K_A \quad \text{(ii)}$$

$$\Delta G^o = \Delta H^o - T\Delta S^o \quad \text{(iii)}$$

b. Displacement Titrations:

The tight binding of bio-5'-AMP and/or btnOH-AMP to wild type BirA and variant proteins K122A, R212A, and R213A necessitated use of the displacement titration method *(105)* for measuring these interactions. In this technique the protein is first saturated with a weaker binding ligand, biotin, through a direct titration as described above and then displaced by btnOH-AMP or bio-5'-AMP. The titrations are performed with 25 x 10µL injections of 40µM biotin into 2µM BirA and then followed by the displacement titration of 35 x 7µL injections of 20µM btnOH-AMP/ bio-5'-AMP into the BirA•biotin solution. The raw data obtained are integrated and corrected for ligand dilution. The binding isotherm is then subjected to non-linear least squares analysis using a single-site binding model. The thermodynamic parameters obtained are the apparent binding constant, K_{app}, and the apparent binding enthalpy, ΔH_{app}. The parameters are then used with the displacement model to obtain the equilibrium binding constant, K_A, and the binding enthalpy, ΔH°_A, for the tighter binding ligand, using the following relationships:

$$K_{app} = \frac{K_A}{1 + K_B[B]} \quad \text{(iv)}$$

$$\text{and} \qquad \Delta H_{app} = \Delta H^\circ_A - \Delta H^\circ_B \frac{K_B[B]}{1 + K_B[B]} \quad \text{(v)}$$

where, K_B and ΔH°_B are the equilibrium binding constant and binding enthalpy, respectively, of the lower affinity ligand, biotin, obtained through the direct titration method. [B] refers to the total biotin concentration in the sample cell.

2. Total Association at Partial Saturation Titrations

Titrations under conditions of total association at partial saturation were used to obtain measurements of the enthalpy of each binding process used in calculation of the heat capacities. In this method, 15 injections of a concentrated ligand solution are introduced into the protein solution under stoichiometric binding conditions. A 2 μM BirA (wild type or variant) solution is titrated with 5 x 5 μL injections of a 20 μM ligand (biotin, bio-5'-AMP or btnOH-AMP) in standard buffer at 20.0 ± 0.1 °C, followed by a 150 μL injection to saturate the protein, and finally followed by 8 x 5 μL injections. The first five injections provide measurements of the uncorrected binding enthalpies (binding + ligand dilution), while the 8 injections post-protein saturation provide the enthalpy of ligand dilution. The enthalpy of binding is calculated using the equation,

$$\Delta H^{\circ}_{binding} = \Delta H^{\circ}_{binding + dilution} - \Delta H^{\circ}_{dilution} \qquad \text{(vi)}$$

In each experiment five measurements of the binding enthalpy are obtained.

D. Heat Capacities of Ligand Binding

Heat capacity changes associated with formation of the protein-ligand complexes were determined by measuring the temperature dependence of the binding enthalpy for the processes. Measurements were performed using the TAPS method

(see above) to obtain enthalpies of binding for wild type BirA and the three ABL variants with biotin, bio-5'-AMP, and btnOH-AMP at temperatures from 5-20 °C. The pH of the standard buffer was adjusted to 7.50 ± 0.02 at each working temperature. The heat capacity change upon binding was obtained by linear regression of the ΔH^o versus T data for each binding interaction, with this relationship:

$$\Delta Cp = \frac{\delta \Delta H^o}{\delta T} \qquad \text{(vii)}$$

E. Sedimentation Equilibrium

Sedimentation Equilibrium Measurements

The dimerization properties of each BirA variant-ligand complex bound to btnOH-AMP or bio-5'-AMP were determined by analytical ultracentrifugation using a Beckman Optima XL-I Analytical Ultracentrifuge equipped with a four-hole An-60 Ti rotor (Beckman Coulter). Double-sector cells with charcoal-filled epon centerpieces with sapphire windows and optical pathlengths of 3 mm and 12 mm were employed *(17)*. The protein was exchanged into and preequilibrated with standard buffer (10 mM Tris-HCl (pH 7.50 ± 0.02 at 20.0 ± 0.1 ^oC), 200 mM KCl, 2.5 mM $MgCl_2$) using a MicroBiospin 6 Chromatography column (BioRad). The concentration of the protein sample was determined spectrophotometrically using the ε_{280} calculated for each BirA variant. The complex was prepared in standard buffer at stoichiometric conditions with a ratio of 1:1.5 of protein to ligand. The buffer density (1.007 g/ml) was determined pycnometrically and the partial specific volume of BirA monomer is 0.755 ml/g as reported previously *(17)*. Scans of absorbance versus radial

position were obtained at 295 nm at three protein loading concentrations from 15 μM to 75 μM and rotor speeds of 18,000, 22,000, 26,000, and 30,000 rpm for 12 hours each. Five measurements were acquired at each radial position with 0.001 cm spacing.

Analysis of Sedimentation Equilibrium Data

The sedimentation equilibrium data were subjected to non-linear least squares analysis using the programs MacNonLin (*144*) or WinNonLin. The σ-values were obtained for each scan individually and related to the molecular weight using the following equation:

$$\sigma = \frac{M(1-\bar{v}\rho)\omega^2}{RT} \qquad \text{(viii)}$$

in which M is the molecular weight, $\bar{v}$ is the partial specific volume of the protein, ρ is the density of the buffer, ω is the angular velocity of the rotor, R is the gas constant and T is the temperature in Kelvin. Data were also analyzed globally to a monomer-dimer association model *(145)* to obtain the monomer-dimer association constant, K_a.

$$c_t(r) = \delta c + c_m(r_o)e^{\sigma_{mon}(\frac{r^2-r_o^2}{2})} + K_a(c_{mon}(r_o))^2 e^{2\sigma_{mon}(\frac{r^2-r_o^2}{2})} \qquad \text{(ix)}$$

where δc is the baseline offset, c_t is the total concentration at each radial position, r, $c_m(r_o)$ is the monomer concentration at r_o, r_o is the reference radial position (at the first data point), σ_{mon} is the reduced molecular weight of the monomer determined by sedimentation of the aporepressor, and K_a is the equilibrium association constant governing assembly of the dimer from the monomers. In the analysis, the reduced molecular weight of the dimer is assumed to be twice that of the monomer. The

quality of each global analysis was evaluated by the magnitude of square root of variance of fit and distribution of residuals.

F. Measurements of Rates of Subtilisin-catalyzed Proteolysis

All BirA histag WT and variant samples were subjected to subtilisin-catalyzed proteolytic digestion following a 30 minute incubation at 20 ˚C in standard buffer (10 mM Tris-HCl (pH 7.50 ± 0.02 at 20.0 ± 0.1 ˚C), 200 mM KCl, 2.5 mM $MgCl_2$) either in the absence or presence of saturating concentrations of biotin or bio-5'-AMP. The apparent rates of subtilisin-catalyzed cleavage were measured by addition of subtilisin prepared freshly in standard buffer to a BirA solution to obtain a final weight ratio of repressor:subtilisin of 33 to 50:1 and incubation was continued at 20 ˚C. All experiments were performed at a BirA concentration at which the protein is 100% monomeric in the absence and presence of ligand. A 10 μL aliquot was removed at 15 minute time intervals and the reaction was quenched into 1 μL of 100 mM PMSF freshly prepared in absolute ethanol. Six microliters of Laemmli gel sample buffer were added and the proteolytic digestion products were separated by electrophoresis on a 15% SDS-polyacrylamide gel. Protein bands were stained with Coomassie Brilliant Blue and the amount of intact BirA for each time point of proteolytic cleavage was quantified using a Molecular Dynamics Laser Scanning Personal Densitometer. Control experiments have shown that high concentrations of the ligands do not affect the catalytic activity of subtilisin *(108)*.

Data Analysis

The rates of subtilisin-catalyzed cleavage of BirA were obtained by relating the time-dependent decrease of intact BirA to a pseudo-first order process. The apparent rates of proteolysis were estimated from linear least-squares analysis using the following equation:

$$\ln\left(\frac{[BirA_{OD}]_t}{[BirA_{OD}]_{t=0}}\right) = -kt \qquad \text{(x)}$$

where $[BirA_{OD}]_t$ and $[BirA_{OD}]_{t=0}$ are the integrated optical densities for the bands corresponding to intact BirA at time t and the zero time point, respectively, t is time in minutes and k, is the rate or slope of the line.

G. DNase I Footprinting

1. Preparation of DNA for Footprinting

The plasmid pBioZ was digested with *Hind III*. The purified and linearized DNA was radiolabelled with ^{32}P- dATP and dGTP and chased with cold dNTPs using the Klenow Fragment (*5, 146*). The resulting labeled DNA was purified using an Elutip column (Scheicher and Schuell), and phenol-chloroform extracted. The mixture was ethanol precipitated followed by digestion with *PstI.* The desired restriction fragment containing bioO, was isolated by electrophoresis on a 1% agarose gel and recovered by electroelution *(146).* The precipitated, radiolabelled DNA was resuspended to a final concentration of approximately 20,000 cpm/µl in TE buffer and stored at 4 º C.

2. Direct DNase I Footprint Titrations

The DNase I footprint titrations were carried out in reaction buffer containing 10 mM Tris-HCl (pH 7.5 ± 0.02 at 20 ± 0.1 °C), 200 mM KCl, 2.5 mM $MgCl_2$, 1.0 mM $CaCl_2$, 100 µg/mL BSA, 2 µg/mL sonicated calf thymus DNA and ligand, 40 µM bio-5'-AMP. This was followed by preparation of 200 µL reaction buffer, along with 12000 cpm of radio-labeled DNA to a final concentration of approximately 20 pM. Footprints were carried out with BirA at a range of concentrations. A DNase I solution of 3 µg/mL was prepared in 10 mM Tris-HCl (pH 7.5 ± 0.02 at 20 ± 0.1 °C), 200 mM KCl, 2.5 mM $MgCl_2$, 1 mM $CaCl_2$. DNA digestion was initiated and followed by quenching with 33 µL of a 50 mM Na_2EDTA solution. The DNA was then precipitated with 700 µL of 0.4 M NH_4OAc, 50 µg/ mL yeast phenylalanyl tRNA in ethanol and incubated in a dry ice/ ethanol bath for about 20 mins (*16*). The samples were centrifuged and pellets are washed with 80% (v/v) ethanol and dried down. The pellets were resuspended in a loading buffer and DNA fragments were resolved by electrophoresis on a 10% denaturing polyacrylamide gel (19:1 acrylamide/ bisacrylamide in 8 M urea).

3. Inhibition DNase I Footprint Titrations

DNase I footprinting was employed to probe the effect of increasing concentration of apoBCCP87 on the equilibrium level of holoBirA occupancy of bioO for the variant repressors. The careful selection of the holoBirA protein concentration for each variant protein at a value just below complete fractional saturation of bioO, was determined from direct DNase I footprinting measurements.

All reactions were performed in buffer containing 10 mM Tris-HCl (pH 7.5 ± 0.02 at 20 ± 0.1 °C), 200 mM KCl, 2.5 mM $MgCl_2$, 1.0 mM $CaCl_2$, 100 µg/mL BSA, 2 µg/mL sonicated calf thymus DNA and saturating concentration of bio-5'-AMP for each variant protein. A range of apoBCCP87 concentrations were used and in each sample apoBCCP87 was combined in buffer with 12,000 cpm labeled bioO to a total volume of 45 µL. The reaction was initiated with the addition of 5 µL of holoBirA to bring both proteins to the desired final concentrations. After a short incubation of 80 seconds, 5 µL of a 0.0055 mg/mL DNaseI solution was added to each reaction followed by a 20 second digestion and quenched with 33 µL of 50 mM Na_2EDTA. Precipitation was carried out with 700 µL of 0.4 M NH_4OAc, 50 µg/ mL yeast phenylalanyl tRNA in Ethanol and incubated in a dry ice/ethanol bath for 20 minutes *(16)*. The samples are centrifuged and pellets are washed with 80% (v/v) Ethanol and dried down. The pellets are resuspended in a loading buffer and DNA fragments separated by electrophoresis on a 10% denaturing polyacrylamide gel (19:1 acrylamide/ bisacrylamide in 8 M urea). For those footprints performed in low salt buffer conditions (10 mM Tris-HCl (pH 7.5 ± 0.02 at 20 ± 0.1 °C), 75 mM KCl, 2.5 mM $MgCl_2$, 1.0 mM $CaCl_2$, 100 µg/mL BSA, 2 µg/mL sonicated calf thymus DNA), 0.002 mg/mL DNaseI was added to the reaction.

4. Quantification and Data Analysis

The gels were dried and exposed to storage phosphor screens for 40 hours or more. Footprints were imaged using a Storm phosphorimaging system (Molecular Dynamics) and the program Image Quant. The optical densities of bands

representative of the bioO binding site at each protein concentration were integrated to produce binding isotherms as described in Brenowitz *et al (147)*. The binding data were analyzed by non-linear least squares analysis using the GraphPad Prism 4.0 software package applying the following expression:

$$\overline{Y} = \frac{K_{TOT}[holoBirA]^2}{1 + K_{TOT}[holoBirA]^2} \quad \text{(xi)}$$

where $\overline{Y}$ is the fractional occupancy of the bioO site. The data are fit to obtain K_{TOT}, the equilibrium constant for total assembly of the holoBirA dimer:bioO complex which is the product of the equilibrium dimerization constant, obtained from the analysis of sedimentation equilibrium data and the equilibrium constant governing dimer binding to bioO, $K_{DIM}K_{bioO}$. The magnitude of total free energies of assembly, ΔG°_{TOT} was calculated using the expression:

$$\Delta G^{\circ}_{TOT} = -RT\ln K_{TOT} \quad \text{(xii)}$$

The quality of the fits was assessed by the magnitude of the sum of the squares of the residuals and the distribution of the residuals.

Similarly, with a modification of the above binding relationship, the fractional saturation of the operator site, bioO, by the repressor was determined as a function of apoBCCP87 concentration. In these competition experiments the fraction occupancy of bioO is perturbed by an interaction between apoBCCP and a certain fraction of holoBirA. The fractional saturation of bioO is 1.0 at the holoBirA concentrations used in these footprints. Hence the fractional occupancies obtained in the presence of apoBCCP were normalized relative to the value obtained in the absence of apoBCCP. The inhibition curve obtained for holoBirA binding to bioO in the presence of

apoBCCP is analyzed by non-linear least squares analysis using GraphPad Prism 4.0 applying the following equation:

$$\overline{Y} = \frac{K_{TOT}([holoBirA](1 - \frac{(K_I[apoBCCP])}{1 + K_I[apoBCCP]}))^2}{1 + K_{TOT}([holoBirA](1 - \frac{(K_I[apoBCCP])}{1 + K_I[apoBCCP]}))^2} \quad \text{(xiii)}$$

K_I, the inhibition constant, is representive of the heterodimeric interaction between holoBirA and apoBCCP. Hence the fractional saturation of holoBirA by apoBCCP is dependent on both the K_I and the apoBCCP concentration.

H. Steady-State Fluorescence Measurements

Stoichiometric and equilibrium titrations of certain variant proteins with the ligands biotin and bio-5'-AMP were performed by steady-state fluorescence using an ISS-PC1 spectrofluorimeter (ISS, Champaign, IL) equipped with a VWR Scientific 1160 constant temperature bath (PolyScience, Niles, IL) maintained at 20.0 ± 0.1 °C. The excitation wavelength was 295 nm and the emission was monitored from 310-450 nm, with both slit widths set at 0.5 nm. All titrations were performed in standard buffer (10 mM Tris-HCl (pH 7.50 ± 0.02 at 20.0 ± 0.1 ˚C), 200 mM KCl, 2.5 mM $MgCl_2$) at 20.0 ± 0.1 °C. Measurements were performed by sequential addition of concentrated biotin or bio-5'-AMP to 600-800 µL of 1-2 µM apo BirA sample. A spectrum of the apo protein is recorded, followed by acquisition of spectra after each addition of ligand sample. Duration of 2 minutes between each ligand addition is allowed for equilibration. The integrated area of each emission spectrum was obtained using the Vinci Software and used in the analysis of titration data. All

integrated areas were corrected for buffer contribution and changes in volume upon addition of ligand.

Data Analysis

The steady-state fluorescence titration data were analyzed by non-linear least-squares analysis using GraphPad Prism 4.0 software package. The stoichiometric titrations performed to measure protein activity after purification of variant proteins were analyzed using a simple stoichiometric titration model as described in Abbott and Beckett *(5)*. The equilibrium titrations of BirA variants with ligands were analyzed using a simple one site binding model, to obtain the equilibrium binding constant.

I. Stopped-Flow Fluorescence Measurements

The initial rates and catalytic efficiency of enzyme-catalyzed synthesis of bio-5'-AMP from biotin and ATP for BirA wild-type and variant proteins were measured by stopped-flow fluorescence using a Kin Tek SF2001 instrument. One syringe contained the protein saturated with biotin in standard buffer (10 mM Tris-HCl (pH 7.50 ± 0.02 at 20.0 ± 0.1 ˚C), 200 mM KCl, 2.5 mM $MgCl_2$), and the other contained an ATP sample prepared in the same buffer. The solutions were rapidly mixed in a 1:1 ratio and the final concentrations of protein and biotin were 1 and 50 μM, with the exception of those variant proteins that required higher concentration of biotin to ensure saturation. The concentration of ATP was varied from 0.5-3.0 mM. The excitation wavelength was set at 295 nm for all measurements and the fluorescence

emission was monitored above 340 nm employing a cut off filter. Upon mixing sample in both syringes to a final volume of 60 μL, the resulting time-dependent decrease in the intrinsic fluorescence was monitored.

Data Analysis

All data obtained from stopped-flow fluorescence measurements were analyzed using the SF 4.0 software package. The initial rates of BirA wild-type and variant-catalyzed synthesis of bio-5'-AMP over a range of ATP concentrations were analyzed employing a single exponential model:

$$F = A\exp\left(\frac{t}{\tau}\right) + C \qquad \text{(xiv)}$$

where, F is the fluorescence intensity, A is the amplitude and τ is the relaxation time. The values for the catalytic efficiency of bio-5'-AMP synthesis by BirA, k_{cat}/K_M, were determined from the initial rates of synthesis versus ATP concentration using the equation:

$$\upsilon_o = \frac{[BirA \bullet biotin]_0 k_2 [ATP]}{[ATP] + K_{M(ATP)}} \qquad \text{(xv)}$$

where, υ_o is the initial velocity, k_2 is the first order rate constant for bio-5'-AMP synthesis from biotin and ATP and K_M is the Michaelis constant for ATP.

J. Michaelis-Menten Kinetics of BirA-catalyzed biotin transfer to apoBCCP87

The kinetics of BirA catalyzed transfer of biotin to BCCP was measured by detecting ^{14}C-biotin incorporation into apoBCCP87. All experiments were performed by preparing a master mix with 1 mM ATP, 10-25 μM ^{14}C-biotin and apoBCCP87,

in standard buffer (10 mM Tris-HCl (pH 7.50 ± 0.02 at 20.0 ± 0.1 ˚C), 200 mM KCl, 2.5 mM $MgCl_2$), over a range of apoBCCP87 concentrations. The BirA wild-type or variant sample was prepared and all samples were incubated at 20 ˚C for 20 minutes. The reaction was initiated by addition of BirA to a final concentration of 150 nM at t=0. At time points ranging from 30 seconds to 8 minute intervals, a 17 µL aliquot is removed from each master mix and quenched with 3.4 µL 1% trifluoroacetic acid and 5.1 µL of Laemmli low-molecular weight gel sample buffer. Samples were frozen immediately in a dry ice/ethanol bath. Samples were heated and loaded onto a 16% low molecular weight SDS-polyacrylamide gel (Schagger and von Jagow) to separate free ^{14}C-biotin from biotinylated-BCCP87 (holoBCCP87). The gels were fixed and dried on Whatmann paper and exposed to a storage phosphor screen for 3 days. Gel images were visualized using a Storm phosphorimaging system (Molecular Dynamics) and quantified with the Image Quant software. The optical densities of bands representative of the ^{14} C-biotinylated BCCP87 were quantified and plotted versus time. Similar quantitation was performed on each gel, representative of a specific apoBCCP87 concentration. The initial velocities were obtained from the slope of the counts versus time plot. The initial velocities were then plotted versus the substrate (apoBCCP87) concentration and fit to the Michaelis-Menten equation:

$$v_\circ = \frac{V_{MAX}[S]}{K_M + [S]} \qquad \text{(xvi)}$$

The K_M for BCCP87 for BirA wild-type and variant proteins was determined from the fit.

VI. Summary and Future Work

A focus of the research in the Beckett Lab is centered on understanding the structural basis of multi-functionality in the *E. coli* Biotin Regulatory System. This requires identification of structural determinants important for the distinct functional properties of BirA. Here, a combination of biochemical and biophysical approaches have been employed to dissect the structural features critical to protein:ligand, protein:protein and protein:DNA interactions of BirA. In this work a mutagenesis approach combined with detailed thermodynamic characterization of key residues has been utilized to probe the role of flexible loops in BirA in the allosteric response and in alternative protein:protein interactions that determine the functional switch. Results obtained from this research have identified the limited structural determinants in BirA required to perform its multiple functions.

A model for the mechanism of allosteric activation in BirA has been formulated and confirmed with extensive thermodynamic, kinetic and structural data acquired over the years. In its transcriptional repression function, binding of the corepressor, bio-5'-AMP drives dimerization of the repressor and subsequent DNA binding. It is therefore, the corepressor-bound form of BirA that is active in DNA binding. Detailed investigations indicated that structural and dynamic changes in the BirA monomer play a critical role in the allosteric activation process. Further, structural and biochemical evidence supported the involvement of a flexible loop in the transmission of the allosteric response. This loop is located distal to the dimerization interface and folds over the adenine in the adenylate-bound dimer

structure. Here, mutations of residues in a hydrophobic cluster in the loop are examined to elucidate the ligand-induced allosteric response. Results obtained from thermodynamic characterization of mutant proteins indicate that the coupling of adenylate ligand binding to dimerization is perturbed. The coupling free energy of dimerization is compromised from 1 to 1.5 kcal/mol for each mutant, confirming the importance of the hydrophobic cluster to the allosteric response. Additionally, formation of the hydrophobic cluster is essential for a disorder-to-order transition of the flexible loop. The folding of this low stability region appears to nucleate the allosteric response in BirA.

Recent efforts have focused on investigating the corepressor-linked changes in the repressor monomer employing hydrogen-deuterium exchange coupled with mass spectrometric analysis *(148)*. In this study, BirA monomer complexed with weak and strong activators was probed to assess the degree of protein backbone exchange, as a means to determine conformational/dynamic changes in response to ligand binding. The results indicated that changes in exchange associated with ligand binding span the entire protein. Moreover, the extent of protection of the backbone from exchange correlates with the magnitude of the allosteric response. The results of hydrogen-deuterium exchange have provided an understanding of the change in dynamics associated with the allosteric response. The work presented in this thesis indicates the importance of the folding of a flexible loop to the functional response in BirA. Combining these results has enabled formulation of a model in which, the ligand-induced folding of the flexible loop appears to nucleate the allosteric response that is

then propagated through the protein *via* changes in dynamics. In order to test this model, future work should include subjecting corepressor-bound variants in the hydrophobic cluster to hydrogen-deuterium exchange. A comparison of the extent of exchange observed for the wild-type and variants should provide information on changes associated with nucleation of the allosteric response. Disruption of the cluster correlates with a decreased magnitude of the allosteric response. This should affect the extent of exchange thereby providing further insight on the transmission of the response.

The structures of apoBirA and ligand-bound BirA dimers have been determined to high resolution by x-ray crystallography. To date a structure of the protein:DNA complex has not been determined. However, a hypothetical model of the holoBirA dimer:operator complex was constructed by Dr. Z.A.Wood. In this thesis, predictions based on the model are tested in an effort to elucidate the structural mechanism of effector-induced protein:DNA interactions in this system. The proposed mechanism involves direct contacts between the DNA backbone and the flexible loops involved in intermediate binding and dimerization. Detailed thermodynamic analyses of the DNA binding properties of single and multiple site mutants in the flexible loops indicated that the structural mechanism does not involve direct interaction between the loops and DNA. However, in this work an interesting phenomenon was observed that should be investigated in the future.

In the allosteric activation mechanism of BirA, ligand binding is thermodynamically linked to DNA binding *via* two coupled processes. Corepressor binding enhances BirA dimerization and subsequent DNA binding. Therefore, the energetics associated with assembly of the repression complex (holoBirA dimer:bioO) is equivalent to the sum of the energetics of ligand-induced dimerization and the energetics of binding bioO. Considering this linkage, defects in ligand-induced dimerization energetics should correlate with defects in free energies of total repression complex assembly. Several corepressor-bound variant proteins, exhibited defects in dimerization energetics ranging from 0.8 to 1.5 kcal/mol compared to the wild-type repressor. The DNase I footprinting technique was utilized to determine the energetics of bioO binding and total repression complex assembly for variants that displayed defects in dimerization. Results of these studies indicated no defects in the energetics of total repression complex assembly relative to wild-type. In all cases, defective dimerization (less favorable free energy) was compensated by a more favorable free energy of binding DNA, consequently no difference in total assembly energetics was detected. The factors contributing to this compensation in energetics are presently unclear. A detailed analysis is imperative to understand this phenomenon and could provide valuable information about the linkage between thermodynamics and structural features of the protein:DNA interaction.

Understanding regulation of protein function through alternative protein:protein interactions has been an important focus in the *E. coli* biotin regulatory system. Extensive and detailed studies have been performed to understand

how the functional switch in BirA is controlled. BirA is its intermediate-bound form, holoBirA, switches between alternative protein:protein interactions. It self-associates to function as a transcriptional repressor or heterodimerizes with an acceptor protein to participate in metabolism. Structural data have revealed that the same BirA surface is utilized in both protein:protein interactions, thus rendering them mutually exclusive. A large body of data collected in the Beckett Lab, has indicated that the two processes are isoenergetic and the functional switch is kinetically controlled. In this thesis, an investigation of structural features important for the two protein:protein interactions is presented. Single site mutants in the ligand binding loops were previously and in this work tested for their homodimerization properties. Results indicated a range of defects. While mutation of residues located close to the dimerization interface resulted in dramatic defects in dimerization, those located in a loop distal to the interface exhibited moderate defects. Employing two methods mutant proteins tested for homodimerization properties were assessed for their defects in heterodimerization. The results obtained revealed a significant overlap in structural determinants important for both protein:protein interactions.

In the *E. coli* protein, BirA, limited structural features are important for performing multiple functions. The combined results of research presented here have indicated the participation of two flexible loops in the multiple functions of the protein. Residues in the flexible loop located distal to the dimerization interface are integral to transmission of the allosteric response. This is evidenced by the compromised coupling between intermediate binding and dimerization of mutant

proteins. Moreover, the allosteric response associated with ligand-induced folding of this flexible loop affects both homo- and hetero-dimerization processes. In addition, the protein has evolved “hotspots” at the dimerization interface that are important for specific interaction with itself or with the acceptor protein.

Several lines of evidence have suggested the involvement of the C-terminal domain of BirA in its two functions. The adenylate-bound structure of BirA indicates that this domain participates in formation of an extended homodimer interface. Structural data have also reveal possible interdomain interactions between the C-terminal domain and the central catalytic domain. Moreover, hydrogen-deuterium exchange studies on the BirA monomer indicate the signal associated with ligand binding is propagated to C-terminal domain. Future work should include an investigation of the role of this domain in hetero- and homodimerization. Such work will further elucidate structural determinants important for the multifunctional features of the *E. coli* Biotin Regulatory System.

References

1. Jacob, F. (1982) *The Possible and the Actual*, Pantheon, New York, USA, 33-36.

2. Cronan, J. E. J. (1989) The *E. coli* bio operon: transcriptional repression by an essential protein modification enzyme. *Cell 58*, 427-429.

3. Barker, D. F., Campbell, A.M. (1981) The birA gene of *Escherichia coli* encodes a biotin holoenzyme synthetase. *J. Mol. Biol. 146*, 451-467.

4. Lane, M. D., Rominger, K.L., Young, D.L., Lynen, F. (1964) The enzymatic synthesis of holocarboxylase from apotranscarboxylase and biotin. *J. Biol. Chem. 239*, 2865-2871.

5. Abbott, J., Beckett, D. (1993) Cooperative binding of the *Escherichia coli* repressor of biotin biosynthesis to the biotin operator sequence. *Biochemistry 32*, 9649-9656.

6. Ostuka, A., Abelson, J. (1978) The regulatory region of the biotin operon in *Escherichia coli*. *Nature 276*, 689-694.

7. Prakash, O., Eisenberg, M.A. (1979) Biotinyl 5'-adenylate: corepressor role in the regulation of the biotin genes of *Escherichia coli* K-12. *Proc. Natl. Acad. Sci. U.S.A 76*, 5592-5595.

8. Gerhart, J. C. (1962) The enzymology of control by feedback inhibition. *J. Biol. Chem. 237*, 891-896.

9. Changeaux, J. P. (1961) The feedback control mechanism of biosynthetic L-threonine deaminase by L-isoleucine. *Cold Spring Harbor Symp. Quant. Biol. 26*, 313-318.

10. Koshland, D. E., Jr., Nemethy, G., and Filmer, D. (1966) Comparison of experimental binding data and the theoretical models in proteins containing subunits. *Biochemistry 5*, 365-385.

11. Koshland, D. E., Jr. (1958) Application of a theory of Enzyme Specificty to Protein Synthesis. *Proc. Natl. Acad. Sci. U.S.A 44*, 98-104.

12. Monod, J., Wyman, J., and Changeux, J.P.,. (1965) On the nature of allosteric transitions: a plausible model. *J. Mol. Biol. 12*, 88-118.

13. Monod, J., Changeux, J.P., and Jacob, F. (1963) Allosteric proteins and cellular control systems. *J. Mol. Biol. 6*, 306-329.

14. Lim, W. A. (2002) The modular logic of signalling proteins: building allosteric switches from simple binding domains. *Curr. Opin. Struct. Biol. 12*, 61-68.

15. Beckett, D. (2001) Regulated assembly of transcription factors and control of transcription initiation. *J. Mol. Biol.* pp 333-352.

16. Streaker, E. D., Beckett, D. (2003) Coupling of protein assembly and DNA binding: biotin repressor dimerization preceeds biotin operator binding. *J. Mol. Biol. 325*.

17. Eisenstein, E., Beckett, D. (1999) Dimerization of the *Escherichia coli* biotin repressor: corepressor function in protein assembly. *Biochemistry 38*, 13077-13084.

18. Wilson, K. P., Shewchuk, L.M., Brennan, R.G., Otsuka, A.J., Matthews, B.W. (1992) *Eshcerichia coli* biotin holoenzyme synthetase/bio repressor crystal

structure delineates the biotin- and DNA binding domains. *Proc. Natl. Acad. Sci. U.S.A 89*, 9257-9261.

19. Abbott, J., and Beckett, D. (1993) Cooperative binding of the *Escherichia coli* repressor of biotin biosynthesis to the biotin operator sequence. *Biochemistry 32*, 9649-9656.

20. Eisenstein, E., and Beckett, D. (1999) Dimerization of the *Escherichia coli* biotin repressor: corepressor function in protein assembly. *Biochemistry 38*, 13077-13084.

21. Kwon, K., Streaker, E. D., Ruparelia, S., and Beckett, D. (2000) Multiple disordered loops function in corepressor-induced dimerization of the biotin repressor. *J. Mol. Biol 304*, 821-833.

22. Streaker, E. D., and Beckett, D. (1999) Ligand- linked structural changes in the *Escherichia coli* biotin repressor: the significance of surface loops for binding and allostery. *Biochemistry 292*, 619-632.

23. Streaker, E. D., and Beckett, D. (2003) Coupling of protein assembly and DNA binding: biotin repressor dimerization preceeds biotin operator binding. *J. Mol. Biol 325*, 937-948.

24. Streaker, E. D., Gupta, A., and Beckett, D. (2002) The biotin repressor: thermodynamic coupling of corepressor binding, protein assembly, and sequence- specific DNA binding. *Biochemistry 41*, 14263-14271.

25. Wilson, K. P., Shewchuk, L. M., Brennan, R. G., Otsuka, A. J., and Matthews, B. W. (1992) *Eshcerichia coli* biotin holoenzyme synthetase/bio repressor

crystal structure delineates the biotin- and DNA binding domains. *Proc. Natl. Acad. Sci. U.S.A 89*, 9257-9261.

26. Weaver, L. H., Kwon, K., Beckett, D., and Matthews, B. W. (2001) Corepressor-induced organization and assembly of the biotin repressor: a model for allosteric activation of a transcriptional regulator. *Proc. Natl. Acad. Sci. U.S.A 98*, 6045-6050.

27. Streaker, E. D., Gupta, A., Beckett, D. (2002) The biotin repressor: thermodynamic coupling of corepressor binding, protein assembly, and sequence- specific DNA binding. *Biochemistry 41*, 14263-14271.

28. Koradi, R., Billeter, M., Wuthrich, K. (1996) MOLMOL: a program for display and analysis of macromolecular structures. *J. Mol. Graph 14*.

29. Brown, P. H., Cronan, J.E., Grotli, M., Beckett, D. (2004) The biotin repressor: Modulation of allostery by corepressor analogs. *J. Mol. Biol. 337*, 857-869.

30. Weaver, L. H., Kwon, K., Beckett, D., Matthews, B.W. (2001) Corepressor-induced organization and assembly of the biotin repressor: a model for allosteric activation of a transcriptional regulator. *Proc. Natl. Acad. Sci. U.S.A 98*, 6045-6050.

31. Wood, Z., Weaver, L.H., Brown, P.H., Beckett, D., Matthews, B.W. (2006) Co-repressor induced order and biotin repressor dimerization: a case for divergent follwoed by convergent evolution. *J. Mol. Biol. 357*.

32. Kwon, K., Streaker, E.D., Ruparelia, S., Beckett, D. (2000) Multiple disordered loops function in corepressor-induced dimerization of the biotin repressor. *J. Mol. Biol. 304*, 821-833.

33. Kwon, K., Beckett, D. (2000) Function of a conserved sequence motif in biotin holoenzyme synthetases. *Protein Sci. 9*, 1530-1539.

34. Xu, Y., Beckett, D. (1996) Evidence for Interdomain Interaction in the *Escherichia coli* Repressor of Biotin Biosynthesis from Studies of an N-terminal Domain Deletion Mutant. *Biochemistry 35*, 1783-1792.

35. Streaker, E. D., Beckett, D. (1999) Ligand- linked structural changes in the *Escherichia coli* biotin repressor: the significance of surface loops for binding and allostery. *Biochemistry 292*, 619-632.

36. Bukau, B., Deuerling, E., Pfund, C., and Craig, E.A. (2000) Getting newly synthesized proteins into shape. *Cell 101*, 119-122.

37. Hartl, F. U., and Hyer-Hartl, M. (2002) Molecular chaperones in the cytosol: from nascent chain to folded protein. *Science 295*, 1852-1858.

38. Jiang, J., Prasad, K., Lafer, E.M., and Sousa, R. (2005) Structural basis of interdomain communication in the Hsc70 chaperone. *Mol. Cell 21*, 359-367.

39. Revington, M., Holder, T.M., and Zuiderweg, E.R. (2004) NMR study of nucleotide-induced changes in the nucleotide binding domain of thermus thermophilus Hsp70 chaperone DnaK:implications for the allosetric mechanism. *J. Biol. Chem. 279*, 33958-33967.

40. Rist, W., Graf, C., Bukau, B. and Mayer, M.P. (2006) Amide hydrogen exchange reveals conformational changes in hsp70 chaperones important for allosetric regulation. *J. Biol. Chem. 281*, 16493-16501.

41. Vogel, M., Bukau, B., and Mayer, M.P. (2006) Allosteric regulation of Hsp70 chaperones by a proline switch. *Mol. Cell 21*, 359-367.

42. Vogel, M., Mayer, M.P., and Bukau, B. (2006) Allosteric regulation of Hsp70 chaperones involves a conserved interdomain linker. *J. Biol. Chem. 281*, 38705-38711.

43. Rawlings, N. D., Tolle, D.P., and Barret, A.J. (2004) MEROPS: the peptidase database. *Nucleic Acids Res. 32*, D160-164.

44. Griffin, J. H. (1995) Blood coagulation. The thrombin paradox. *Nature 378*, 337-338.

45. Trumbo, T. A., and Maurer, M.C. (2000) Examining thrmobin hydrolysis of the factor XIII activation peptide segment leads to a proposal for explaining the cardioprotective effects observed with the factor XIII V34L mutation. *J. Biol. Chem. 275*, 20627-20631.

46. Lorand, L., Downey, J., Gotoh, T., Jacobsen, A., Tokura, S. (1968) The transpeptidase system which crosslinks fibrin by gamma-glutamyle-episilon-lysine bonds. *Biochem. Biophys. Res. Commun. 31*, 222-230.

47. Esmon, C. T. (2003) The protein C pathway. *Chest 124*, 26S-32s.

48. Wells, J. A., McClendon, C.L. (2007) Reaching for high-hanging fruit in drug discovery at protein-protein interfaces. *Nature 450*, 1001-1008.

49. Bone, S. (2006) Dielectric studies of water clusters in cyclodextrins: Relevance to the transition between slow and fast forms of thrombin. *J. Phys. Chem. B 110*, 20609-20614.

50. Di Cera, E. (2006) A structural perspective on enzymes activated by monovalent cations. *J. Biol. Chem. 281*, 1305-1308.

51. Pineda, A. O., Carrell, C.J., Bush, L.A., Prasad, S., Caccia, S., CHen, Z.W., Mathews, F.S., and Di Cera, E. (2004) Molecular dissection of Na+ binding to thrombin. *J. Biol. Chem. 279*, 31842-31853.

52. Pineda, A. O., Savvides, S.N., Waksman, G., and Di Cera, E. (2002) Crystal structure of the anticoagulant slow form of thrombin. *J. Biol. Chem. 277*, 40177-40180.

53. Bah, A., Garvey, L.C., Ge, J., and Di Cera, E. (2006) Rapid kinetics of Na+ binding to thrombin. *J. Biol. Chem. 281*, 40049-40056.

54. Mengwasser, K. E., Bush, L.A., Shih, P., Cantwell, A.M., and Di Cera, E. (2005) Hirudin binding reveals key determinants of thrombin allostery. *J. Biol. Chem. 280*, 23997-27003.

55. Rose, T., and Di Cera, E. (2002) Three-dimensional modeling of thrombin-fibrinogen interaction. *J. Biol. Chem. 277*, 18875-18880.

56. Stubbs, M. T., Oschkinat, H., Mayr, I., Huber, R., Angliker, H., Stone, S.R., Bode, W. (1992) The interaction of thrombin with fibrinogen. A strcutural basis for its specificity. *Eur. J. Bichem 206*, 187-195.

57. Braun, V. (1997) Avoidance of iron toxicity through regulation of bacterial iron transport. *Biol. Chem. 378*, 779-786.

58. Morse, D. E., and Yanofsky, C. (1969) Amber mutants of the trpR regulatory gene. *J. Mol. Biol. 44*, 185-193.

59. Lawson, C. L., and Carey, J. (1993) Tandem binding in crystals of a trp repressor/operator half-site complex. *Nature 366*, 178-182.

60. Arrowsmith, C., Pachter, R., Altman, R., and Jardetzky, O. (1991) The solution structures of Escherichia coli trp repressor and trp aporepressor at an intermediate resolution. *Eur. J. Bichem 202*, 53-66.

61. Schevitz, R. W., Otwinowski, Z., Joachimiak, A., Lawson, C.L., and Sigler, P.B. (1985) The three-dimensional structure of trp repressor. *Nature 317*, 782-786.

62. Zhao, D., Arrowsmith, C.H., Jia, X., and Jardetzky, O. (1993) Refined solution structures of the Escherichia coli trp holo- and aporepressor. *J. Mol. Biol. 229*.

63. Zhang, R. G., Joachimiak, A., Lawson, C.L., Schevitz, R.W., Otwinowski, Z., and Sigler, P.B. (1987) The crystal structure of trp aporepressor at 1.8A shows how binding tryptophan enhances DNA affinity. *Nature 327*, 591-597.

64. Otwinowski, Z., Schevitz, R.W., Zhang, R.G., LAwson, C.L.,Joachimiak, A., Marmorstein, R.Q., Luisi, B.F., and Sigler, P.B. (1988) Crystal structure of trp repressor/operator complex at atomic resolution. *Nature 335*, 321-329.

65. Marmorstein, R. Q., Sprinzl, M., Sigler, P.B. (1991) An alkaline phosphatase protection assay to investigate trp repressor/operator interactions. *Biochemistry 30*, 1141-1148.

66. Guenot, J., Fletterick, R.J., Kollman, P.A. (1994) A negative electrostatic determinant mediates the association between the Escherichia coli trp repressor and its operator DNA. *Protein Sci. 3*, 1276-1285.

67. De Pina, K., Desjardin, V., Mandrand-Berthetol, M.A., Giordano, G., Wu, L.F. (1999) Isolation and characterization of the nikR gene encoding a nickel responsive regulator in Escherichia coli. *J. Bacteriol. 181*, 670-674.

68. Chivers, P. T., Sauer, R.T. (2000) Regulation of high affinity uptake in bacteria.

Ni2+-Dependent interaction of NikR with wild-type and mutant operator sites. *J. Biol. Chem. 275*, 19735-19741.

69. Chivers, P. T., Sauer, R.T. (2002) NikR repressor: high-affinity nickel binding to

the C-terminal domain regulates binding to operator DNA. *Chem. Biol. 9*, 1141-1148.

70. Wang, S. C., Dias, A.V., Bloom, S.L., Zamble, D.B. (2004) Selectivity of metal

binding and metal-induced stability of Escherichia coli NikR. *Biochemistry 43*, 10018-10028.

71. Schreiter, S., M.D., Guo, Y., Chivers, P.T, Sauer, R.T., Drennan, C.L. (2003) Crystal structure of the nickel-responsive transcription factor NikR. *Nat. Struct. Biol. 10*, 794-799.

72. Schreiter, E. R., Wang, S.C., Zamble, D.B., Drennan, C.L. (2006) NikR-operator complex structure and the mechanism of repressor activation by metal ions. *Proc. Natl. Acad. Sci. U.S.A 103*, 13676-13681.

73. Raumann, B. E., Rould, M.A., Pabo, C.O., Sauer, R.T. (1994) DNA recognition by beta-sheets in the Arc repressor-operator crystal structure. *Nature 367*, 754-757.

74. Somers, W. S., Phillips, S.E. (1992) Crystal structure of the met repressor-operator complex at 2.8 A resolution reveals DNA recognition by beta-strands. *Nature 359*, 387-393.

75. Bohm, A., and Boos, W. (2004) Gene regulation in prokaryotes by subcellular relocalization of transcription factors. *Curr. Opin. Microbiol. 7*, 151-156.

76. Tanaka, Y., Kimata, K., and Aiba, H. (2000) A novel regulatory role of glucose transporter of *Escherichia coli*: membrane sequestration of a global repressor MIc. *EMBO J 19*, 5344-5352.

77. Kho, C. J., and Zarbl, H. (1992) Fte-1, a v-fos transformation effector gene, encodes the mammalian homologue of a yeast gene involved in protein import into mitochondria. *Proc. Natl. Acad. Sci. U.S.A 89*, 2200-2204.

78. Cui, K., Coutts, M., Stahl, J., Sytkowski, A.J. (2000) Novel interaction between the transcription factor CHOP (GADD153) and the ribosomal protein FTE/S3a modulates erythropoiesis. *J. Biol. Chem. 275*, 7591-7596.

79. Kewley, R. J., Whitelaw, M.L., and Chapman-Smith, A.,. (2004) The mammalian basic helix-loop-helix/PAS family of transcriptional regulators. *Int. J. Biochem. Cell Biol 36*, 189-204.

80. Joly, N., Bohm, A., Boos, W., and Richet, E. (2004) MalK, the ATP-binding cassette component of the Escherichia coli maltodextrin trsncporter, inhibits the transcriptional activator malt by anatagonizing inducer binding. *J. Biol. Chem. 279*, 33123-33130.

81. Kholti, A., Charlier, D., Gigot, D., Huysveld, N., Roovers, M., and Glansdorff, N. (1998) pyrH-encoded UMP-kinase directly participates in pyrimidine-specific modulation of promoter activity in Escherichia coli. *J. Mol. Biol. 280*, 571-582.

82. Bachler, C., Schneider, P., Bahler, P., Lusting, A., and Emi, B. (2005) Escherichia coli dihydroxyacetone kinase controls gene expression by binding to transcription factor DhaR. *EMBO J 24*, 283-293.

83. Honda, R., Yasuda, H. (2000) Activity of MDM2, a ubiquitin ligase, toward p53 or itself is dependent on the RING finger domain of the ligase.*Oncogene 19*, 1473-1476.

84. Fang, S., Jensen, J.P., Ludwig, R.L., Vousden, K.H. and Weissman, A.M. (2000) Mdm2 is a RING finger-dependent ubiquitin ligase for itself and p53. *J. Biol. Chem. 275*, 8945-8951.

85. Li, M., Brooks, C.L., Kon, N., Gu, W. (2004) A dynamic role of HAUSP in the p53-Mdm2 pathway. *Mol. Cell 13*, 879-886.

86. Cummins, J. M., Rago, C., Kohli, M., Kinzler, K.W., Lengauer, C. (2004) Tumor supression: disruption of HAUSP gene stabilizes p53. *Nature 428*, 486.

87. Hu, M., Gu, L., Li, M., Jeffrey, P., Gu, W. and Shi, Y. (2006) Structural basis of competitive recognition of p53 and MDM2 by HAUSP/USP7: implications for the regulation of the p53-MDM2 pathway. *PLoS Biol. 4*, e27.

88. Chitaev, N. A., Averbakh, A.Z., Troyanovsky, R.B. and Troyanovsky, S.M. (1998) Molecular organization of the desmoglein-plakoglobin complex. *J. Cell. Sci. 111*, 1941-1949.

89. Yap, A. S., Briecher, W.M., and Gumbiner, B.M. (1997) Molecular and functional analysis of cadherin-based adheres junctions. *Annu. Rev. Cell Dev. Biol. 13*, 119-146.

90. Polakis, P. (2000) Wnt signaling and cancer. *Genes Dev. 14*, 1837-1851.

91. Huber, A. H., And Weis, W.I. (2001) The structure of the beta-catenin/E-cadherin complex and the molecular basis of diverse ligand recognition by beta-catenin. *Cell 105*, 391-402.

92. Graham, T. A., Weaver, C., Mao, F., Kimelman, D. and Xu, W. (2000) Crystal structure of a beta-catenin/Tcf complex. *Cell 103*, 885-896.

93. Chapman-Smith, A., Morris, T.W., Wallace, J.C., and Cronan, J.E., Jr. (1999) Molecular recognition in a post-translational modification of exceptional specifcity. Mutants of the biotinylated domain of acetyl- CoA carboxylase defective in recognition by biotin protein ligase. *J. Biol. Chem. 274*, 1449-1457.

94. Cronan, J. E. J. (1988) Exprssion of biotin biosynthetic operon of *Escherichia coli* is regulated by the rate of portein biotination. *J. Biol. Chem. 263*, 10332-10336.

95. Zhao, H., Beckett, D. (2008) Protein-protein interactions dominate the assmebly thermodynamics of a transcription repression complex. *J. Mol. Biol. in press*.

96. Streaker, E. D., Beckett, D. (2006) The Biotin Regulatory System: Kinetic Control of a Transcriptional Switch. *Biochemistry 45*, 6417-6425.

97. Weaver, L. H., Kwon, K., Beckett, D., Matthews, B.W. (2001) Competing protein:protein interactions are proposed to control the biological switch of the *E. coli* biotin repressor. *Protein Sci. 10*, 2618-2622.

98. Reche, P., Li, Y.L., Fuller, C., Eichhorn, K., and Perham, R.N. (1998) Selectivity of post-translational modification in biotinylated proteins: The carboxy carrier protein of the acetyl-CoA carboxylase of *Escherichia coli. Biochem. J. 329*, 589-596.

99. Gerhart JC, P. A. (1964) Aspartate Transcarbamylase, as enzyme designed for feedback inhibition. *Fed. Proc. 23*, 727-735.

100. Horwich AL, F. W., Hirshfield IN, Furtak K. (1993) Folding *in vivo* of bacterial cytoplasmic proteins: role of GroEL. *Cell 74*, 909-917.

101. Jobe, A., Bourgeois, S. (1973) Lac repressor-operator interaction: Lactose is an anti-inducer of the lac operon. *J. Mol. Biol. 75*, 303-313.

102. Torres, E., Rosen, M.K. (2006) Protein-tyrosine kinase and GTPase signals cooperate to phosphorylate and activate Wiskott-Aldrich syndrome protein (WASP)/ neuronal WASP. *J. Biol. Chem. 281*, 3513-3520.

103. Wickiser, J. K., Cheah, M.T., Breaker, R.R., Crothers, D.M. (2005) The kinetics of ligand binding by an adenine-sensing riboswitch. *Biochemistry 44*, 13404-13414.

104. Brown, P. H., Beckett, D. (2005) Use of binding enthalpy to drive an allosteric response. *Biochemistry 44*, 3112-3121.

105. Sigurskjold, B. W. (2000) Exact analysis of competition ligand binding by displacement isothermal titration calorimetry. *Anal. Biochem. 227*, 260-266.

106. Bains, G., Freire, E. (1991) Calorimetric determination of cooperative interactions in high affinity binding processes. *Anal. Biochem. 192*, 203-206.

107. Zhao, H., Streaker, E.D., Pan, W., Beckett, D. (2007) Protein-protein intercations dominate the assembly thermodynamics of a transcription repression complex. *Biochemistry 46*, 13667-13676.

108. Xu, Y., Nenortas, E., Beckett, D. (1995) Evidence for distinct ligand-bound conformational states of the multifunctional *Escherichia coli* repressor of biotin biosynthesis. *Biochemistry 34*, 16624-16631.

109. Sturtevant, J. M. (1977) Heat capacity and entrpy change in processes involving proteins. *Proc. Natl. Acad. Sci. U.S.A 74*, 2236-2240.

110. Spolar, R. S., Ha, J.H., Record, M.T, Jr. (1989) Hydrophobic effect in protein folding and other noncovalent processes involving proteins. *Proc. Natl. Acad. Sci. U.S.A 86*, 8382-8385.

111. Baldwin, R. L. (1986) Temperature dependence of the hydrophoibic interaction in protein folding. *Proc. Natl. Acad. Sci. U.S.A 83*, 8069-8072.

112. Bruzzese, F. J., Connelly, P.R. (1997) Allosteric properties of inosine monophosphate dehydrogenase revealed through the thermodynamics of binding of inosine 5'- monophosphate and mycophenolic acid. Temperature dependent heat capacity of binding as a signature of ligand- coupled conformational equilibria. *Biochemistry 36*, 10428-10438.

113. Keramisanou, D., Biris, N., Gelis, I., Sianidis, G., Karamanou, S., Economou, A., Kalodimos, C.G. (2006) Disorder-order folding transitions underlie catalysis in the helicase motor of SecA. *Nat. Struct. Mol. Biol. 13*, 594-602.

114. Kozlov, A. G., Lohman, T.M. (2006) Effects of monovalent anions on a temperature- dependent heat capacity change for *Escherichia coli* SSB tetramer binding to single-stranded DNA. *Biochemistry 45*, 5190-5205.

115. Kumaran, S., Grucza, R.A., Waksman, G. (2003) The tandem Src homology 2 domain of the Syk kinase: a molecular device that adapts to interphophotyrosine distances. *Proc. Natl. Acad. Sci. U.S.A 100*, 14828-14833.

116. Rodionov, D. A., Mironov, A.A., Gelfand, M.S. (2002) Conservation of the biotin regulon and the BirA regulatory signal in Eubacteria and Archaea. *Genome Res. 12*, 1507-1516.

117. Bagautidinov, B., Kuroishi, C., Sgahara, M., Kunishima, N. (2005) Crystal structure of biotin protein ligase from *Pyrococcus horikoshii* OT3 and its complexes: Structural basis of biotin activation. *J. Mol. Biol. 353*, 322-333.

118. Kern, D., Zuiderweg, E.R. (2003) The role of dynamics in allosteric regulation. *Curr. Opin. Struct. Biol. 13*, 748-757.

119. Popovych, N., Sun, S., Ebright, R.H., Kalodimos, C.G. (2006) Dynamically driven protein allostery. *Nat. Struct. Mol. Biol. 13*, 831-838.

120. Huffman, J. L., Brennan, R.G. (2002) Prokaryotic transcription regulators: more than just the helix-trun-helix motif. *Curr. Opin. Struct. Biol. 12*, 98-106.

121. Brennan, R. G. a. M., B.W. (1989) The helix-turn-helix DNA binding motif. *J. Biol. Chem. 264*, 1903-1906.

122. Gallegos, M. T., Schleif, R., bairoch, A., Hofmann, K., and Ramos, J.L. (1997) *Microbiol. Mol. Biol. Rev. 61*, 393-410.

123. Mo.Y., V., B., Johnston, K., Marmorstein, R. (2000) Structure of the elk-1-DNA complex reveals how DNA-distal residues affect ETS domain recognition of DNA. *Nat. Struct. Biol. 7*, 292-297.

124. Lewis, M., Chang, G., Horton, N.C., Kercher, M.A., Pace, H.C., Schumacher, M.A., Brennan, R.G., and Lu, P. (1996) Crystal structure of the lactose operon repressor and its complexes with DNA and inducer.*Science 271*, 1247-1254.

125. Jin, L., Yang, J., and Carey, J. (1993) Thermodynamics of ligand binding to trp repressor. *Biochemistry 32*, 7302-7309.

126. Reedstrom, R. J., and Royer, C.A. (1995) Evidence for coupling of folding and function in trp repressor: physical characterization of the superrepressor mutant AV77. *J. Mol. Biol. 253*.

127. Bell, C. E., and Lewis, M. (2000) A closer view of the conformation of the Lac

repressor bound to operator. *Nat. Struct. Biol. 7*, 209-214.

128. Naganathan, S., Beckett, D. (2007) Nucleation of an Allosteric Response *via* Ligand-induced Loop Folding. *J. Mol. Biol. 373*, 96-111.

129. Streaker, E. D., Beckett, D. (1998) A Map of the Biotin Repressor-Biotin Operator Interface: Binding of a Winged Helix-turn-helix Protein Dimer to a Forty Base-pair Site. *J. Mol. Biol. 278*, 787-800.

130. Record, M. T., Jr, de Haseth, P.L., Lohman, T.M. (1977) Interpretation of monovalent and divalent cation effects on the lac repreoor-operator interaction. *Biochemistry 16*, 4791-4796.

131. Ha, J. H., Capp, M.W., Hohenwalter, M.D., Baskerville, M., Record, M.T. (1992) Thermodynamic stoichiometries of participation of water, cations and anions in specific and non-specific binding of lac repressor to DNA. Possible thermodynamic origins of the "glutamate effect" on protein-DNA interactions. *J. Mol. Biol. 228*, 252-264.

132. Baichoo, N., and Heyduk, T. (1997) Mapping conformational changes in a protein: application of a protein footprinting technique to cAMP-induced conformational changes in cAMP receptor protein. *Biochemistry 36*, 10830-10836.

133. Morozov, A. V., Havranek, J.J., Baker, D., Siqqia, E.D. (2005) Protein-DNA specifcity predictions with structural models. *Nucleic Acids Res. 33*, 5781-5798.

134. Commichau, F. M. a. S., J. (2008) Trigger enzymes: bifunctional proteins active in metabolism and in controlling gene expression. *Mol. Microbiol. 67*, 692-702.

135. Athappilly, F. K., and Hendrickson, W.A. (1995) Structure of the biotnyl domain of acetyl-coenzyme A carboxylase deteremined by MAD phasing.*Structure 3*, 1407-1419.

136. Nenortas, E., and Beckett, D. (1996) Purification and characterization of intact and truncated forms of *Escherichia coli* biotin carboxyl carrier subunit of acetyl-CoA carboxylase. *J. Biol. Chem. 271*, 7559-7567.

137. Bagautidinov, B., Matsuura, Y., Bagautdinov, S., Kunishima, N. (2008) Protein biotinylation visualized by a complex structure of biotin protein ligase with a substrate. *J. Biol. Chem. 283*, 14739-50.

138. Li, S. J., Cronan, J.E. Jr. (1993) Growth rate regulation of *Eshcerichia coli* acetyl coenzyme A carboxylase, which catalyzes the first committed step of lipid biosynthesis. *J. Bacteriol. 175*, 332-340.

139. Kwon, K., Streaker, E.D., Beckett, D. (2002) Binding specificty and the ligand dissociation process in the *E. coli* biotin holoenzyme synthetase. *Protein Sci. 11*, 558-570.

140. Xu, Y., Beckett, D. (1994) Kinetics of Biotinyl-5'-adenylate Synthesis Catalyzed by the *Escherichia coli* Repressor of the Biotin Biosynthesis and the Stability of the Enzyme-Product Complex. *Biochemistry 33*, 7354-7360.

141. Tissot, G., Douce, R., and Alban, C. (1997) Evidence for multiple forms of biotin holocarboxylase synthetase in pea (pisum sativum) and in arabidopsis thaliana: subcellular franctionation studies and isolation of a cDNA clone. *Biochem. J. 323*, 179-188.

142. Buoncristiani, M. R., Howard, P.K., and Ostuka, A.J. (1986) DNA-binding and enzymatic domains of the bifunctional biotin operon repressor (BirA) of Escherichia coli. *Gene 44*, 255-261.

143. Gill, S. C., von Hippel, P.H. (1989) Calculation of protein extinction coeffiecients from amino acid sequence data. *Anal. Biochem. 182*, 319-326.

144. Johnson, M. L., Correia, J.J., Yphantis, D.A., Halvorson, H.R. (1981) Analysis of data from the analytical ultracentrifuge by nonlinear least-squares techniques. *Biophys. J. 36*, 575-588.

145. Laue, T. M. (1995) Sedimentation equilibrium as a thermodynamic tool. *Methods Enzymol. 259*, 427-452.

146. Maniatis, T., Fritsch, E.F., and Sambrook, J. (1982) Molecular Cloning, A Laboratory Manual, *Cold Spring Harbor, New York*.

147. Brenowitz, M., Senear, D.F., Shea, M.A., and Ackers, G.K. (1986) Quantitative DNase footprint titration: a method for studying protein-DNA interactions. *Methods Enzymol. 130*, 132-181.

148. Laine, O., Streaker, E.D., Navabi, M., Fensleau, C., Beckett, D. (2008) Allosteric signaling in the biotin repressor occurs through local folding coupled to global dampening of protein dynamics. *J. Mol. Biol. In press*.